STATISTICAL ANALYSIS OF RESILIENCE DISTRIBUTION AND APPLICATION TO RURAL ELECTRIC DISTRIBUTION SYSTEM SUBJECTED TO HURRICANE WIND

A DISSERTATION IN
Civil Engineering
And
Geosciences

Presented to the Faculty of the University
of Missouri-Kansas City in partial fulfillment of
the requirements for the degree

DOCTOR OF PHILOSOPHY

by
Prativa Sharma

B.C.E, Himalaya College of Engineering, Tribhuvan University, 2014
M.S.C.E., University of Missouri-Kansas City, 2019

Kansas City, Missouri
2021

STATISTICAL ANALYSIS OF RESILIENCE DISTRIBUTION AND APPLICATION TO RURAL ELECTRICAL DISTRIBUTION SYSTEM SUBJECTED TO HURRICANE WIND

Prativa Sharma, Candidate for the Doctor of Philosophy Degree

University of Missouri-Kansas City, 2021

ABSTRACT

Several mathematical frameworks and models are proposed to quantify the resilience of power systems against hurricane events. However, these frameworks contribute to the urban area's large-scale transmission system or networked power delivery system. They are barely applicable to the rural power distribution system, whose intrinsic properties vary distinctively compared to an urban area. These inherent properties such as less robustness due to the high vulnerability of aged wooden poles, topology characterization as a set of linear subsystems that emanate from one power substation and individually feature zero redundancy and cascading effect, and slow recovery due to low socio-economic resources and geospatially sparse customers make it less resilient.

This study thus proposes a fully probabilistic and analytical measurement framework for assessing the resilience of linear power distribution systems affected by hurricane wind. The proposed framework includes the mechanical analysis of coupled wooden-pole and feeder-line as a system unit, the definition of component restoration and system-level recovery functions, and a new resilience measure termed the total mean system-resilience (TMSR). Numerical experimentation is provided that validates the effectiveness and the analytical tractability of the framework. The insight that how physical aging, local resourcefulness, and spatial sparseness interplay and affect the system resilience is shed quantitatively.

On the other hand, from a critical synthesis of the existing literature towards several quantitative resilience measures or ambiguously termed metrics frameworks for quantifying the resilience of civil infrastructure, the author found informational inadequacy on taking objective decisions such as resilience acceptance or parameter strengthening prioritization. Two ingrained drawbacks of such measurements are lack of theoretical basis in 1. Discriminating relatively how a parametric infrastructure system is more resilient than a different one or the same one subject to some changed conditions and, 2. answering which input parameter is most influential while assessing the resilience measure.

This study thus explores and suggests several statistical tools such as 1. A nonparametric approach to perform sensitivity analysis of each input parameter to output resilience and check for the robustness of the proposed resilience assessment framework. 2. Copula-based dependence analysis to determine the most influential parameter and tail dependencies of the resilience measure with each input parameter. 3. Information-theoretic distance measures termed Resilience Distance (RD) measures to characterize how a system evolves as a function of system variables from the realm of materials, hazards, or socioeconomic resourcefulness. 4. Nonparametric two-sample test to check if the calculated resilience can be accepted when compared to targeted resilience of the same system.

Numerical evaluation is conducted using these statistical tools on the proposed probabilistic resilience assessment framework of stochastically modeled rural electrical distribution system, and numerical measures show that the proposed statistical analysis of the resilience distribution can be a possible objective decision-making tool.

APPROVAL PAGE

The faculty listed below, appointed by the Dean of School of Graduate Studies have examined the dissertation titled, "Statistical Analysis of Resilience Distribution and Application to Rural Electrical Distribution System Subjected to Hurricane Wind" presented Prativa Sharma, candidate for the Doctor of Philosophy degree, and certify that in their opinion it is worthy of acceptance.

Supervisory Committee

ZhiQiang Chen, Ph.D., Committee Chair
Department of Civil and Mechanical Engineering

Jejung Lee, Ph.D., Co-advisor
Department of Geosciences

Yong Zeng, Ph.D.
Department of Mathematics and Statistics

Ganesh Thiagarajan, Ph.D.
Department of Civil and Mechanical Engineering

John Kevern, Ph.D.
Department of Civil and Mechanical Engineering

FengPeng Sun, Ph.D.
Department of Geosciences

Bandana Kar, Ph.D., Outside Reader
Research Scientist, Oak Ridge National Laboratory

TABLE OF CONTENTS

LIST OF ILLUSTRATIONS

LIST OF TABLES

ACKNOWLEDGEMENTS

I would like to express my deepest humble gratitude to my advisor, Associate Prof. ZhiQiang Chen. I will forever be grateful to him for the opportunity, directions, motivation, knowledge, wisdom, and support he provided throughout my research during graduate studies. I also would like to thank Prof. Jejung Lee, Prof. Yong Zeng, Prof Ganesh Thiagarajan, Prof. John Kevern, Assistant Prof. FengPeng Sun, and Dr. Bandana Kar for valuable suggestions, availability, and feedback. I am blessed to have all my committee members and will always cherish their guidance.

I sincerely appreciate the excellent resources and experience that I got. I am thankful for all the support I got from the highly humble faculty and staff of the Department of Civil and Mechanical Engineering and Department of Geosciences at the University of Missouri-Kansas City. I also would like to convey my special thanks to Instructor Michael Kelly for his valuable time and knowledge on power transmission and distribution. I am also thankful to my excellent, cheerful, and supportive lab mates, including Shimin, Mostafa, and Max.

I want to take this opportunity to appreciate my parents Mrs. Manju Sharma and Mr. Huta Raj Sharma, for their love, sacrifice, nurture, care, constant support, and encouragement which shaped my life to where I am. I am also eternally thankful to my eldest sister Mrs. Pragya Sharma and brother-in-law Dr. Tara Nath Subedi, for guiding me throughout the academics path, for the motivational support and encouragement. Also, I am genuinely grateful to my sisters Pratigya and Prashamsha, brother Aashish, friends Sonafi and Sudha, and my in-laws for their endless support, love, and motivation. Finally, I put forward my humble appreciation to the love of my life, my dearest friend, classmate, lab mate, and confidant, my husband Sameer, who has been solid support in every aspect with his selflessness, love, and care.

A dedication to my family.

CHAPTER 1. INTRODUCTION

1.1. Problem Statement and Background

Communities continue to suffer from economic and financial loss due to many blackouts following extreme events such as hurricanes, lightning, storms, wildfires, ice storms, flooding and, Tornadoes. According to the Climate Central analysis, there is a 67% increase in significant power outages within the states from weather-related events since 2000. The hurricane alone is causing to lose $25 to $70 billion annually (Central, C. 2020). The Saffir-Simpson Hurricane Wind Scale is the most adopted hurricane category system. It categorizes hurricanes on a severity scale of Category 1-5 based on sustained wind speeds, as shown in Table 1.1. While every category of storms poses a significant risk to human and infrastructure assets, hurricanes of Category III and higher are considered to be "Major" hurricanes as they have the potential to cause extensive damage as for every increase in the category of hurricane, damage rises by a factor of four.

Table 1.1 Saffir-Simpson Hurricane Wind Scale

Category	1	2	3	4	5
Sustained Winds on miles per hour	74-95	96-110	111-129	130-156	157 or higher

Few such major outages based on Disaster type within the USA and affected customers due to blackout are summarized in Table 1.2. Hurricanes are responsible for the outages that affect a relatively massive number of customers.

Table 1.2 Summary of major outages since 2002

Date	Disaster Type	Place	Affected Customers
30th January, 2002	Ice storm	Kansas City, MO, USA	270,000
30th April, 2002	Lightening	Jacksonville, FL	355,000
22nd July, 2003	Windstorm	Memphis, Tennessee	300,000
18th September, 2003	Hurricane Isabel	East Coast USA	4 million
16th September 2004	Hurricane Ivan	Florida, Alabama, Louisiana, Mississippi, Georgia, Tennessee, North Carolina	1,700,935
13th August, 2004	Hurricane Charley	North Carolina, South Carolina, Florida	427,000
3rd September, 2004	Hurricane Frances	Florida	1,715,400
24th October, 2005	Hurricane Wilma	Florida	3,241000
24th September,2005	Hurricane Rita	Texas and Louisiana	1.2 million
29th August 2005	Hurricane Katrina	Louisiana, Mississippi, Alabama, Florida, Kentucky, and Tennessee	2.6 million
13th September 2008	Hurricane Ike	Galveston, Texas	2 million
11th December 2008	Snowfall	Southern Louisiana	10,000
11th December 2008	Ice Storm	Massachusetts and New Hampshire	1 million

12th December 2008	Ice Storm	Northeast US	1.5 million
27th January 2009	Ice Storm	Kentucky, Southern Indiana	769000
9th February 2010	Blizzard	Northeastern US	200,000
14th March 2010	Windstorm	Southwestern Connecticut, Westchester County of long Island, and New Jersey	260,000
15th July 2010	Windstorm	Oakland and Wayne counties of Michigan	76,000
25th July 2010	Windstorm	Washington, D.C.	250,000
27th April 2011	Tornado	Northern Alabama	675,000
11th July 2011	Windstorm	Chicago Area	850,000
27th August 2011	Hurricane Irene	Caribbean and East coast	6.69 million
29th October 2011	Snowstorm	East Coast	3.2 million
29th June 2012	Thunderstorms with Hurricane-force winds	Iowa to mid-Atlantic Coast	3.8 million
29th October 2012	Hurricane Sandy	Eastern United States	8 million
17th November 2015	Windstorm	Spokane County, Washington	161,000
1st, September 2016	Hurricane Hermine	Florida and Southern Georgia	350,000
8th March 2017	Windstorm	Michigan	1 million

20th September 2017	Hurricane Maria	Puerto Rico	3.4 million
10th September 2017	Hurricane Irma	Florida, Puerto Rico	6.7 million
25th August 2017	Hurricane Harvey	Southern Texas	347,000
14th September 2018	Hurricane Florence	East Coast of USA	1.7 million
10th October 2018	Hurricane Michael	South East of USA	1.7 million
28th August 2019	Hurricane Dorian	Florida. Georgia, South Carolina, North Carolina, Virginia	470,176
17th September 2019	Tropical Storm Imelda	Texas, Louisiana	75,000
4th August 2020	Hurricane Isaias	Eastern US	2 million
27th August 2020	Hurricane Laura	Louisiana, Texas, Arkansas	900,000
16th September 2020	Hurricane Sally	Gulf Coast and Alabama, Florida, Georgia	540,000

Amongst three components of Electricity Sector systems: Electricity Generation, Electricity Transmission, and Electricity Distribution, the level of risk to the electric distribution system due to the high-speed wind of hurricanes are high (Preston, B. L. et al. 2016). This is mainly because of the low reliability of the significant wooden distribution poles with service ages exceeding 40-60 years or more (Brown, R. E. and Willis, H. L. 2006) and

overhead distribution line discontinuity due to fallen trees and high wind. Another striding fact is that although the economic losses concentrate on densely populated urban areas, the outage frequencies and duration are prolonged in rural areas (Mukherjee, S. et al. 2018). The primary reasons behind this fact being: 1. Lack of enough resources; 2. Aging Infrastructural Component 3. Low Redundancy and; 4. Less attention from utility companies towards operation and maintenance frequency considering sparsely populated rural areas and economic justification. A brief discussion of these factors will be discussed in Chapter 3. Towards the risk status and management of the electric distribution, many practices such as assessing reliability indices and improving them are established; however, there is still space for improvements (Preston, B. L., Backhaus, S. N., Ewers, M., Phillips, J. A., Silva Monroy, C. A., Tarditi, A. G., Looney, J. P. and King, T. J., Jr. 2016).

From a system engineering perspective, reliability is the ability of a system to perform its functions under normal and extreme circumstances. Towards the reliability assessment of the electric distribution system, "Guide for Electric Distribution Reliability Indices," standard number P1366 (IEEE 2012) developed by the Institute of Electrical and Electronic Engineers (IEEE), has defined several reliability indices to measure the distribution system reliability. These reliability indices measure system performance by measuring outage duration, frequency outages, system availability, and response time. And, these reliability indices are widely used by Utilities Company to compare their performance over time and other companies. The few most common distribution indices include the System Average Interruption Duration Index (SAIDI), Customer Average Interruption Duration Index (CAIDI), System Average Interruption Frequency Index (SAIFI), Momentary Average Interruption Frequency Index (MAIFI), Customer Average Frequency Index (CAIFI), Customers

Interrupted per Interruption index (CIII), and the Average Service Availability Index (ASAI). The concept of reliability is well known, and numerous power system reliability studies have been developed in the last decades and have been utilized. However, with increased extreme natural hazards brought by climate change and inevitable economic and financial loss, the research regime has been shifted to assess and maintain resilience and is not limited to reliability.

Resilience in the context of a civil infrastructural system is the ability of a system to be fully functional within a short period after losing the system's functionality due to extreme circumstances such that minimal loss is ensured. The higher reliability and maintaining the highest possible functionality during extreme events is one of the properties of the resilient system, followed by enough resourcefulness, redundancy, and rapid recovery. With this shift towards assessing the resilience of an infrastructural system, several mathematical frameworks are developed to evaluate the resilience of electricity distribution systems, and numerous researchers propose resilience enhancement techniques. However, a widely accepted framework is yet to define. Additionally, the author of this dissertation research found a critical gap of inapplicability of this resilience assessment framework of the electrical distribution system in the rural setting, i.e., the inclusion of geospatial sparseness and resourcefulness into the framework. Furthermore, the author argues if based on such measurements, objective decisions of acceptance of as such measurement and/or prioritization to strengthen the parameters are not ready to make. Two ingrained drawbacks of such measurements are lack of theoretical basis in 1. discriminating relatively that how a parametric infrastructure system is more resilient than a different one or the same one subject to some changed conditions and, 2.

answering which input parameter is most influential towards the resilience output and requires more attention and consideration.

1.2. Goals and Objectives of the Study

The goals of this research are threefold first is to develop a probabilistic and structural mechanics-based framework for quantifying the resilience of power distribution systems in the rural area setting. The second is to perform sensitivity analysis to see the robustness of the developed framework and do the dependence modeling to find the most dependent parameter and tail dependence of each parameter using copula. Finally, the third is to develop fully theoretic probabilistic resilience distance measures that relatively answer how close is measured resilience when compared to targeted resilience of the same system or similar other systems. Hence towards achieving the desired framework following objectives are introduced:

- Development of mechanics-based fragility modeling for the capacity assessment of power distribution components, coupled wooden pole and conductors.
- Probabilistic assessment of the system performance including probabilistic loss measurement in terms of the number of customers without power.
- Analytical formulation and validation of a set of resilience measures considering disaster-response resourcefulness and geospatial sparseness of rural areas.
- The inclusion of various recovery patterns based on resources available and depicts the change in resilience.
- Perform the nonparametric sensitivity analysis to check the robustness of the proposed framework

- Find the correlation and tail dependence of each input parameter with measured resilience using nonparametric copula density.
- Conceptualize the use of terms *Measures*, *Metrics and, Statistical Distances* towards the resilience assessment framework
- Using *Statistical Distance* as Resilience Distance on discriminating relatively that how a parametric infrastructure system is more resilient than a different one or the same one subject to some changed conditions.
- Hypothesize the similarity of targeted and measured resilience distribution and perform the non-parametric test to accept the hypothesis.

1.3. Organization of the Dissertation

The remainder of this dissertation is organized as follows: Chapter 2 presents state of art about the definition, properties and, dimensions of Resilience; the brief review of available assessment frameworks towards community resilience and electricity distribution system. The study will also include the basic terminology used to define tropical cyclones and anthropogenic influence for their current state and future projection. Chapter 3 consists of the developed probabilistic and analytical measurement framework for assessing the resilience of linear power-distribution systems affected by high-speed hurricane wind. The first four sets of objectives are achieved in this chapter. Chapter 4 includes the adopted sensitivity analysis and dependence modeling. Chapter 5 includes the methodology to achieve the last three objectives of this study. The key conclusions and final remarks of the study are presented in Chapter 6.

CHAPTER 2. STATE OF ART

2.1. Resilience: Definition, Properties, and Dimensions

Originally the concept of *Resilience* was introduced by Holling in 1973 in the field of ecology stating resilience as a measure of the ability of the ecological system to absorb change and disturbance while keeping the system's persistence on the relationship between the variables of the system. As such the resilience is mathematics-based and model-oriented (Holling, C. S. 1973). It was only after the late 1980s, the concept started in the analysis of human-environmental interactions. In 1999, a philosophy of reducing losses from natural hazards and disasters by the development of disaster-resistant communities was sought by Mileti (Mileti, D. 1999). Afterward in 2002, Multidisciplinary Center for Earthquake Engineering Research (MCEER) task group identified the critical need to establish earthquake-resilient communities as the pressing challenge. Following this task, Bruneau et al. (2003) developed a conceptual framework of resilience and proposed eleven aspects of resilience as shown in Figure 2.1 and defined the seismic resilience of communities as "the ability of organizations/communities to mitigate hazards, contain/absorb the effects during the disaster and carry out recovery activities rapidly to ensure minimize social disruption and economic losses" (Bruneau, M. et al. 2003). In the civil infrastructure engineering community, this definition and eleven aspects of resilience become the most widely adopted definition and the defined aspects of resilience left a significant impact.

Four properties of the Resilience that apply to both social and physical systems include:

- "Robustness: strength, or the ability of elements, systems, and other units of analysis to withstand a given level of stress or demand without suffering degradation or loss of function.

- Redundancy: the extent to which elements, systems, or other units of analysis exist that are substitutable, i.e., capable of satisfying functional requirements in the event of a disruption, degradation, or loss of functionality.
- Resourcefulness: the capacity to identify problems, establish priorities, and mobilize resources when conditions exist that threaten to disrupt some element, system, or another unit of analysis; resourcefulness can be further conceptualized as consisting of the ability to apply material (i.e., monetary, physical, technological, and informational) and human resources to meet established priorities and achieve goals.
- Rapidity: the capacity to meet priorities and achieve goals promptly to contain losses and avoid future disruption."

The elven aspects also encompass four interrelated dimensions: "The *technical* dimension refers to the ability of physical systems (including components, their interconnections, and interactions) to perform to acceptable/desired levels when subject to earthquake forces. The *organizational* dimension refers to the capacity of organizations that manage critical facilities and have the responsibility for carrying out critical disaster-related functions to make decisions and take actions that contribute to achieving the properties of resilience outlined above, that is, that help to achieve greater robustness, redundancy, resourcefulness, and rapidity. The *social* dimension of resilience consists of measures specifically designed to lessen the extent to which earthquake-stricken communities and governmental jurisdictions suffer negative consequences due to the loss of critical services as a result of earthquakes. The *economic* dimension of resilience refers to the capacity to reduce both direct and indirect economic losses resulting from earthquakes. Hence the resilient system

shows 1. Higher reliability i.e. reduced failure probabilities; 2. Lower Consequences from failures in terms of loss of lives, damage and, negative economic and social consequences; 3. Quick restoration i.e. reduced time to respond and recover a specific system or set of systems to their normal level of performance.

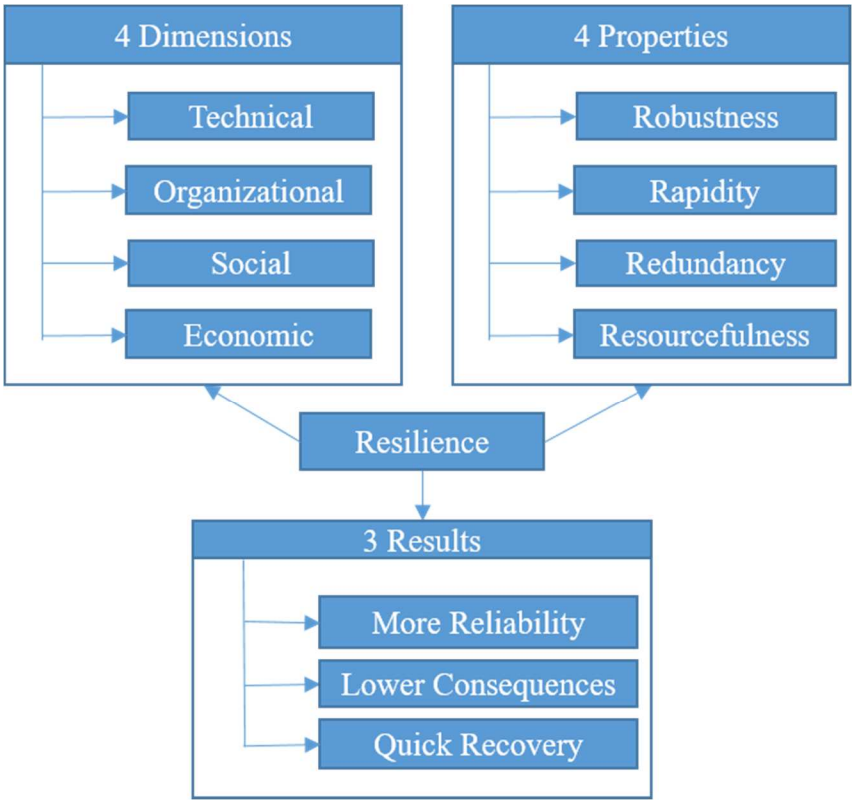

Figure 2.1. Eleven Aspects of Resilience proposed by Bruneau et al. (2003)

After 2003, several other definitions were also proposed for a different infrastructural system such as (Bruneau, M. and Reinhorn, A. 2007; Miles, S. B. and Chang, S. E. 2006) defined and measured resilience applying to lifelines and to other distributed systems. The comprehensive list of the definition of resilience can be found in Zhou et al. (2010) (Zhou, H. et al. 2010).

2.2 Community Resilience Assessment

Communities are viewed as the totality of population living within a defined geographical space such as neighborhood, census tract, city, county, state, or country sharing the interactions between the social/economic system, built environment, and natural processes (Cutter, S. L. et al. 2008). Thus within these geographically defined spaces, there could be many different communities with different levels of resilience. Measuring the resilience of communities thus given such interrelated dimensions is complex and challenging. As such the Cutter et al., (2008) developed a place-based conceptual DROP model which starts from the antecedent conditions that should include the inherent vulnerability and inherent resilience, characterized by the six dimensions and corresponding candidate variables as shown in Table 2.1. These antecedent conditions interact with the hazard event producing the immediate effects. This effect can either be attenuated or amplified depending on coping responses. The cumulative effect of the antecedent conditions, event characteristics, and coping responses is the disaster impact. The degree of recovery is considered high a hence higher resilience if this disaster impact is well absorbed by the community and low if the absorptive capacity exceeded and follows the adaptive techniques i.e. improvisation and learning.

Table 2.1. Community resilience indicators summarized by Cutter et al., (2008) (Cutter, S. L., Barnes, L., Berry, M., Burton, C., Evans, E., Tate, E. and Webb, J. 2008).

Dimension	Candidate Variables
Ecological	Wetlands acreage and loss
	Erosion rates
	% Impervious surface
	Biodiversity

	# Coastal defense structure
Social	Demographics (age, race, class, gender occupation)
	Social networks and social embeddedness
	Community values-cohesion
	Faith-based Organizations
Economic	Employment
	Value of Property
	Wealth generation
	Municipal finance/revenues
Institutional	Participation in hazard reduction programs (NFIP, Storm Ready)
	Hazard mitigation plans
	Emergency services
	Zoning and Building Standards
	Emergency response plans
	Interoperable communications
	Continuity of operational plans
Infrastructure	Lifelines and critical infrastructure
	Transportation network
	Residential housing stock and age
	Commercial and manufacturing establishments
Community Competence	Local understanding of risk
	Counseling Services
	Absence of psychopathologies (alcohol, drug, spousal abuse)

	Health and wellness (low rates of mental illness, stress-related outcomes)
	Quality of life (high satisfaction)

Similarly, Cimellaro et al. (2016) developed a PEOPLES framework, a toolkit identifying 7 dimensions (population and demographics, environmental and ecosystem, organized governmental services, physical infrastructures, lifestyle and community competence, economic development, and socio-cultural capital) characterized by the corresponding performance metric to calculate the community resilience at different temporal and spatial scale (Renschler, C. et al. 2010). This PEOPLES framework is claimed to have favorable characteristics based on comprehensiveness, utility, impacts assessed, techniques used, and critical assessment according to the review done by (NIST 2016). Several other toolkits, scorecard, index, models that are proposed to measure community resilience are reviewed by (Johansen, C. et al. 2017; Sharifi, A. 2016).

2.3. Resilience Quantification

Especially within the civil infrastructure, the notion of resilience measurement has been classically illustrated as a piece-wise function model with the phases of performance or functionality degrading, dropping, and recovering [e.g. (Bilal, A., M. 2015; Cimellaro, G. P. et al. 2010)]. As shown in Figure 2.2, the pre-event performance is assumed to be a constant at a perfect (100%) functionality level with slow degradation by developing aging-induced loss. After, incidentally due to minor or moderate-level hazards, functionality drop either

abruptly (brittle), with ductility, or gracefully and then recovery efforts start. After recovery, the functionality may or may not matches prior functionality prior incident.

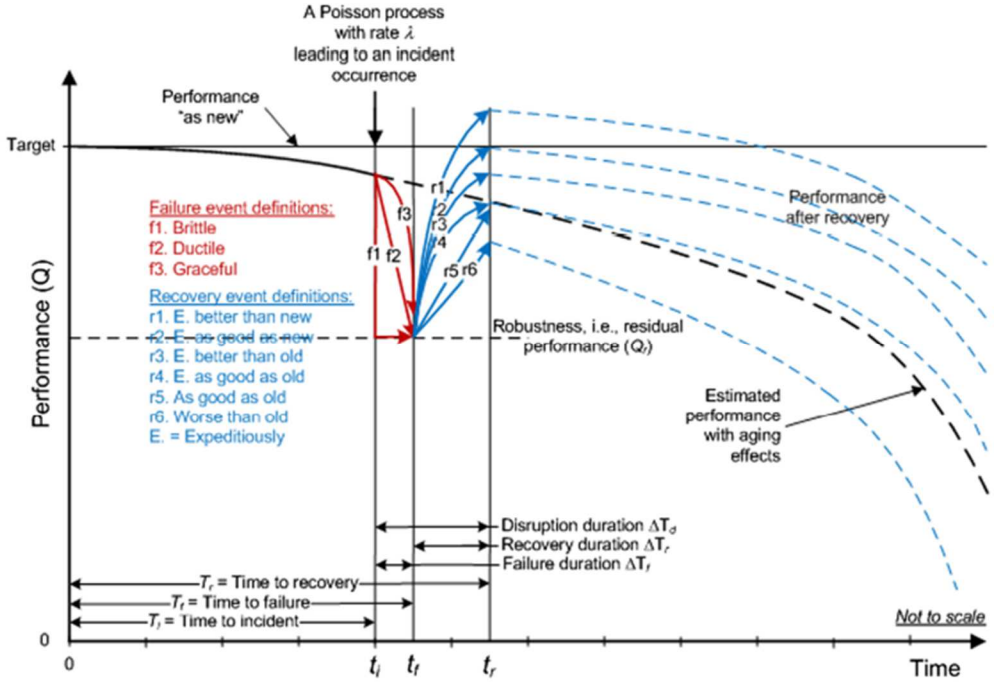

Figure 2.2 Resilience Quantification approach defined by Bilal (2015)

Thus, mathematically, resilience is measured as the normalized area underneath the system recovery function as given in Eq. 2.1 within the interval of the functionality-drop time and the defined control period ($T = t_h - t_i$), (for a single event) t_i is a time of incidence and t_h is the time of specified control period. This mathematical definition of resilience has thus been adopted by several researchers such as (Bilal, A., M. 2015; Cimellaro, G. P. and Piqué, M. 2016; Cimellaro, G. P., Reinhorn, A. M. and Bruneau, M. 2010; Cimellaro, G. P. et al. 2010; Decò, A. et al. 2013; Ouyang, M. and Dueñas-Osorio, L. 2014; Ouyang, M. et al. 2012) in their study. .

$$R = \frac{\int_{t_i}^{t_h} Q(t)dt}{Q(100)*T} \text{ (Single event);} \qquad R = \frac{\int_{0}^{t_h} Q(t)dt}{Q(100)*t_h} \text{ (Multiple events)}$$

(2.1)

The major challenge is to mathematically model and quantify the piece-wise function of the functionality (Bruneau, M. and Reinhorn, A. M. 2019). Table 2.2 summarizes the number of ways for how the functionality can be defined depending upon the services of the system being provided adopted from (Bruneau, M. and Reinhorn, A. M. 2019).

Table 2.2 Examples of functionality depending on system considered (Bruneau, M. and Reinhorn, A. M. 2019)

System	Functionality
Physical Civil Infrastructure	The ratio of residual strength and strength demand
Physical, Economic and Environmental dimensions of resilience	The ratio of available space to original space
Infrastructure networks; health of a population; organizational networks	The ratio of number of customers served to the total number of customer
Public transportation; Emergency Room of the hospital;	The ratio of waiting time in an emergency condition to normal condition
Acute care facilities	Number of patients provided treatment per day

These functionality measures, though quantify true global societal measure for the resilience assessment, obtaining quantifiable data is rather tough and linking functionality with a performance of engineered infrastructure is even more challenging in the pre-event scenario. Some researchers, however, quantified the resilience of infrastructures as a function of time such as Henry& Emmanuel Ramirez-Marquez (2012) calculates the ratio of recovery at

time t to loss suffered by the system at some previous point in time and inferred that sooner the ratio is 1 more resilient the system is (Henry, D. and Emmanuel Ramirez-Marquez, J. 2012). Similarly, Hashimoto et al (1982) calculated the resilience as the inverse of the time required for the system to be fully recovered (Hashimoto, T. et al. 1982) whereas (Mahzarnia, M. et al. 2020) calculated the resilience as the inverse of the cost imposed on the system after it losses the functionality.

2.4. Resilience Assessment for Electricity Distribution Systems due to Extreme Events

In this review, the literature that appeared in 2010 and onwards that developed framework applicable to quantify electricity distribution system are briefly studied.

2.4.1. Literature Review Criteria

Table 2.3 summarizes the reviewed study based on the review criteria defined herein:

- Network Configuration: The electricity distribution network can either be *Radial* or *Network*. A radial system is arranged like a tree where each customer has only one source of supply whereas a network system has multiple sources of supply operating in parallel.
- Hurricane Hazard Modelling: Hurricane is Low Probability High Impact (LPHI) impact and two approaches are found to be followed for modeling Hurricane. First, is the Probabilistic Based Approach (PBA) where the probability density function of wind speed is considered such that lower wind speed has a higher chance of occurrence. Hence, if PBA is used the occurrence of high wind is very unlikely and therefore, the probability of failure of the component becomes very small. The second is Scenario-Based Approach

(SBA) where specific wind speed or hurricane category is considered and the probability of failure of a component is investigated.

- Fragility Modeling of Component: The main component of the Electricity Distribution system are Wooden/Steel Pole (W/SP), Distributing Lines (DL), Substation (S), Transformer (T) and, Switches (Sw). The review will characterize if the fragility modeling of any or all of these components is included in the proposed framework to assess resilience.
- Aging: This study review if the aging of the component is considered in the fragility modeling of a component.
- Uncertainty of Disruption scenarios: Following the hazard, several failure events with different outcome and loss is possible. It is integral that the framework considers this uncertainty.
- Cascading effect: Failure of one component may result in the functionality disruption of consequent loads especially in the radial network and cascading effect should be incorporated in the model.
- Redundancy: This study review if the framework includes the network reconfiguration by the use of sectionalizing-switch, tie-switch, or Distributed Generator (DG) to ensure redundancy while modeling the functionality loss.
- Resourcefulness: Study reviews if the framework considers resources available while modeling the restoration time.
- Time to Response: Immediate after the hazard, the system requires time to comprehend the impact before beginning the recovery of loss. Thus it is crucial to incorporate time to respond while assessing resilience.

- Inclusion of Resilience Enhanced Technique (RET) (such as adding/ including DG and sectionalizing-switch, hardening the components) with (w) or without (wo) Cost-Benefit Analysis CBA)
- Resilience Calculation: As mentioned in 2.3 if the resilience is calculated using Area method (AM) i.e. similar to Equation 2.1 or Inverse of Time to recovery (IoT) or Inverse of Cost (IoC).

2.4.2. Overview of the Literature

Several efforts are found that focus on either resilience/risk assessment, performance assessment, or resilience enhancement of the power system as reviewed in (Chi, Y. et al. 2018; Gasser, P. et al. 2019) subject to extreme weather or terrorist attacks or malfunctions. However, the author of this study finds relatively few studies as summarized in Table 2.3 that focus primarily on resilience assessment framework on electricity distribution due to extreme weather such as Hurricane or Typhoon. The methodologies of these studies are briefly summarized herein:

Mahzarnia et al. 2020 adopted the definition of resilience as the inverse of the cost to any system imposed by an event and proposed a snapshot resilience assessment to evaluate the power system resilience against a single intensity of a hurricane (Mahzarnia, M., Parsa Moghaddam, M., Siano, P. and Haghifam, M.-R. 2020). Amongst all the components of the power system, the vulnerability of only the transmission line is considered, and for which the corresponding fragility curve (probability of failure of transmission line vs speed of wind) is adopted. Monte-Carlo Simulation (MCS) technique followed by a scenario reduction algorithm is adopted to generate the number of scenarios of transmission line failure and the consecutive probability of each failure scenario. The optimization problem is then formulated

to solve the Conditional Value at Risk (CVaR) of Cost of Energy not supplied (CENS) considering all the failure scenarios, corresponding load shedding on the buses at each hour for 24 hours, weighting parameter (parameter for user to define risk [0,1]) and confidence level. The CVaR of CENS is to be minimized such that the critical load (Grade 1) defined in this paper has less load shedding. Finally, the snapshot resilience of the power system is the inverse of value CVaR of CENS as showed in Eq. 2.2

$$\text{Power System Snapshot Resilience } \alpha \frac{1}{CVaR\ of\ CENS} \tag{2.2}$$

This snapshot resilience assessment is done over a range of intensities of the event to capture the trend of the change of the measured snapshot resilience values. Lower the change of these snapshot resilience measures higher the comprehensive resilience of the overall system is considered. Towards that end, a resilience graph is introduced whose smoothness is proposed as an index for a comprehensive assessment of power system resilience. The transmission line switching approach is further added to the optimization problem as a resilience improvement method.

The research done by (Darestani, Y. M. and Shafieezadeh, A. 2019) first incorporated the fragility modeling of wooden poles developed by (Mohammadi Darestani, Y. and Shafieezadeh, A. 2019). This fragility modeling is followed by the performance model of the radial network of the distribution system of the power supply to assess the resilience of the power supply. This performance model uses the MCS technique and Dichotomized Gaussian Method (DGM) to generate the correlated failure or survival events for the wooden pole followed by the network connectivity analysis to get the outage nodes and number of affected customers. For the restoration model, the Normal distribution with an average of 5 hours and a standard deviation of 2.5 hours to repair a wooden pole and Normal distribution with an

average of 4 hours and a standard deviation of 2 hours to repair a conductor adapted from (Ouyang, M. and Dueñas-Osorio, L. 2014) is utilized. Finally the concept of the area under the functionality curve over the period proposed by (Cimellaro, G. P., Reinhorn, A. M. and Bruneau, M. 2010) as shown in Eq. 2.1 to calculate the resilience.

The study, (Bazargani, N. T. and Bathaee, S. M. T. 2018) adopted the amount of active power as the functionality and calculated resilience as the expected value of probabilistic resilience $E[R]$ measured for a considered number of hurricanes (NH). The mathematical concept of resilience proposed in (Cimellaro, G. P., Reinhorn, A. M. and Bruneau, M. 2010) is adopted to calculate the resilience of the system for each hurricane such that the resilience is the ratio of the area between the functionality curve available active power function and time ($P_{avial}(Nh, Pd_k(t), P_{PV}(t))$) after Nh hurricane and area between the total amount of active power required ($P_{reql}(Pd_k(t), P_{PV}(t))$) to serve all the loads types (k = residential (*res*), commercial (*com*) and, critical (*cri*)) within study period T as shown in Eq. 2.3.

$$E[R] = \sum_{Nh-1}^{NH} P(Nh) \,.\, E\left[\frac{\int_0^T P_{avail}(Nh, Pd_k(t), P_{pV}(t)).dt}{\int_0^T P_{req}(\, Pd_k(t), P_{pV}(t)).dt}\right] \tag{2.3}$$

The active power, however, is a function of active power consumption Pd_k for each consumer load k and Photovoltaic (P_{pV}) system generation and the uncertainties of these input variables are handled using Point Estimation Method (PEM) to lower the computational burden. For the load scenario generated from PEM, followed by the generation of characteristics (type, start time, wind speed) of Nh^{th} = [1,5] hurricane event, the probability of failure of wooden pole and distribution line is calculated using the fragility curve developed by (Panteli, M. et al. 2017). The pole (node) and line (edges) is considered failed if generated uniform random number (U(0,1)) is less than the probability of failure. Subsequently, repair time to pole and conductor are estimated using the approach as adopted in (Ouyang, M. and

Dueñas-Osorio, L. 2014). The graph model is hence utilized to model the system response and calculate the system resilience.

(Bhat, R. et al. 2018) utilized the SBA for the hurricane modeling, the fragility model for the Distribution line and wooden pole as proposed in the (Onyewuchi, U. P. et al. 2015) followed by the restoration model adapted from (Ouyang, M. and Dueñas-Osorio, L. 2014) and Eq. 2.1 for the resilience quantification to the radial network of the electricity distribution. The novelty of this study is the use of a connectivity model to quantify the network performance i.e. to find the number of failed poles and consequently outage nodes followed by the network reconfiguration to minimize the outages.

(Poudel, S. et al. 2020) defined resilience using risk-based quantitative measures which are Value at Risk ($V_\alpha R_\alpha$) that measures the maximum probable loss of the system during an event and Conditional Value at Risk ($CV_\alpha R_\alpha$) that measures the expected loss due to the HILP events i.e. beyond a specified risk threshold α. The $V_\alpha R_\alpha$ and $CV_\alpha R_\alpha$ are calculated using the proposed probability density function of the system performance loss which in turn is the function of energy not served aftermath of an event until recovery starts and, total time of an event and time required for the damage assessment (i.e. response time).

In (Mensah, A. F. and Dueñas-Osorio, L. 2016), authors first use SBA approach to model the hurricane hazard on ArcGIS to generate spatially varying winds with specific gust speeds for locations at 1-km^2 block level within the entire electric grid considered. The probability of failure of components (transmission line, distribution poles and, distribution line) on these grids due to this speed is obtained from the fragility curve of each component adapted from (Technology, Q. 2008; Technology, Q. 2009). The numbers of damaged components are then determined by comparing the uniformly distributed random variable

realizations and their probability of failure. Then for the transmission system response, Bayesian Network-based model is developed to evaluate the outage probability of substation as a function of failure probability of transmission line and failure events. These outage probabilities then provide functional constraints to obtain the outages on the distribution nodes i.e., 1-km^2 block. For the distribution system response, distribution systems are represented as minimum spanning trees, and the number of poles along a distribution line is determined by the ratio of line length to average adjacent span length between two poles. For the restoration model, restoration time for each component is considered, resource mobilization is modeled as the dynamic function, and repair sequence is prioritized for the critical loads first. Finally, the resilience is quantified as a normalized area under a time-dependent restoration curve.

The study (Nateghi, R. 2018) proposed an approach of supervised machine learning to approximate the resilience of the power distribution system. The proposed model utilizes the system's inoperability data (outage duration, outage counts and, customers affected), hurricane hazards data (wind speed and wind duration), the topology of the system data (tree trimming., protective devices, miles of overhead lines), topographical data (Aspect Ratio, Elevation, Slope, Mean annual precipitation, Standardized precipitation index, Compound topographic index, soil moisture, soil type) and, landcover data provided by an electric utility company as the independent variables. These variables are used to train the tree-based algorithms to approximate the response surface and dependency of individual variables with these response variables. The multivariate response variables include 1. The cumulative duration of outages, 2. The number of customer meters without power, and 3. The number of outages.

(Sun, S. et al. 2019) modeled the typhoon disaster using the key parameters such as annual occurrences, minimum distance from the study point, center pressure difference,

moving speed and, moving azimuth. The probability distribution of these five key parameters is built based on the historical data to characterize the intensity and probability of typhoons. Batts's typhoon model is then selected to simulate the wind field and characterize the feature of typhoons. The fault trip rate of distribution lines is characterized using supervised machine learning wherein the characteristics of typhoon modeled from Batts and key parameters are used as the predictor variables. This fault trip rate is used on a piecewise exponential function to give the outage rate function of simulated time. The random outage time of the distribution line is thus determined according to the inverse function method applied to the outage rate function. For each fault of the distribution line, load-loss and the actual total power supply of the bus in the distribution system are calculated. The repair time for the damaged distribution line is assumed to obey the exponential distribution. Finally, using all these parameters three resilience indices are calculated: 1. System Maximum Loss of load ratio index. 2. System total restoration duration index and System Annual Loos of Energy Index.

In (Gautam, P. et al. 2021), authors defined the expected probability of interruption per system active demand load, the average outage duration per system active demand load and, the average energy not served for the overall system due to supply interruption as the resilience metrics to assess the resilience for the radial power distribution system. The severity-based wind event is modeled based on the historical data of the considered region and the fragility of the wooden pole due to wind speed is adopted from (Ouyang, M. and Dueñas-Osorio, L. 2014). The failure probability of the line section is then the function of the failure probability of the pole. The status of the line section is evaluated by comparing the failure probability with random realizations. Graph theory is then utilized to find if the affected segments can be islanded to microgrid mode with distributed energy resources, and if the faulted section can be

islanded using sectionalizer for the repair thus giving the total outage duration and energy not supplied because of each line segments interruptions. The optimization is included for each islanded microgrids including renewable energy input, load demand and the energy limitation of the energy storage system.

Few notable other efforts that are found focused on system performance assessment for either or both power-delivery (transmission or distribution) infrastructure subject to extreme weather or terrorist attacks are: Panteli and Mancarella used sequential Monte-Carlo simulation to model weather-related fragility models for transmission towers and further assessed the resilience of power systems (Panteli, M. and Mancarella, P. 2017). This fragility model was used by Espinoza et al. (2016) as one of the phases to access the resilience of transmission network calculating the expected energy-not-supplied (EENS) resilience index and the energy index of reliability (EIU) when subjected to extreme events and flooding (Espinoza, S. et al. 2016; Panteli, M., Pickering, C., Wilkinson, S., Dawson, R. and Mancarella, P. 2017). Some studies identified the most critical line in a transmission network that could cause the maximum outage and proposed to harden the same transmission line for improved resilience (Bier, V. M. et al. 2007; Yao, Y. et al. 2007). A fragility study of a three-span pole-wire system of power distribution network subjected to strong wind was conducted by (Yuan, H. et al. 2018) for determining the hardening of poles and the inspection priority. (Kwasinski, A. 2016) proposed metrics for resilience assessment and verified the interrelation between resilience, resistance, and brittleness for power grids. Historical data of power outages were explored by several studies to give the estimated power outage during extreme events. For instance, (Guikema, S., D. and Goffelt, J., P. 2008) assessed the reliability of power-delivery systems using regression analysis that was useful for under-dispersed and over-dispersed outages. (Liu, H. et al. 2005)

used a negative binomial regression model based on the Geographic Information System (GIS) database of outages to predict the number of outages likely to occur in each square kilometer grid cell of the specified region. (Zhu, D. et al. 2007) created empirical models using historical outages data and used those models to predict outages in real-time storms. Some researchers, however, emphasized the concept of microgrids and resource allocation for enhancing the resilience of distribution networks (Chen, C. et al. 2016; Gao, H. et al. 2016; Li, J. et al. 2014).

Table 2.3 Summary of the reviewed literature towards power distribution system

Authors	Type of Network	Hazard Modeling	Fragility Modeling	Aging	Scenarios of Disruptions	Cascading Damage	Redundancy	Resourcefulness	Time to response	RET W/O C/B Analysis	Resilience Calculation
(Mahzarnia, M., Parsa Moghaddam, M., Siano, P. and Haghifam, M.-R. 2020)	Grid	SBA	TL	No	Yes	Yes	Yes	No	No	Yes-wo CBA	IoC
(Darestani, Y. M. and Shafieezadeh, A. 2019)	Radial	SBA	WP	No	Yes	Yes	No	No	No	No	AM

(Bazargani, N. T. and Bathaee, S. M. T. 2018)	Grid	PBA	DL and WP	No	Yes	Yes	Yes	No	No	Yes-wo CB	AM
(Bhat, R., Darestani, Y. M., Shafieezadeh, A., Meliopoulos, A. P. and DesRoches, R. 2018)	Radial	SBA	DP and DL	Yes	Yes	Yes	Yes	Yes	No	No	AM
(Poudel, S., Dubey, A. and Bose, A. 2020)	Radial	SBA	N/A	NA	Yes	Yes	Yes	No	Yes	Yes-wo CBA	AM
(Mensah, A. F. and Dueñas-Osorio, L. 2016)	Grid	SBA	TL, WP and DL	No	Yes	Yes	No	Yes	No	No	AM
(Sun, S., Lyu, Q., Li, G., Lin, Y., Bie, Z. and Wen, W. 2019)	Radial	SBA	No	No	Yes	No	No	No	No	No	N/A

(Gautam, P., Piya, P. and Karki, R. 2021)	Radial	SBA	DP	No	Yes	Yes	No	No	Yes	No	N/A

2.4.3 Literature Review Summary and Research Gaps

To this end, several research gaps are recognized considering the efforts reviewed previously. First, several frameworks do not systematically account for system robustness, redundancy, and resourcefulness collectively for power-delivery systems. If redundancy and robustness are well defined, then the author realizes the framework lacks the inclusion of resourcefulness towards response and recovery of the impaired system or lacks the inclusion of response time at all such that the model seems to have inadequate consideration of interdependency among auxiliaries. Second, few proposed frameworks are seen as highly data-driven, and, it is very unlikely to obtain accurate data in all regions and cases. Third, regardless of rural or urban power systems, empirical functions are often used without a mechanical (or first-principle) basis when computing the system reliability or vulnerability. Fourth, rural power-delivery systems are rarely treated in any previous research efforts in the area of quantitative resilience assessment. Fifth and lastly, the author argues if based on these proposed framework measurements, objective decisions of acceptance or prioritization to strengthen the parameters are not ready to make. Two ingrained drawbacks of such measurements are lack of theoretical basis in 1. discriminating relatively that how a parametric infrastructure system is more resilient than a different one or the same one subject to some changed conditions and, 2. answering which input parameter is most influential towards the resilience output and requires more attention and consideration.

2.5 Tropical Cyclones

Tropical Cyclones is a rotating, organized system of clouds and a spiral arrangement of a thunderstorm that originates over tropical or subtropical waters and has closed, low-level atmospheric circulation that produces heavy rain or squalls. The weakest tropical cyclones are called tropical depressions. If this depression intensifies and maximum sustained winds reach 39 MPH then a tropical cyclone is now termed a tropical storm. Similarly, if maximum sustained winds reach 74 MPH or higher, it is then termed as a hurricane within the geographical area of North Atlantic, central North Pacific, and eastern North Pacific. The same disturbance is termed a Typhoon in Northwest Pacific. Meanwhile, in the South Pacific and the Indian Ocean, the generic term tropical cyclone is used.

The combination of pre-existing weather disturbance like large-scale cyclonic vorticity, conditional convective instability, low vertical wind shear with warm tropical cyclones, moisture and relatively light winds cause the tropical cyclones. And, the potential hazards include powerful winds, heavy rainfall, storm surges, coastal and inland flooding, rip currents, tornadoes, and landslides.

2.5.1 Definition and Annotations of the Terminology used when studying Tropical Cyclones:

Power dissipation Index (PDI): measures the accumulated cube of maximum wind speeds across all TCs and storm lifetimes

Potential Intensity (PI): a theoretical estimate of the maximum intensity a TC can attain for a given thermodynamic environment

Atlantic meridional overturning circulation (AMOC): the northward flow of warm, salty water in the upper layers of the Atlantic, and a southward flow of colder water in the deep Atlantic

Atlantic Multi-decadal Oscillation (AMO): is a North Atlantic basin-wide sea surface temperature fluctuation on multi-decadal time series

El Niño–Southern Oscillation (ENSO): are periodic departures from expected sea surface temperatures (SSTs) in the equatorial Pacific Ocean. These warmer or cooler than normal ocean temperatures can affect weather patterns around the world by influencing high and low-pressure systems, winds, and precipitation

Pacific decadal oscillation: The Pacific Decadal Oscillation (PDO) is a pattern of Pacific climate variability similar to ENSO in character, but which varies over a much longer time scale. The PDO can remain in the same phase for 20 to 30 years, while ENSO cycles typically only last 6 to 18 months

Interdecadal Pacific Oscillation (IPO): It is a phenomenon similar to PDO but occurs in the wider area of the pacific. While the PDO occurs in the mid-latitudes of the Pacific Ocean in the northern hemisphere, the IPO stretches from the southern hemisphere into the northern hemisphere. It has two phases: Positive phases of the IPO are characterized by a warmer than average tropical Pacific and cooler than average northern Pacific. Negative phases are characterized by an inversion of this pattern, with cool tropics and warm northern regions.

Hadley Circulation (HC): It is a constant, low latitude global scale tropical atmospheric circulation in which air rises near the Equator, flowing poleward at a height of 10 to 15 kilometers above the earth's surface, descending in the subtropics, and then returning equatorward near the surface.

Vertical mixing**:** In the atmosphere or oceans, it is an upward and downward movement of air or water that occurs as a result of the temperature gradients (temperature differences between layers of the fluid). In the atmosphere, vertical mixing is sometimes discernible as a form of atmospheric turbulence.

Steering Flow: A basic flow that exerts a strong influence upon the direction of movement of disturbances embedded in it. In the case of tropical cyclones, the steering flow is largely responsible for their actual track.

Coupled Model Intercomparison Project (CMIP): The project is to better understand past, present, and future climate changes arising from natural, unforced variability or in response to changes in radiative forcing in a multi-model context. This understanding includes assessments of model performance during the historical period and quantifications of the causes of the spread in future projections. Idealized experiments are also used to increase understanding of the model responses.

2.5.2 Observed Changes on the Trends of Tropical Cyclones:

a. Poleward migration of Latitude of Lifetime Maximum Intensity(LMI)

Several studies studied the latitudinal migration of LMI of TC and concluded the poleward migration of LMI (Choi, J.-W. et al. 2016; He, H. et al. 2015; Kossin, J. 2018; Kossin, J. P. et al. 2014; Oey, L.-Y. and Chou, S. 2016; Tennille, S. A. and Ellis, K. N. 2017). This poleward migration is particularly well observed and robust in the Western North Pacific Ocean (WNP). Observed changes because of this shift which also proves the latitudinal poleward migration of LMI includes the decreased TC exposure in the region of the Philippine and South China Seas, including the Marianas, the Philippines, Vietnam, and southern China, and increased exposure in the region of the East China Sea, including Japan and its the Ryukyu Islands, the Korea

Peninsula, and parts of eastern China (Kossin, J. P. et al. 2016; Park, D.-S. R. et al. 2014). Liang et al. (2017) observed 64-year rainfall around Taiwan and showed that the rainfall trends are significantly rising west and north of the island but are insignificant east and southeast in recent decades for TCs to veer more poleward (Liang, A. et al. 2017). Poleward migration of latitude of LMI is also verified by the study using a unique tree-ring approach that searched for the detection of canopy disturbances rate within the region of coastal northeast Asia(Altman, J. et al. 2018).

Several causes are speculated and studied that could result from this shift and most of the study concluded because of the weakening of the steering flow consistent with the expansion of the tropics and decadal change in tropical Indo-Pacific sea surface temperature which in turn is due to the climate change(Colbert, A. J. et al. 2013; He, H., Yang, J., Gong, D., Mao, R., Wang, Y. and Gao, M. 2015; Liang, A., Oey, L., Huang, S. and Chou, S. 2017; Oey, L.-Y. and Chou, S. 2016; Zhan, R. and Wang, Y. 2017). Wang and Wu (2019) study, however, concluded that the temporal change in the environmental parameters (sea surface temperature, outflow temperature, vertical wind shear, and ocean mixed layer depth) has little influence on the observed shift of the mean LMI latitude. The poleward migration of the mean LMI latitude is mainly due to the TC track shift, which results primarily from the change in the large-scale steering flow (Wang, R. and Wu, L. 2019). On the other hand, Song and Klotzbach (2018) linked the interdecadal fluctuations of TC genesis latitude with IPO such that TC form in the northwestern quadrant of WNP during the negative phase of IPO and in the southeastern quadrant during a positive phase of IPO. And, the increases in latitudinal distance between genesis position and LMI location primarily result from the continuous warming of WNP sea surface temperature (Song, J. and Klotzbach, P. J. 2018). Studholme and

Gulev (2018) linked the poleward move of HC to reduced meridional SST gradients and warm SST anomalies at TC latitudes (Studholme, J. and Gulev, S. 2018). Moon et al (2015) speculated the strong roles of Interbasin frequency changes in the poleward shift and also suggest that if the phase of multidecadal variability in the NH is reversed, as found in earlier TC records, the poleward trend could be changed to an opposite, equatorward, trend in the future (Moon, I.-J. et al. 2015). Peng (2015) demonstrates that the weakening ocean vertical mixing in the ocean after the mid-1970s could be the main cause of poleward migration (Peng, S. 2015). In the review paper done by Knutson et al. (2019), most of the authors suggested that the anthropogenic forces contributed towards the poleward migration of latitude of LMI (Knutson, T. et al. 2019).

b. Landfall records and intensity of TC

Stronger TCs have become more intense globally with dramatic changes in the frequency distribution of LMI in the North Atlantic. However, small changes in the frequency of LMI are observed within South Pacific and South Indian Oceans (Klotzbach, P. J. 2006; Kossin, J. P. et al. 2013; Webster, P. J. et al. 2005). Park et al (2013) studied the spatial distribution of trends in TC intensity over WNP and concluded that the trend is weakening in the tropical Philippine Sea and strengthening in southern Japan and its southeastern ocean (Park, D.-S. R. et al. 2013). Mei and Xie (2016) found increased intensities of typhoons by 12% to 15% with the doubled proportion of land falling category 4–5 storms within the East and Southeast Asia over the past 37 years (Mei, W. and Xie, S.-P. 2016). A study done by Holland and Bruyere (2014) concluded the increase in the proportion of Category 4 and 5 hurricanes at a rate of ~25–30 % per °C of global warming but a similar decrease in Category 1 and 2 hurricane with no anthropogenic forces contribution to the frequency changes

(Holland, G. and Bruyère, C. L. 2014). A recent study, done by Bhatia et al (2019) also concluded the increase in the TC intensity with positive contribution from anthropogenic forces (Bhatia, K. T. et al. 2019). However, in Knutson et al. (2019), most of the authors suggested that the anthropogenic forces do not contribute to the observed frequency change trend of TC but do contribute to the intensification of TC (Knutson, T., Camargo, S. J., Chan, J. C. L., Emanuel, K., Ho, C.-H., Kossin, J., Mohapatra, M., Satoh, M., Sugi, M., Walsh, K. and Wu, L. 2019).

2.5.3 Near and Long term TC Projections and Predictability

Extensive experiments and study, done by Knutson et al (2013) based on CMIP3 and CMIP5 model to project the potential changes in hurricane activity in the early and late Twenty-First Century suggested: 1. Significant reduction, 27% for CMIP3-late; 20 % for CMIP5-early and 23% for CMIP-late for TC frequency. 2. Significant increase in LMI intensity by 4%-6% for CMIP3 and CMIP5. 3. Increase in the frequency of very intense (categories 4 and 5) hurricane with 87% increase for CMIP3, 45% and 39% increase for the CMIP5-early and CMIP5-late scenarios. 4. Hurricane rainfall rates increase robustly for both CMIP3 and CMIP5 scenarios (Knutson, T. R. et al. 2013). Zhang and Wang (2017) projected the late twenty-first-century changes of TC activity over the WNP and Southwest Pacific (SP) suggesting no significant change on overall WNP but decrease over the SP in the frequency of TC genesis. The change in maximum near-surface wind speed is robust with more strong TCs than weak TCs over both WNP and SP (Zhang, C. and Wang, Y. 2017). (Knutson, T., Camargo, S. J., Chan, J. C. L., Emanuel, K., Ho, C.-H., Kossin, J., Mohapatra, M., Satoh, M., Sugi, M., Walsh, K. and Wu, L. 2019) also assessed the change in tropical activity in an environment with 2°C anthropogenic warmings and projected the following impact: 1. High

confidence in higher storm inundation level. 2. 14% median increase in TC precipitation rate. 3. Medium to high confidence that TC intensity increases globally with TC's that reach very intense (Category 4-5). 4. Low confidence on further poleward expansion of the latitude of maximum TC intensity in the western North Pacific. 5. A decrease of global TC frequency, an increase in global very intense TC frequency (Category 4–5) and slowdown in TC translation speed. Choi et al (2019) projected the near future tropical cyclones (2016-2030) and concluded East Asian coastal area will be affected by fewer TC landfalls but the number of stronger TC landfalls may increase. Authors also demonstrate that ENSO, the North Pacific SST variation and basin-wide warming of the pacific modulates near-future TC activity with last factor being least responsible (Choi, W. et al. 2019).

From this brief review, the author realizes that shortly, the high wind speed due to intense TC is highly likely and it is of the utmost importance that our community be prepared to counteract such events. One of the steps toward preparation would be assessing the resilience of infrastructures against such hurricane events, finding the weaknesses, and strengthening the same.

CHAPTER 3. PROBABILISTIC RESILIENCE MEASUREMENT FOR RURAL ELECTRIC DISTRIBUTION SYSTEM AFFECTED BY HURRICANE EVENTS

3.1 Introduction

Electricity infrastructure including power transmission and distribution systems are of paramount importance among all civil infrastructure systems (CISs) as electricity is the most universal and direct energy source for supporting other CISs (DHS 2011). Among different types of climatic events that cause power outages, coastal hurricanes and tropic storms are reportedly the major cause in the United States from 1984 to 2012 (Kenward, A. and Raja, U. 2014). Particularly, those deadliest hurricane landfalls have triggered an average economic loss of $25 to $70 billion annually due to power outages(Vugrin, E. D. et al. 2017). These soaring losses may hide a striking fact – although the economic losses concentrate on densely populated urban centers, the post-disaster recovery in rural areas is much slower than that is in urban centers. The prominent instance is the recovery from power outages, which may last from a few hours in urban areas but weeks and sometimes months in rural areas. One of the examples is found in Puerto Rico, where the power outage in the rural village of Adjuntas lasted for almost a year after being hit by Hurricane Maria in September 2017 (Danica Coto 2018, July 16). Adopting the notion of resilience in the context of civil infrastructure engineering, which is the ability to prepare for, withstand, and recover from the disruption (Bilal, A., M. 2015; Cimellaro, G. P., Reinhorn, A. M. and Bruneau, M. 2010). This signifies the low resilience of power systems in these rural areas. In this paper, the authors identify three intrinsic indicators that account for the low *resilience* of rural power systems.

1) Material aging. A report indicates that among the six largest utility companies in the US, the percentage of wood distribution poles with service ages exceeding 40 years ranges

from 15% to 50%, and the percentage of ages exceeding 60 years is still up to 5% to 15% (Brown, R. E. and Willis, H. L. 2006). Wood poles are susceptible to aging due to fungal decay and other environmental deterioration(Morrell, J. J. 2012). These poles after serving for years often suffer from a significant loss of structural capacity against wind loads, which hence statistically results in low system reliability. On the other hand, wood poles are much more widely used in rural distribution systems than in urban areas. One previous FEMA's hurricane report suggested the replacement of wood poles with concrete or metal poles after observing the significant losses of utility structures but also indicated that rural electric cooperatives are likely to continue the use of wood poles (Burbank, K. et al. 2005).

2) Low redundancy. In urban areas, infrastructure systems are mostly networked, including connected substations, transmission, distribution systems, and power switches. In such a networked system, redundancy is essential and enforced. As such, any failure in a confined area can be isolated and the remaining system continues to function (Dueñas-Osorio, L. et al. 2007; Reed, D. A. et al. 2009). Comparatively, the power systems in rural areas usually feature a pattern of linear distributions, which emanate from a central substation, then pass through the service area without alternative connections to other substations or power sources. Such a linear power-delivery subsystem has zero redundancy; even with more than one substation servicing the same area, the redundancy is still at a very low level.

3) Low resourcefulness. The third lies in the social/economic dimensions measured by the local resourcefulness. In urban areas, local resourcefulness (including trained personnel, vehicle support, safety support, and use of technologies) are relatively abundant. This abundance of resources directly determines the rapidity of recovery or the rate of recovery. On the contrary, lower resourcefulness in disaster preparation and response is a signature of most

rural areas and rural communities increasingly find themselves short of resources in dealing with climate changes and hazards (Brennan, M. A. and Flint, C. G. 2007; Kapucu, N. et al. 2013).

> Resourcefulness is dynamic not only when socioeconomic conditions are improved or worsened upon a time but when distributions of interconnected infrastructure systems change spatially. In urban areas, the physical and social infrastructure systems are closely distributed, whereas, in rural areas, they are geospatially sparse. Very little research concerns the relation of resources (e.g., technologies) and geospatial sparseness of infrastructure. A recent study proposes a general framework for bridging the digital divide in rural preparedness and response for emergencies, which particularly mentioned the factor of geospatial sparseness in civil infrastructure and population in rural areas (Gascó-Hernandez, M. et al. 2019). As a result of this geospatial sparseness, the aforementioned resourceful weakness in rural areas is further exacerbated and should be coupled with geospatial factors (Britt, E. 2017). The Center Point Energy Houston Electric (CEH) pointed out that the use of advanced meters, intelligent grids, All Terrain Vehicles (ATVs) and, drones and helicopters based remote sensing, have helped to shorten the outages (Britt, E. 2017). The two resilience examples (including the Puerto Rico example mentioned earlier) reveal that for a similar type of infrastructure, resilience disparity is evidential and real due to different degrees of resourcefulness in urban and rural areas.

As the first step to fully understand and assess rural power-system resilience, this section aims to develop an analytical framework for quantifying the linear power-delivery subsystems typically found in rural power systems. The framework includes mechanical

analysis of a coupled wood-pole and feeder-line as a system unit, the system performance following the hazard, the definition of component restoration (including system response and system-level recovery functions), and finally the definition of a new resilience measure termed as the total mean system-resilience (TMSR). When formulating the component-based restoration and system-level recovery functions, the novelty also lies in that both resourcefulness and spatial-sparseness parameters are parametrically integrated into the framework.

3.2 Model Idealization and Methodology Framework

Most distribution networks in rural areas operate in a linear configuration and can be represented as a minimum spanning tree (Warwick, M. and Hoffman, M. 2016). Figure 3.1a depicts an illustrative example, in which one can see that a 'leaf' can be recognized when a substation is selected. Taking advantage of this topological characteristic and without losing the generality, this paper considers a generic 'leaf' as the object of interest as shown in Figure 3.1b. This leaf-like power-delivery subsystem is assumed to have N poles and N conductor cable segments (counting from the end to the substation, i = 1, 2, ..., N). This linear power-delivery subsystem is referred to as a *system* hereinafter for the sake of simplicity in this paper. Given this linear conductor-pole system, any failure of an upstream feeder line or pole will cause the outage to all the downstream customers (Davidson, R., A. et al. 2003). Assuming that for the i^{th} pole, it individually feeds the power to Nc_i customers, and hence the total number of customers served by this power delivery system is $\sum_{i=1}^{N} N_{c_i}$. It is noted that the failure of substations, transmission towers, and other electrical components, is out of the scope of this study.

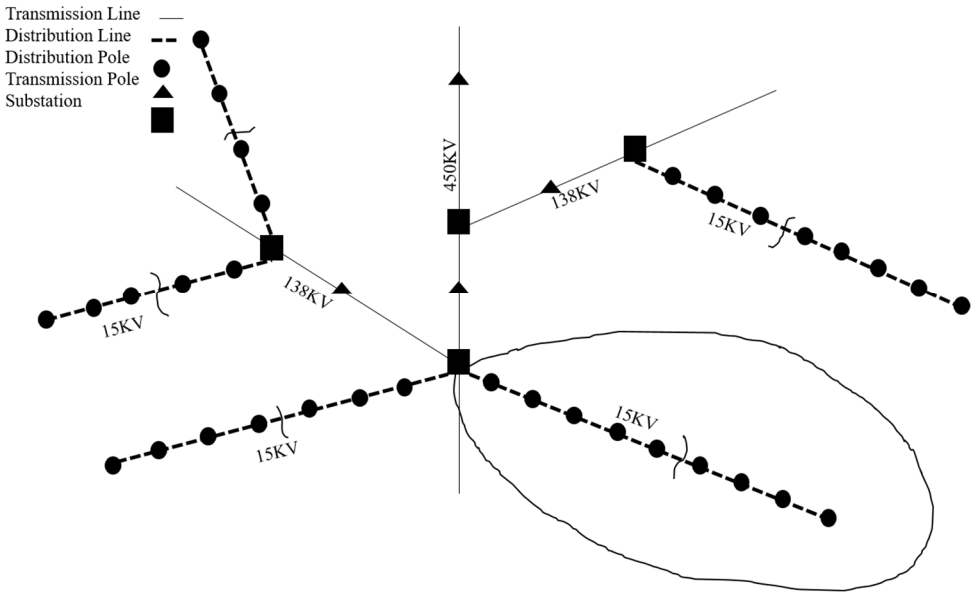

(a)

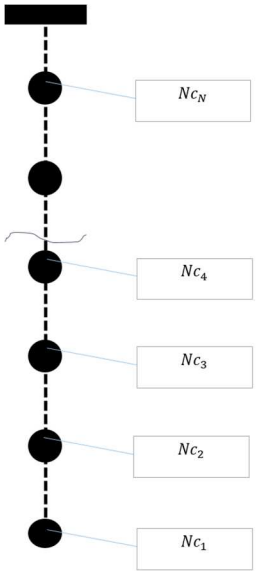

(b)

Figure 3.1. (a) Typical rural power-distribution configuration; and (b) a single span with N poles in a radial subsystem

With this general rural power-delivery system, a probabilistic resilience measurement framework is proposed in this paper. This framework has four sequential steps and the description of these steps is elaborated as follows:

1. *Probabilistic system vulnerability modeling*. This step produces the failure probability given a hurricane event characterized by its Hurricane Category (H). Mechanical analysis based on the material properties of wood poles and feeder conductors of the system is the core element of this step. Two reduced-order analysis methods are adopted, including the analytical cable method and the empirical pole-capacity model in this paper, which yield the conditional failure probability distributions for a generic pole and a conductor.
2. *Probabilistic system functionality modeling*. The probabilistic system functionality model incorporates the structural-system vulnerability model and the notion of loss in the power-delivery system. In this work, the functionality loss is characterized in terms of the number of customers collectively summed up due to the failure event, upon which the discrete probability mass function (PMF) for the system function is defined.
3. *Probabilistic system recovery modeling.* Towards quantifying the system recovery and measuring the resilience, local resourcefulness and geographical sparseness are crucial parameters that control the system recovery. In this paper, a novel and general component-level restoration model is proposed, which is then used to formulate the system-level restoration time and the system recovery function.
4. *Probabilistic resilience modeling*. This final step measures the resilience of the system as described in Equation 1, where the recovery function is integrated mathematically (leading to an area calculation, essentially). The final resilience measure is formulated probabilistically, which leads to the definition of the total mean system-resilience (TMSR).

3.2.1 Probabilistic System Vulnerability Modeling

3.2.1.1 Order-Reduced Conductor-Pole Model

To assess the vulnerability of poles and cables, ideally, a mechanics-based structural model is required. The widely adopted solution is a finite-element (FE) based modeling of the complete and connected system of poles and conductors, where multiple poles with multiple spans of sagged cables with the proper material- and element models are subjected to the wind loads of select intensity levels (Pang, W. et al. 2013). However, such a model would be computationally prohibitive when conducting a stochastic simulation. As will be shown later, the probability of failure for a conductor or a pole is as small as can be stochastically sampled; the system-level probability of failure at many scenarios can be extremely small, hence not manageable if a sampling approach is used. In this work, an order-reduced model with a single span of a sagged cable pinned at two nodes is adopted as shown in Figure 3.2b.

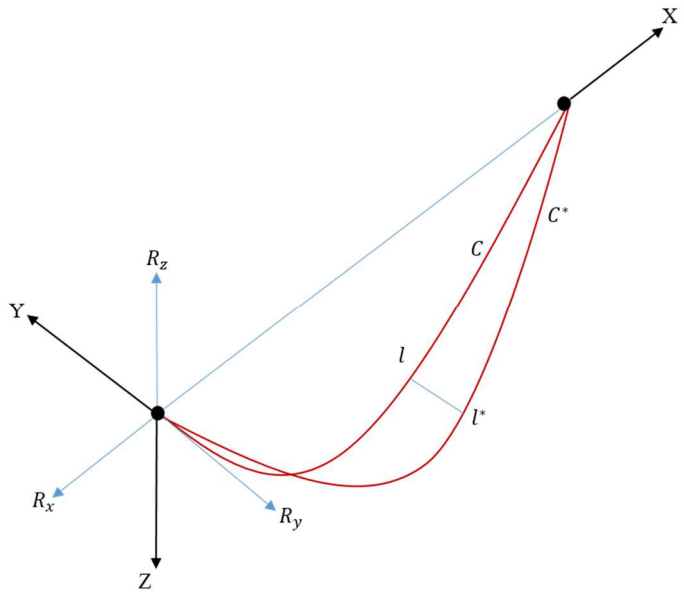

(a)

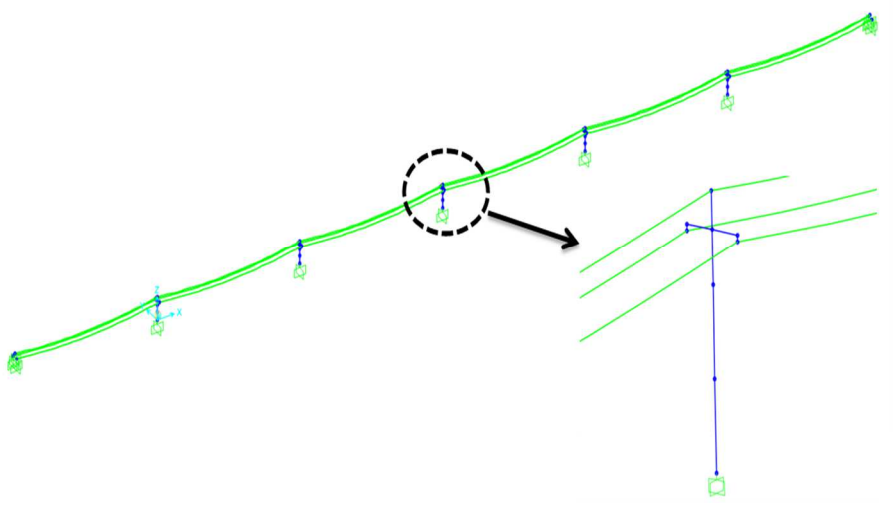

(b)

Figure 3.2 (a) Finite element model of a 6 span power-delivery system; and (b) a single span with N poles in a radial subsystem

This model, fully solvable analytically (Impollonia, N. et al. 2011), can account for the geometric nonlinearity of the cable and the elasticity of the supports. Considering uniformly distributed wind loads (with a variable wind direction angle in 3D) and the self-weight load of the cable, t41he tension in the cable can be expressed as:

$$\mathbf{T}(\ell) = \mathbf{R_0} - \mathbf{P}\ell \tag{3.1}$$

where $\mathbf{R_0} = [Rx, Ry, Rz]$ is the reaction force vector at the origin (the left-end support); $\mathbf{P} = p\,\boldsymbol{\pi}$ is a vector of a distributed load with an intensity p acting along the cable in the directivity defined by a vector $\boldsymbol{\pi}$, and $\mathbf{T}$ is the cable tension vector as a function of the Lagrangian coordinate l that represents a unit length of the unstrained cable. The wind speed and directivity are chosen as the major load parameter. However, it is noted that heavy rainfalls accompanying a hurricane landfall and the ensuing flooding may also contribute to structural failure. In this paper, the effects of flooding or rainfalls are not included in the framework. If one desired to include these effects, the mechanical model subject to these hazards needs to be considered,

leading to different failure probabilities of poles and conductors. For solving Equation 3.1, the closed-form solution is derived at the position l satisfying a stretched configuration, which is expressed in Equation 3.2:

$$\boldsymbol{\mathcal{E}}(s) = C\left(\mathbf{r}\,s - \boldsymbol{\pi}\frac{s^2}{2}\right) + (I - \boldsymbol{\pi}\,\boldsymbol{\pi}^{\mathrm{T}})r * ln\left[\frac{\rho(\boldsymbol{\pi}\,s)}{\rho(0)}\right] - \boldsymbol{\pi}(\|\mathbf{r} - \boldsymbol{\pi}s\| - \|\mathbf{r}\|) + \mathcal{E}\boldsymbol{(0)} \quad (3.2)$$

where $\boldsymbol{\mathcal{E}}(s)$ is a dimensionless position vector, $C = (p\,L)/(E\,A)$ (L is the unstrained cable length, and E and A are Young's modulus and area of the cable section, respectively), $\mathbf{r}$ is the dimensionless reaction force at the cable origin, s is a dimensionless coordinate of l, and $\rho(\cdot)$ is operator performing $\rho(\cdot) = \|\mathbf{r} - \cdot\| - \boldsymbol{\pi}^T[\mathbf{r} - (\cdot)]$. The detailed formulation for Equations 3.1 and 3.2 is found in (Impollonia, N., Ricciardi, G. and Saitta, F. 2011). A verification study using the finite-element-based multi-span model as seen in Figure 3.1a is found in (Pang, W., Chen, Z., Liu, F. and Holmes, R. 2013), which shows sufficient accuracy when comparing the nonlinear behavior of a mid-span cable of the 3D model against the reduced-order model.

Furthermore, the resultant reaction force vectors at the supports provide the force demands unto the poles. This contributes to the bending moment and shear demands for the pole structures, which are in general maximal at the base of the poles. In addition to this demand coming from the conductors, the wind on the vertical profile of the poles contributes to the base moment and shear-force demands as well. Thus, the two sources of bending moment demands at the ground line of the pole (M_B) are combined and then compared with the bending capacity (S). Namely, if $M_B > S$, a failure event occurs. For treated wood poles, the following equation recommended by the ASCE report "Reliability-based Design of Utility Pole Structures" is adopted to define the bending capacity (Dagher, H. J. 2006).

$$\mathrm{S} = 0.000264 * F_b * {C_g}^3 \quad (3.3)$$

where F_b is the fiber stress in psi for the type of wood considered and C_g is the ground-line circumference of the pole in inches, and the resulting S is has a unit in lbf-ft. Untreated wood poles are more prone to aging due to material decay reducing the strength capacity of the pole (Wang, C.-h. et al. 2008). The bending capacity S after considering aging is calculated as:

$$S = 0.000264 * F_b * \left[C_g - \pi d(t)\right]^3 \quad (3.4)$$

where $d(t)$ is the decay depth at a time t (year) and it depends on the rate of decay (defined as $r = k_{wood}\ k_{climate}$, where the k parameters relate to the type of wood and the climate of the region being considered). The detailed procedure to calculate $d(t)$ is found in (Wang, C.-h., Leicester, R. H. and Nguyen, M. 2008).

3.2.1.2 Stochastic Estimation of Failure Probabilities

The random variables used in this study are the wind speed, wind directivity for the desired hurricane category, the fiber strength of timber for the pole, and the tensile strength of the cable material. These random variables are treated probabilistically independently, and Table 3.1 lists the distribution types and parameters for the involved variables in this work. Specifically, the Lognormal distribution has been considered as a proper statistical distribution for modeling random material-strength variables (Sakai, T. et al. 1997; Torrent, R. J. 1978), including the rated fiber strength (F_b) of timber and the tensile strength of the feeder-line conductors (F_y). The mean value for the fiber strength for common wood species for pole can be obtained from (2017). The mean value for the tensile strength of solid/stranded bare copper wires and cables can be obtained from standard and specifications available [e.g.,(Southwire 2013)]. The standard deviations for these material properties depend on the quality of the select manufacturers and other operational factors. In this paper, 1% of the mean value is taken as the standard deviation for the distributions.

Table 3.1. List of distribution types and distribution parameters of the variables involved.

Variable	Distribution	Parameters	
Fiber strength (fb)	Lognormal	8000 psi (mean)	1200 psi (standard deviation)
Tensile strength (fc)	Lognormal	6453 lbf (mean)	645.3 lbf (standard deviation)
Wind Speed	Weibull	2 (*k,* shape parameter)	λ (scale parameter) *
Wind Directivity	Uniform	0^o - 180^o (range)	

* λ is calculated using $\mu = \lambda\,\gamma(1+1/k)$ given a value of k, where μ is the mean wind speed based on the saffir-simpson hurricane wind scale for a selected hurricane category.

For hurricane winds, however, the Weibull distribution with the shape parameter of 2 fairly matches the wind distribution for inconsistent wind with high speed (Archer, C. L. and Jacobson, M. Z. 2003; Edwards, P. and B. Hurst, R. 2001) and thus used in this paper to model the wind pressure given a hurricane category. For the site-specific case, users can estimate the distribution parameters and perform the goodness of fit test to check the adequacy of the distribution model to the recorded wind speed data. In the literature, Gumbel Type I distributions have been adopted for modeling the distribution of hurricane wind speed (Carlos Agustín, E.-S. 2013; Vivekanandan, N. 2012). Users can select these distributions while adopting the proposed framework. By adopting the Weibull distribution, the mean wind speed at a Hurricane Category H is determined based on the Saffir-Simpson Hurricane Wind Scale (SSHWS); and the scale parameter of the Weibull distribution is calculated as mentioned in

Table 3.1. To consider the randomness in wind directivity, a random direction vector in the *x-y* plane is considered. Denoting the relative angle to *x* by θ, which follows a Uniform distribution in the range of [0, π], the random direction of the wind in 3D coordinates is expressed as a vector of [Cos(θ), Sin(θ), 0].

Based on the closed-form solution as shown in Equation 3.2, which shows the analytical solution for a cable in a 3D subject to a uniform force vector in a designated direction, the first-order or second-order approximation method can be used to estimate the failure probability of the cable. Nonetheless, the sampling technique provides a more straightforward and efficient solution without using any analytical approximation. In this paper, the Latin Hypercube sampling (LHS) method is selected considering its more convergent property than a basic Monte-Carlo method in approximating the distribution means and other higher-order moments of the random variables(Bilal, A. M. and Lai, K.-L. 1989).

With Equations 3.1-3.4 and the LHS sampling technique, the response-surface of the failure events for the two generic components are estimated based on the following definitions:

- $P_w = \mathrm{P}(S - M_B < 0 \mid H)$
- $P_c = \mathrm{P}(F_y - T(\ell) < 0 \mid H, G)$

where the two limit states, $F_y - T(\ell) < 0$ and $S - M_B < 0$, define the failure events for the wood pole and the feeder conductor, respectively and, P_c and P_w are the conditional failure probability of the feeder conductor and the wood poles, respectively. Figure 3.3a and Figure 3.3b show the sampled response surfaces for the conductors (subject to the wind speed and the directivity) and the pole (subject to the wind speed, directivity, and the aging), both considering a hurricane category H = III. With this sample response surface, the failure probability is estimated as the frequency that corresponds to the percentage of the failure events over the

total sampling size as P(failure) ≅ (# of failed sampled points) /(# total simulation samples). The failure criterion at a sampled point is determined based on the limit-state definitions: F_y - $T(\ell) < 0$ and S - $M_B < 0$. From the sampled response surfaces, the failure probabilities are calculated as 9% for the cable, 18% for the non-aged pole, and 41% for the 60-year aged pole, respectively.

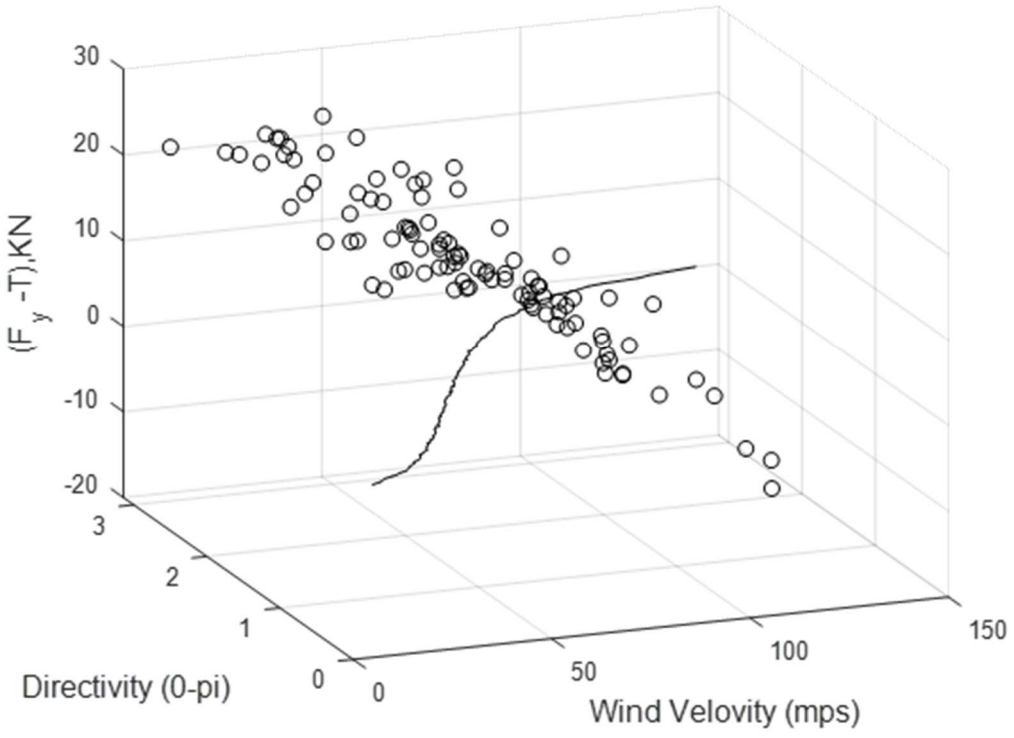

(a)

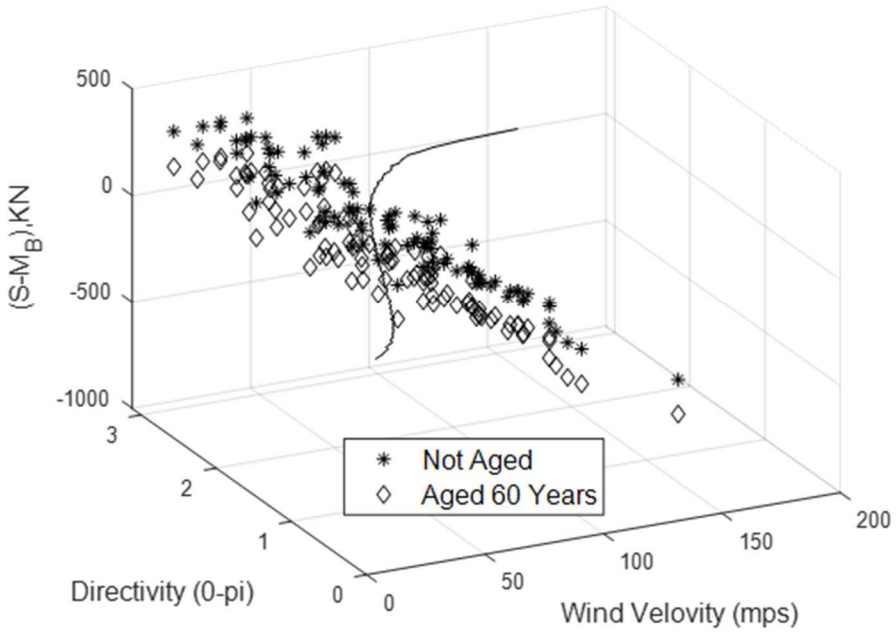

(b)

Figure 3.3. Sampled response surface subjected to hurricane category III for (a) conductors; and (b) poles

It is noted that to consider the effect of aging, the aging factor is not treated as a random variable but a deterministic condition to directly evaluate its effects on resilience measurement. Second, the conditional failure probabilities are calculated for a 47set of different hurricane categories at the select location. In the latter phase of the modeling, for the sake of simplicity, the variables P_c and P_w are used in the formulation without expressing the conditional variables (the hurricane category H and the aging factor G). Further, it is noted that if the fragility model for poles and conductors exist as a function of the wind speed (V_w), i.e., P(S - M_B < 0 | V_w, H) and Pc = P(Fy -T(l) < 0 | V_w, H, G), one can directly estimate the probability of failure by integrating out V_w given its distribution to obtain P_w and P_c, respectively.

3.2.2 Probabilistic System Functionality Modeling

The system considered in this study has cascading effects such as a single failure of an upstream distribution feeder line, either a conductor or a pole causes power outage to all the customers downstream. Therefore, a natural function measure is the number of customers that are affected by the outage resulting from a failure event. Given a hurricane category *H* and an aging factor *G,* considering *N* poles (and *N* conductor lines) from the linear power-delivery system, and that at the i^{th} conductor-pole unit, the number of customers served is Nc_i (i = 1 to *N*), the sample space ($\mathcal{A}$) of the Affected Customers (AC) considering all failure events is defined in Equation 3.5:

$$\mathcal{A} = \left\{0, \sum_{i=1}^{PS_1} Nc_i, \sum_{i=1}^{PS_2} Nc_i, \sum_{i=1}^{PS_3} Nc_i, \ldots\ldots \sum_{i=1}^{PS_n} Nc_i\right\} \quad (3.5)$$

Where, PS_m (m = 1 to n), is the position of Sectionalizer and m+1 is the number of possible events. Sectionalizer islands the faulty section of the distribution span for the recovery such that the upper section and also the lower section (only if a switch is close and power is not interrupted on adjacent distribution span with which switch is connected) gets the power uninterrupted. For instance, if the first Sectionalizer is present in the 44th pole counting from an end of distribution span then, PS_1 = 44 and so on till n number of Sectionalizer is reached. Thus a total of n + 1 different event is possible. For the sake of simplicity, these AC events are redefined as $\mathcal{A} = \{A_m \mid m=0, 1, \ldots, n\}$, where except that $A_0 = 0$, $A_m = \sum_{i=1}^{PS_m} Nc_i$ $(m = 1, 2, \ldots, n)$.

It is obvious that the maximum affected customers (A_n) also defines the total number of customers that the linear power-delivery system serves. In this paper, this quantity is treated as a proxy to define the 100% functionality of the system, denoted by Q_{100}. Given a hurricane event, if A_m ($A_m \in \mathcal{A}$) customers are affected, then the functionality drop is A_m, and the

remaining number of customers (Q_{100} - A_m), defines the system robustness. Given a sample value from the space $\mathcal{A}$, A_m, the probability mass distribution (PMD) is denoted by $P_{AC}(\cdot)$, which has the following mathematical expression:

$$P_{AC}(A_m|H,G) = \left\{P_{E_{i=0}}, \sum_{i=1}^{PS_1} P_{E_i}, \sum_{i=PS_1+1}^{PS_2} P_{E_i}, \sum_{i=PS_2+1}^{PS_3} P_{E_i}, \ldots\ldots \sum_{i=PS_{n-1}+1}^{PS_n} P_{E_i}\right\} \tag{3.6}$$

Where, P_{E_i}(i = 0 to N) is the mass probability of the failure event in which i^{th} pole-conductor unit fails but none of the units fails from N to i^{th} and the unit from i^{th} to end may or may not fail. Mathematically, P_{E_i} is expressed using Equation 3.7:

$$P_{E_i} = \begin{cases} (1-P_c)^N(1-P_w)^N & \text{if } i = 0 \\ (1-P_c)^{N-i}(1-P_w)^{N-i}(P_c + P_w - P_cP_w) & \text{if } 1 \le i < N \\ (P_c + P_w - P_cP_w) & \text{if } i = N \end{cases} \tag{3.7}$$

Appendix A provides more details on the formulation of Equation 3.7, and an illustrative example is given to enhance the understanding. It is noted that when $m = 0$ and denoting $P_{ZL} = (1 - P_c)^N (1 - P_w)^N$, P_{ZL} defines the conditional probability of 'zero-loss of affected customers, which is essentially the reliability of the power delivery system. On the other hand, when $m = N$ and denoting $P_{TL} = P_c + P_w - P_c P_w$, P_{TL} defines the probability of the maximal total loss of customers (i.e., Q_{100}). Now with the expression in Equation 3.7 and the definition of A_m, the mean affected customers, denoted as $Q(H, G)$, can be defined using the Law of Total Expectation:

$$Q(H,G) = \sum_{A_m \in \mathcal{A}} A_m \; P_{AC}(A_m|H,G) \tag{3.8}$$

Equation 3.8 defines the expectation of the affected customers, which can be treated as the variable mean of the dropped system functionality given the hurricane category H and a select aging factor G. Accordingly, the mean robustness of the system Q_R is expressed $Q_{100} - Q(H, G)$. It is noted that if desired, the variance of affected customers can be calculated.

Figure 3.4 illustrates the distribution plots based on Equation 8 (defined over 100 randomly generated A_m with A_{100} = 500) given two analytical cases with an equal number of sectionalizer: (1) Case 1 – high-reliability system (assuming P_c = 1/500, P_w = 1/200); and Case 2 – low-reliability system (P_c = 1/100, P_w = 1/50). Both cases use a randomly generated 100 different number of customers for 100 conductor-pole units (each unit serves from one to 10 customers). For Case 1, the system reliability P_{ZL} is 49.6%; whereas in Case 2, P_{ZL} = 4.9%. One can further see that (as predicted by Equation 1) that for the low-reliability system, although the probability of losing the least number of customer (i.e. A_1 that is served by the ending power-conductor unit) is smaller, the probabilities of losing a higher number of customers increase much faster than the high-reliability system due to the cascading effect. As a result, using A_m set, the mean loss of the high-reliability system is 157.4 customers; whereas the low-reliability system is 386.2 customers. This is consistent with the understanding of either a low or high-reliability system or its effects on affecting system functionality.

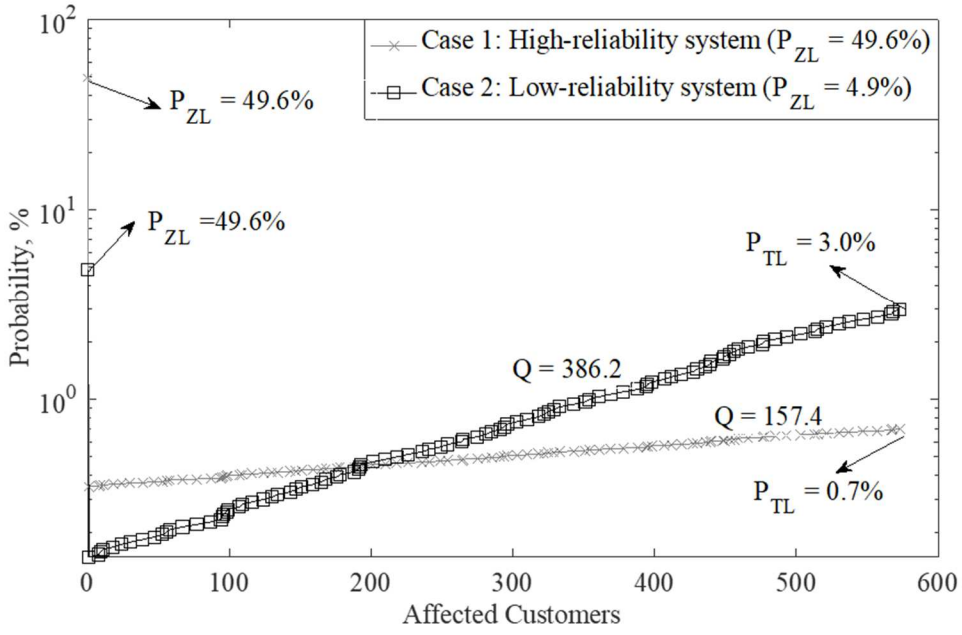

Figure 3.4. The analytical distribution function of affected customers

3.2.3 Probabilistic System Recovery Modeling

The concept of variable restoration time for civil infrastructure components has been proposed in the literature (Anghel, M. et al. 2007; Ouyang, M., Dueñas-Osorio, L. and Min, X. 2012). For example, the restoration time of any failed component by repairing or replacing is taken as the summation of two random time variables *a* and *b* (e.g., *a* takes a uniform distribution and *b* takes an exponential distribution). In this paper, a general and analytical restoration-time modeling approach for power-delivery components is proposed (which are different from the system-level restoration to be introduced later). (Cutter, S. L., Barnes, L., Berry, M., Burton, C., Evans, E., Tate, E. and Webb, J. 2008) mentioned in the DROP (Disaster Resilience of Place) model that the immediate aftermath of the hazard comes the coping responses wherein the first-responders identify disaster extent, evaluate the severity and then plan and prioritize the allocation of resources towards taking action on series of efforts for containing losses. These coping responses are the function of the antecedent condition of the social system or community such as Social/Economic soundness, organizational preparedness and, technical ability. During this time it is obvious that the functionality of the physical system (infrastructure) remains unaltered. As descriptive as all other four properties, coping responses can be treated as an intrinsic property of a resilient physical system, namely being less or more responsive to disruption or extreme events depending on the inherent condition. To the work in this paper, since this response phase is an important period of considering and adopting technologies, which tend to make the system more responsive to the disruption (e.g., in terms of collecting data or providing critical information for the ensuing recovery), 'response' as a new property is explicitly included as the first phase towards restoration known as Response

Phase and time passed in this phase as Response Time (*RS*). This response phase is followed by the system Recovery Phase in which the functionality of the system starts to recover and the time required is Recovery Time (*RC*). The significant differentiation of this approach from the previous efforts is the inclusion of two parameters that account for local resourcefulness and spatial distribution.

First, the authors state that the local resources for the component-level restoration affect the system-level recovery rate and the resulting recovery function as well. Quantification of available resources within the system is a crucial task for selecting the component restoration function. However, it is challenging to characterize local resourcefulness, since it spans multiple resilience dimensions (social, organizational, behavioral, and technological) (Bruneau, M., Chang, S. E., Eguchi, R. T., Lee, G. C., O'Rourke, T. D., Reinhorn, A. M., Shinozuka, M., Tierney, K., Wallace, W. A. and Winterfeldt, D. v. 2003). Besides, if a failure occurs within more than two local power delivery systems, local competition and cooperation are expected in resource allocation, which further complicates component restoration and system recovery. Without addressing such local competition and cooperation, a simplified modeling approach may be developed in terms of a weighting variable from each of the resilience dimensions (Zona, A. et al. 2020). Due to the scope of this study, such possibility is not included in this paper; rather with an objective towards the power restoration, authors have integrated three weighted orthogonal dimensions of resourcefulness to get a lumped static resourcefulness parameter (κ).

Amongst the three dimensions first one is the Social/ Economic (R_{SE}) dimension and the variables/indicators to quantify this dimension can be not limited to relief fund allocated by the government towards the recovery, population of the society effectively using a

smartphone, population active/inactive in any of the various social media platform, population knowledgeable and using free communication services such as weather alert, power outage alert, and outage tracker map and, population properly utilizing the helpline for reporting an outage. Similarly, the second dimension is Organizational Preparedness (R_{OP}) for which indicators can be the availability of enough emergency fund, organization-wide plans, and drills to respond to an emergency, partnerships on mutual assistance programs with other electric companies such that one will be aided with maintenance crew and equipment on need, good public relation and, the efficacy of routine maintenance such as tree trimming, quality inspection and replacement of infrastructure such as a transmitter, fuse, Sectionalizer, tapping device and so on. Finally, the third dimension is Technical (R_T) for which the indicators can be the number of high-trained personnel and their availability within the organization, advanced technology for rapid damage assessment and, advanced equipment and vehicles required for effective response and recovery. Thus, a lumped static resourcefulness parameter (κ) is lower and upper bounded by 0 (absolute absence of resources) and 1 (adequate resources of the system and society that this system serves) respectively and, weightage W_{SE}, W_{OP}, and W_T is assigned for dimension R_{SE}, R_{OP}, and R_T respectively such that $W_{SE} + W_{OP} + W_T = 1$. These weights however are not necessarily constant while calculating *RS* and *RC*. For example, strong R_{SE} and R_T play a more vital role to minimize the response time when compared to R_{OP} and, in contrast, R_T and R_{OP} play a major role in increasing the rapidity of the recovery. Consequently, this study will adopt two resources parameter for the resilience calculation κ_1 (resourcefulness parameter towards response) κ_1 (resourcefulness parameter towards recovery). Thus, the empirical formula is proposed to calculate *RS* time as

$$RS = \ RS_{min} * e^{(1-\kappa_1)} \tag{3.9}$$

where $\kappa_1 = W_{SE} * R_{SE} + W_{OP} * R_{OP} + W_T * R_T$ and RS_{min} is the user-defined parameter representing the minimum response time possible when the organization is fully prepared to go in the action with enough resources to mobilize and hierarchical chain of action in order soon after the event strike. It is noted that the RS_{min} is still conditional to H as with the higher category comes the larger impacted area to cover with greater damage and the responsibility.

The other variable that influences the restoration for a component is the geospatial location of the component that couples with the dynamic availability of resources. Specifically, for a rural power-delivery system, this distance is taken as the relative distance from the substation to a remote pole or cable, assuming that the restoration times increase monotonically as this relative distance increases. In this paper, considering a pole or a cable at the i^{th} unit that potentially fails, D_i denotes the geospatial distance at this component. In practical implementation, one may further consider local terrain or other geospatial challenging factors when calculating D_i values. In this study, the simple 2-dimensional Euclidean distance metric is used to calculate D_i's.

With the definitions of κ and D_i, a general component restoration model is proposed in Equation 3.10.

$$R(i) = r_0 * e^{\lambda_1 * Di} * e^{\lambda_2 (1-\kappa)} \tag{3.10}$$

This component restoration model assumes that the restoration time for a generic pole or a conductor cable decreases exponentially as the distance to the substation (D_i) increases, and increases exponentially as the resourcefulness (κ) increases. In Equation 9, r_0, λ_1 ($\lambda_1 > 0$), and λ_2 ($\lambda_2 > 0$) are empirical (user-defined) constant parameters. The constant r_0 is a user-determined parameter that approximates the expected hours for repairing the pole or conductor closest to the substation with the maximal resource. The constants of λ_1 and λ_2 are parameters

that incorporate other uncertainties such as flooded streets, traffic blockades, and fallen trees, etc., which may interrupt the restoration. In this paper, an empirical procedure is used to estimate λ_1 and λ_2 and is detailed in the numerical experiment later. When the restoration times for the i^{th} pole and cable are calculated, they are denoted as $Rw(i)$ and $Rc(i)$, respectively.

With $Rw(i)$, $Rc(i)$, the PMF, $P_{AC}(A_m|H, G)$, and position of the sectionalizers (PS_m) the mean recovery time of the system considering all components at A_m is determined, denoted by $RC(\kappa_2, A_m)$. As in shown Equation 3.11, it is a mathematical expectation of the restoring times for all the possible combinations of the failed poles and conductors and the successful ones, conditional on the event of A_m. Appendix A provides the key steps to obtain this expression

$$RC(\kappa_2, A_m) = \begin{cases} 0, & \text{if } m = 0 \\ P_c\left(\sum_{i=1}^{PS_m-1} Rc(i) + \frac{Rc(PS_m)}{P_c+P_w-P_cP_w}\right) + P_w\left(\sum_{i=1}^{PS_m-1} Rw(i) + \frac{Rw(PS_m)}{P_c+P_w-P_cP_w}\right), & \text{if } 1 \le m \le n \end{cases} \quad (3.11)$$

Given this function, the total mean restoration time, T_{sys}^t considering the distribution of all failure events and the component restoration times can be further obtained based on the Law of Total Expectation:

$$T_{sys}^t = \sum_{m=0}^{n} RC\left(\kappa_2, A_m\right)\ P_{AC}(A_m|H, G) \quad (3.12)$$

which can be used as a scalar measure of the total restoration time cost.. Subsequently, the variance of the total restoration time and the coefficient of variation (denoted by COV_T) can be calculated in Equation 3.13 and 3.14, respectively.

$$\sigma_T^2 = \sum_{m=0}^{N}\left[T^t{}_{sys} - RC\left(\kappa_2, A_m\right)\right]^2 P_{AC}(A_m|H, G) \quad (3.13)$$

$$\text{COV}_\text{T} = \frac{\sigma_T}{T_{sys}^t} \times 100\% \quad (3.14)$$

3.2.4. Probabilistic Resilience Modeling

This study adopts the concept of varying functionality and hence resilience is calculated as the normalized area underneath the illustrated piece-wise function model of functionality

that degrades after hazard and starts to recover to its full potential following the response period over the controlled time as shown in Figure 1. Following this notion and graphical illustration of Figure 1, Q is the functionality measures over time such that Q_{100} is the full functionality measure before the hazard strike and Q_R is the residual functionality of the infrastructure system and its quantification should assimilate the Robustness and Redundancy (if any) which are two inherent properties of resilience among four as described in (Bruneau, M., Chang, S. E., Eguchi, R. T., Lee, G. C., O'Rourke, T. D., Reinhorn, A. M., Shinozuka, M., Tierney, K., Wallace, W. A. and Winterfeldt, D. v. 2003); t_{oe} is the time of the event, t_{rs} is the time from when the recovery of the infrastructure starts, t_{rc} is the time for an entire system to be fully recovered and, t_c is the control time or the planning horizon to calculate the resilience. Hence with these timelines, three time-period, Response Time (RS) = t_{rs} - t_{oe}, Recovery Time (RC) = t_{rc} - t_{rs}, and Control Period (T_C): time-period from beginning to t_c are defined.

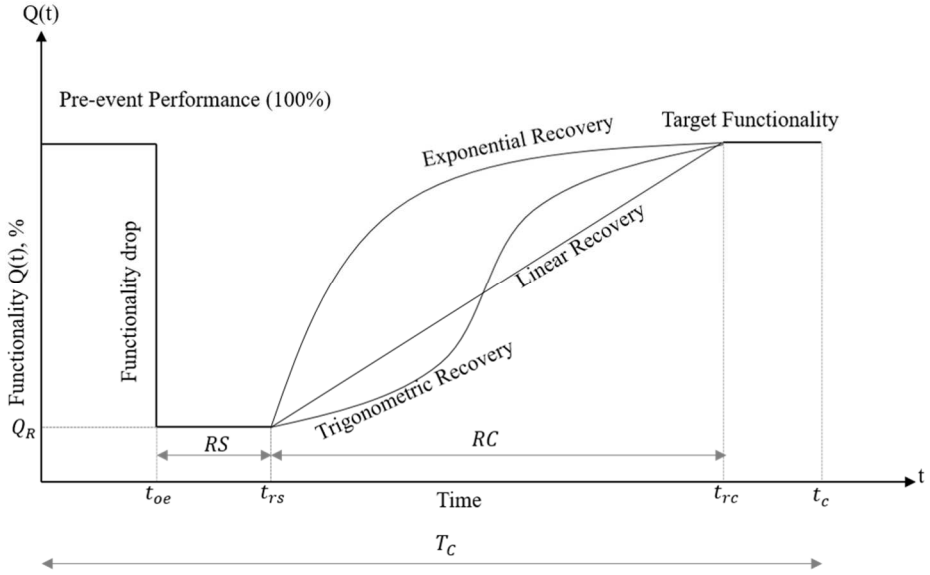

Figure 3.5. Graphical representation of resilience measurement

Hence analytically, resilience in this study calculated as:

$$\mathrm{R_{sys}} = \frac{Q_R * RS + \int_{trs}^{trc} f_{rec}(t)\,\mathrm{dt} + (T_C - (RS+RC)Q_{100}}{T_C * Q_{100}} \tag{3.15}$$

Where $f_{rec}(t)$ is the system recovery function of time and indeed is key towards measuring resilience. Different from the restoration time for a component or a system, a system recovery function is a continuous model that can measure the rate of recovery However, the rate of recovery poses to be a much challenging problem mathematically. In the literature (Cimellaro, G. P., Reinhorn, A. M. and Bruneau, M. 2010), three canonical forms, linear, exponential, and trigonometric, are expressed in the following.

$$\text{Linear:} \quad f_{rec}(t) = \frac{(Q_{100}-Q_R)(t-t_{rs})}{RC} + Q_R \tag{3.16}$$

$$\text{Trigonometric:} \quad f_{rec}(t) = (Q_{100} - Q_R)\left(1 - cos\left(\frac{\pi(t-t_{rs})}{2*RC}\right)\right) + Q_R \tag{3.17}$$

$$\text{Exponential:} \quad f_{rec}(t) = \gamma\left(exp^{\frac{t-t_{rs}}{RC}}\right) + Q_R - \gamma \tag{3.18}$$

where Q_{100} is the full functionality of the system before the strike, Q_R is residual functionality after the strike, t_{oe} is a time of the strike, and $\gamma = (Q_{100}\text{-}Q_R)/(e\text{-}1)$. Given Equations 3.16-3.18, choosing a recovery function is highly empirical and is regarded as a higher-level decision-making process; namely, it is determined by the stakeholders for the power system. In general, the Trigonometric recovery function is more realistic demonstrating an initially slow-pacing recovery rate; then a fast rate in the later phase. Nonetheless, if the resourcefulness towards recovery is very high (e.g. $\kappa_2 = 0.9$), one may proceed with the Exponential function. When no knowledge about the recovery rate exists or the resourcefulness is considered low, the linear recovery function may be preferred.

Hence, given a select system recovery function (f_{rec}), the controlling period (T_C), the mean restoration time at A_m or $RC(\kappa_2, A_m)$the mean system-resilience (MSR) given a failure event A_m, denoted by $R_{sys}(\kappa, A_m)$, is computed using Equation 3.15 over the time interval [t_{oe},

t_c]. From the calculated resilience measurements $R_{sys}(\kappa, A_m)$, the total mean system-resilience (TMSR) is further computed using the Law of Total Expectation:

$$R_{sys}^{t} = \sum_{m=1}^{N} R_{sys}(\kappa, A_m) \;\; P_{AC}(A_m|H, G) \tag{3.19}$$

It is noted that both MSR and TMSR defined herein are still retrospectively conditional on the hurricane category H and the aging factor G. As similarly expressed previously, the variance for the total system resilience can be calculated $\sigma_R^2 = \sum_{m=1}^{N}\left[\left(R^{t}{}_{sys-} R_{sys}(\kappa, A_m)\right]^2 \;\; P_{AC}(A_m|H, G)\right.$. The coefficient of variation for the total system resilience denoted as $\mathrm{COV_R} = \sigma_R / R_{sys}^{t} \times 100\%$, can be used to measure the variability of the total system resilience.

3.3 Numerical Example

3.3.1 System Configuration and Parameters

Given the simplified configuration in Figure 2a, it is assumed that one transmission line with a voltage level of 450KV runs in the middle of the area. This transmission line passes through the substation where the voltage level steps down to the distribution level of 15KV. From the substation, three-phase feeder (primary) lines (each of 15KV) emanate radially for the rural distribution. These primary feeder lines are assumed to have 4/0 AWG cu i.e. 25.4 mm (0.53 in) diameter without insulation, which is commonly found in rural distribution systems. The average total length considered for a feeder line is 16.09 km (10 miles) with timber poles (Southern pine, Class 3, average diameter 0.24 m (9.5 in) with a height of 7.93 m (26 ft) above and 2.74 m (9ft) below ground respectively) at a distance of 76.2 m (250 ft). such that, a total of 211 poles (and 211 spans) are considered. Five sectionalizer are assumed to be present at the 42nd, 84th, 127^{th,}, 169th and 211thpole, respectively counting from the end of the distribution span. These primary lines are branched off at the transverse direction to

smaller three-phase secondary conductors (300 kcmil cu, 16.51 mm diameter) with insulation and then into single-phase laterals, which finally deliver power to local residences. This distribution span is assumed to serve 800 customers in total.

3.3.2 System Vulnerability and Function Calculation

A Matlab® program was written that implements the proposed framework in this paper. With the stochastic sampling described previously, the variable hurricane categories, the aging factor (G = 5, 20, 30, 60, and 90 years; and G = *5* years is considered as a non-aged condition). Figure 6a and Figure 6b show the failure probability curves for a generic conductor and a wood pole, respectively.

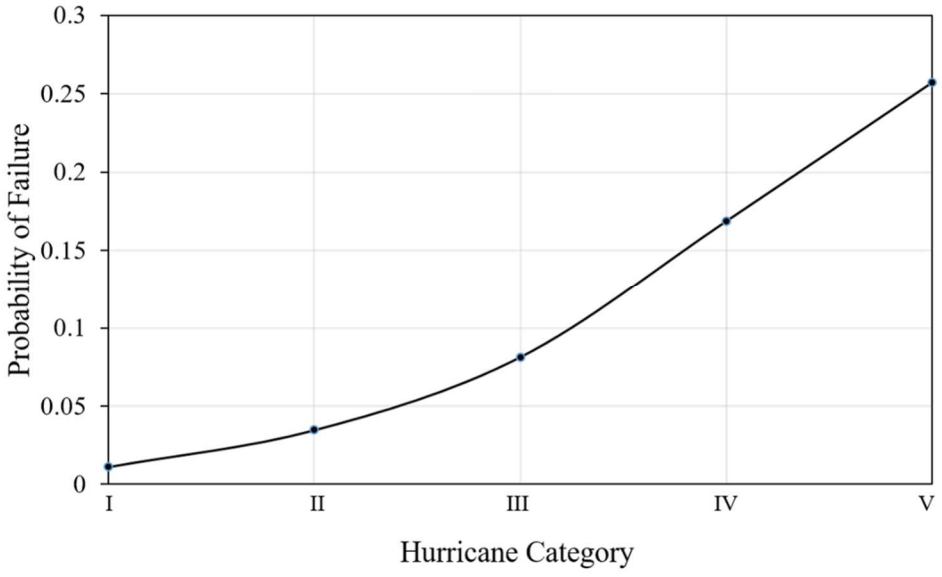

(a)

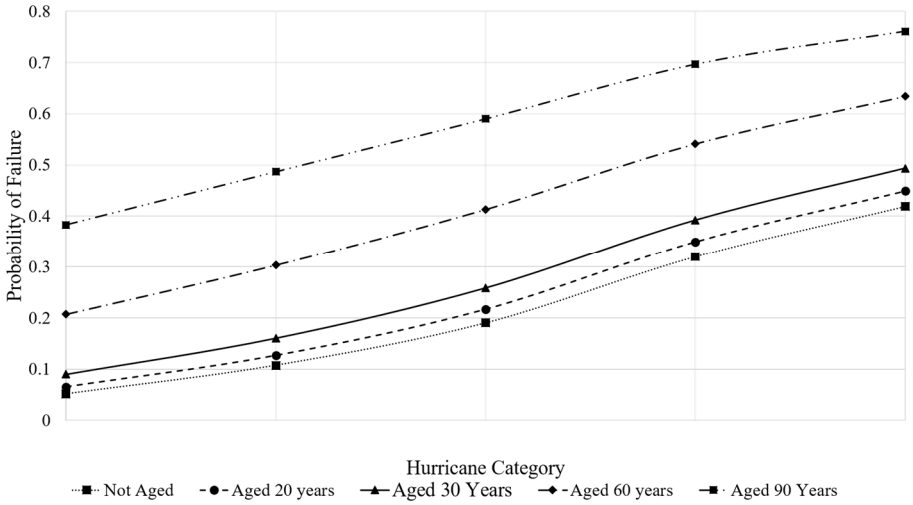

(b)

Figure 3.6. Probability of failure as a function of the hurricane category for (a) conductors; and (b) poles

The PMF (P_{AC}) defined upon the sample space of affected customers given the hurricane category III and three different aging factors (G = 5, 20, and 60 years) are shown in Figure 3.7. With the relatively high failure probabilities for the poles and the conductors (e.g. $Pc \approx 0.0853$; and $Pw \approx 0.2$ for non-aged poles; both at the hurricane category III), the probabilities at a small number of affected customers are very small; then it increases rapidly as A_m reaches to the total number of customers (Q_{100}). Using Equation 8, the expected mean affected customers are obtained as 382, 385, and 390 customers, for G = 5, 20, and 60 years, respectively, at the hurricane category of III. These mean loss values of affected customers are consistent with the aging factors.

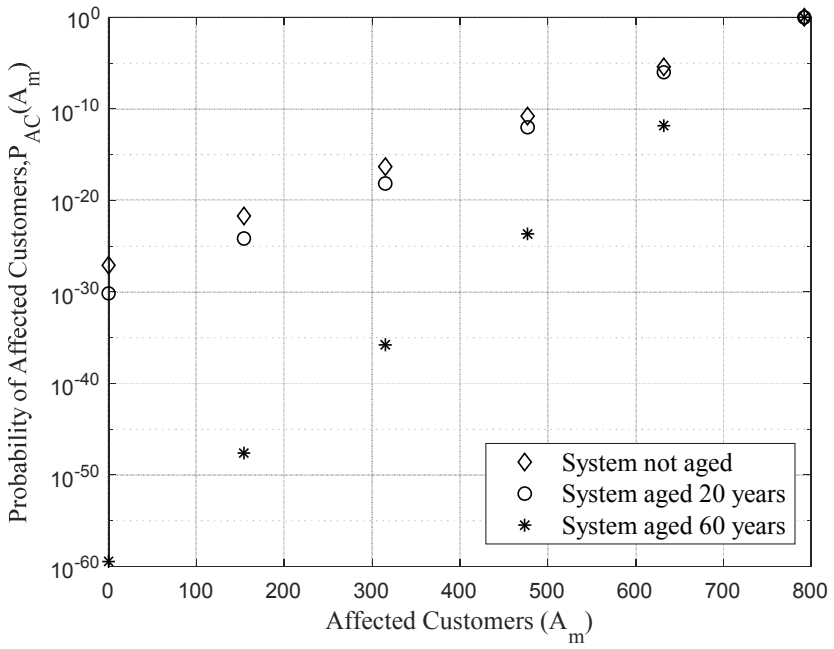

Figure 3.7. Probability density of affected customers with different aging parameters.

3.3.3 Component Restoration and System Recovery Calculation

To proceed with the recovery time and resilience calculation, an empirical parameterization procedure is adopted in this paper, which is summarized in the following steps:

1) The minimal hours for repairing a wood pole (r^w_0) and a conductor (r^c_0) is set as 5 hours and 3 hours, respectively, which were similarly used in (Ouyang, M., Dueñas-Osorio, L. and Min, X. 2012).
2) Considering the instance of a pole, the constants λ^w_1 and λ^w_2 in Equation 3.10 are estimated by assuming two empirical conditions. First, it is assumed that the maximal restoration times occur at the remotest component, namely at the end pole where D_{211} = 16.09km (10 miles). Taking the first condition, two different maximal restoration times occur at these two extreme resourcefulness conditions, namely κ_2 = 0 and κ_2 = 1. In this paper, for the numerical experiment, the authors consider

$R_w(211)$ = 36 hours with $\kappa_2 = 0$, and $R_w(211)$ = 10 hours with $\kappa_2 = 1$. By applying these two results into Equation 9, the two restoration constants are solved, which yields $\lambda^w_1 = 1.313 \times 10^{-5}$ and $\lambda^w_2 = 1.281$.

3) Similarly for the restoration time for a conductor, by repeating the previous step expect with considering, $Rc(211)$ = 20 hours with $\kappa_2 = 0$, and $Rc(211)$ = 7 hours with $\kappa_2 = 1$, the resulting restoration constants are solved as well: $\lambda^c_1 = 1.06 \times 10^{-5}$ and $\lambda^c_2 = 1.05$.

4) With this empirical and simplified procedure, the two restoration functions are obtained: $Rw(i) = 5\ e^{0.00001313*Di}\ e^{1.281(1-\kappa_2)}$ and $Rc(i) = 3\ e^{0.0000106*Di}\ e^{1.05(1-\kappa_2)}$.

By choosing a moderate-level resourcefulness value, in this example, R_{SE}, R_{OP}, and R_T = 0.65, 0.55, 0.6 respectively with the weightages towards κ_2 as 0.2, 0.3 and, 0.5 respectively such that the κ_2 = 0.595, distribution of the $RC(\kappa_2, A_m)$, is shown in Figure 3.8, where three aging conditions (G = 5, G = 20, and G = 60 years) are considered (given a Category III hurricane). The total mean recovery times and their variabilities for the different cases are computed based on Equations 11-13, which are T^t_{sys} = 459.85, 494.47, and 771.54 hours with the COV_T of 0.03%. 0.01% and 0.000018%, for G = 5, G = 20, and G = 60 years, respectively.

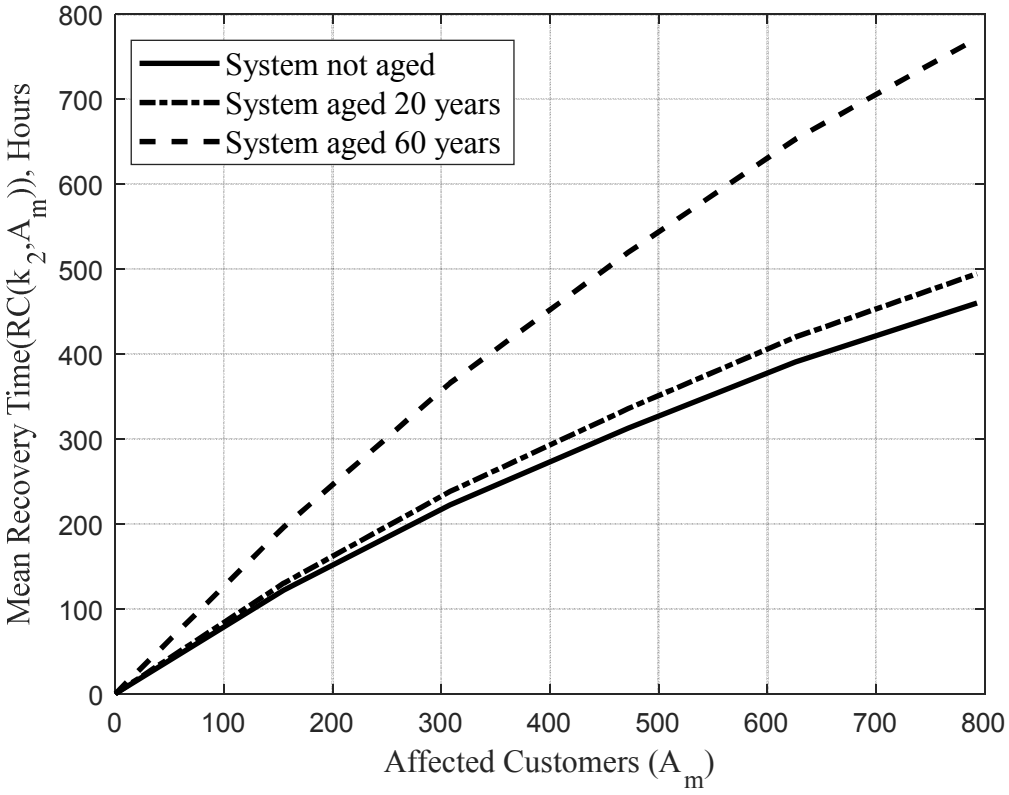

Figure 3.8. Mean Recovery Time conditional to Affected customers for H=III

3.3.4 Resilience Calculation

To proceed with the resilience calculation, the minimum response time is assumed to be 2, 3, 8, 16, and 26 hours respectively for H = I, II, III, IV and, V. *Ncrew* is as mentioned in Section 3.3.1 and trigonometric recovery function is used unless $\kappa 2 > 0.9$ where exponential recovery function is used. Hence, following the description previously, the MSR of the system as a function of a customer loss event, or $R_{sys}(A_m)$, is obtained as shown in Figure 3.9. It is noted that aging factors adversely affect the system resilience at different levels of functionality losses in terms of the affected customers. Particularly, when the aging is taken as 60 years, the system resilience decreases significantly at all levels of function losses.

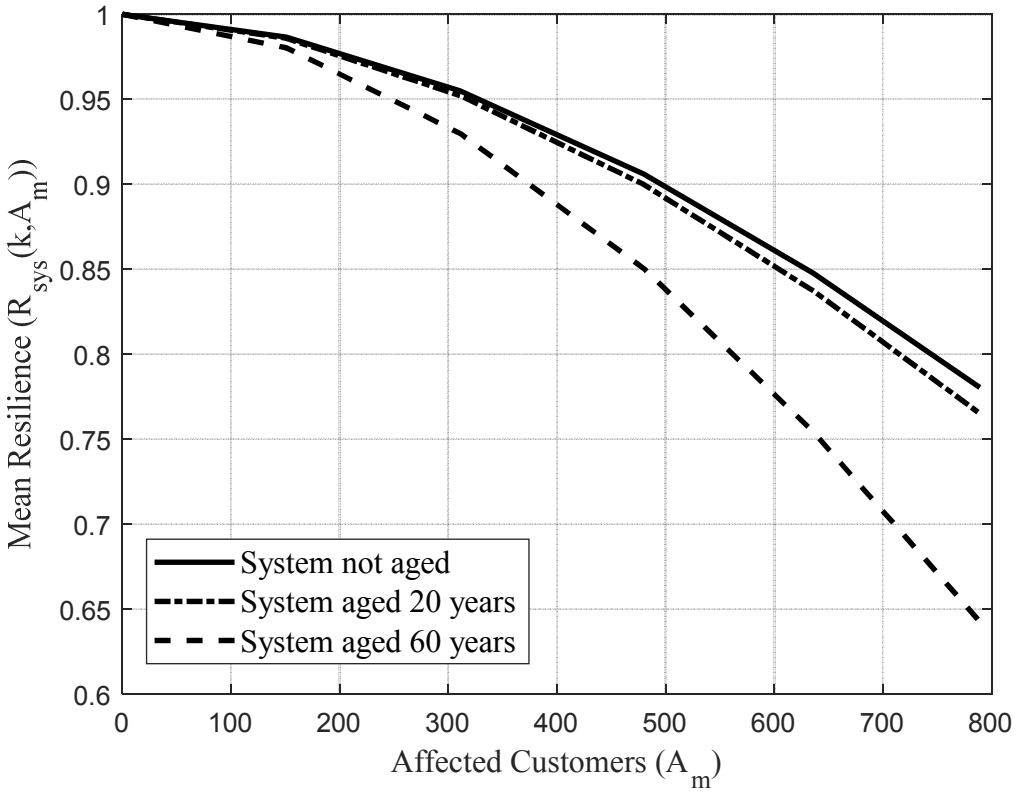

Figure 3.9. Mean System Resilience conditional to Affected customers for H=III

Equation 3.19 provides the expression of the total-mean system-resilience (TMSR), which yields a scalar-value statistic that characterizes the system resilience. Besides, this TMSR measure can be used to evaluate the effects of resourcefulness. Three lower to higher-level resourcefulness values are considered to compute TMSRs, Table 2 reports all the TMSR measurements, and Table 3 reports the COV_R considering the parameter matrix of the aging factor (G = 5, 20, and 60 years) and the hurricane categories (H = I, II, III, IV, and V) for the assumed resourcefulness parameter of each dimension, respectively. Figure 3.9 partially summarizes the results in Table 2 by graphing the variations of TMSRs against the hurricane categories with a moderate aging value G = 20. It is observed that within the same system with the same control period, the resilience can be very small (e.g. under G = 20 years and resources are low or perhaps negative, TMSR = -0.216 for the hurricane $H = IV$; and -0.7382 for $H = V$);

yet they increase significantly when the resourcefulness increases. Under the same *G* and with moderate resources, TMSR increases to 0.5908 and 0.4135, respectively. Figure 3.10 confirms this trend as well. This change in resilience thus proves the importance of incorporating a resourcefulness parameter to quantify system resilience. When the variability of the measure of the total system resilience is concerned as shown in Table 3, it is observed that in general, the hurricane category and level of resourcefulness decreases the variability.

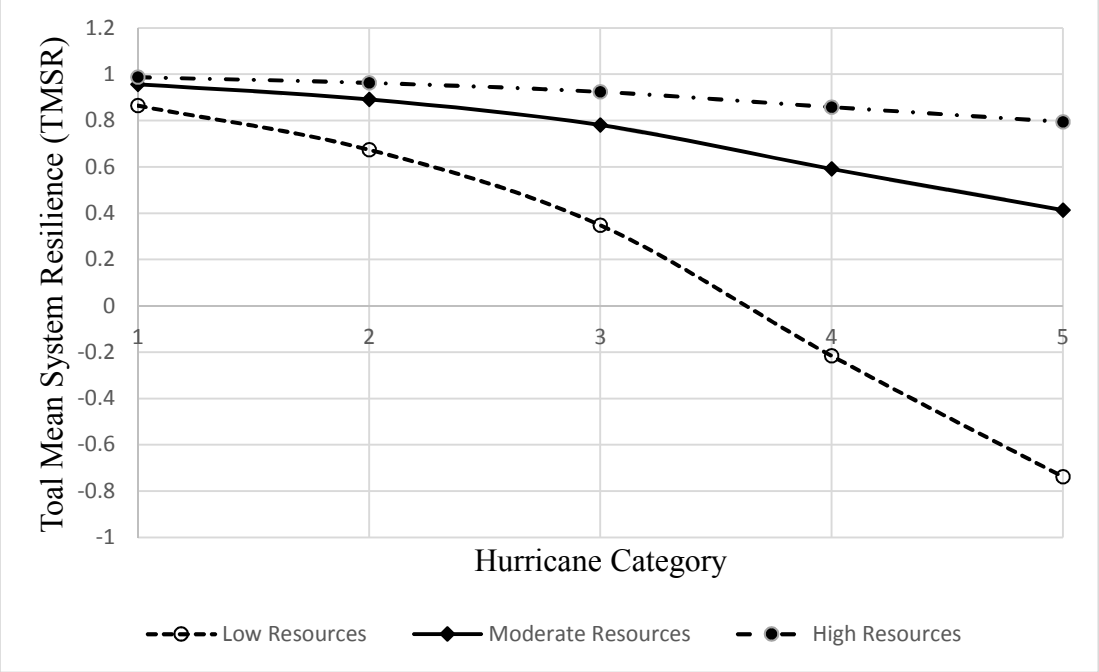

Figure 3.10 Total Mean System resilience at different hurricane levels and resourcefulness levels

Table 3.2. Total mean system resilience at different resourcefulness and hurricane category levels.

Hurricane Category	Resourcefulness		
	R_{SE}=0.2, R_{OP}=0.15, R_I=0.27	R_{SE}=0.65, R_{OP}=0.55, R_I=0.6	R_{SE}=0.85, R_{OP}=0.9, R_I=0.97
I	(0.865,0.839,0.595)*	(0.9128,0.8949,0.7292)	(0.9461,0.9339,0.8258)

II	(0.675,0.642,0.343)	(0.7878,0.7656,0.5638)	(0.8661,0.8517,0.7212)
III	(0.348,0.303,-0.061)	(0.5770,0.5464,0.3014)	(0.7338,0.7140,0.5556)
IV	(-0.216,-0.267,-0.592**)	(0.2145,0.1802,-0.0392)	(0.5073,0.4851,0.3432)
V	(-0.738,-0.79,-1.102)	(-0.1197,-0.1547,-0.0392)	(0.2987,0.2761,0.1393)

* The three numbers from the left provide the estimation of TMSRs at the aging of 5, 20, and 60 years.

** The negative value herein is because the calculated *Tsys* is longer than the assumed *Tc*; to avoid a negative resilience value, a larger *Tc* can be used.

Table 3.3. Coefficient of variations (%) for the total system resilience at different resourcefulness and hurricane category levels.

Hurricane Category	Resourcefulness		
	R_{SE}=0.2, R_{OP}=0.15, R_T=0.27	R_{SE}=0.65, R_{OP}=0.55, R_T=0.6	R_{SE}=0.85, R_{OP}=0.9, R_T=0.97
I	(1.43, 1.22, 0.13)	(0.97,0.79,0.07)	(0.689,0.535,0.041)
II	(0.66, 0.49, 0.02)	(0.37,0.27,0.006)	(0.215,0.153,0.0030)
III	(0.12,0.072,0.00068)	(0.0468,0.0262,9.01e-5)	(0.023,0.0126,3.10e-5)
IV	(0.001, 0.0004, 1.4e-7)	(7.4e-4, 3.6e-4, 1.4e-6)	(1.9e-4,8.3e-5,9.8e-8)
V	(1.6e-6,5.1e-7,7.9e-11)	(6.5e-6, 1.7e-6,1.6e-10)	(1.67e-6, 5.8e-7, 2.6e-10)

* The three numbers from the left provide the COVs at the aging of 5, 20, and 60 years.

3.4. Conclusions and Remarks

By focusing on power-delivery systems typically found in rural areas, this paper proposes a probabilistic framework for measuring the resilience of such systems. The framework starts with an order-reduced mechanics-based modeling approach, which yields the conditional failure probability for wood poles and conductors. The remaining steps are fully mathematically tractable with closed-form formulations. First, the system functionality probability is defined upon the event space of affected customers. Second, a component-level restoration model is proposed, and the mean restoration time-cost is formulated probabilistically considering the cascading effects. Last, the mean resilience distribution and the total-system mean-resilience of the system are both formulated, the latter of which yields a scalar measure for linear power-delivery systems in rural areas. A numerical example is provided with realistic aging-related material degrading effects and considering different categories of hurricane winds. The resulting probabilistic distribution of affected customers, restoration times, and system resilience are calculated using the proposed framework. The plots of the mean system resilience subject to different aging factors and the total-system mean-resilience subject to the resourcefulness parameters insightfully demonstrate the effects of aging and local resourcefulness, one in the physical dimension and the other in the socio-economic dimension.

Different from the previous framework in the literature, the methodology provided in this study provides a basis for probabilistically characterizing the system vulnerability and resilience at a local level (i.e., one linear power-delivery system that may spans miles long in the US). This framework can be used to quantitatively assess systems- or network-level

resilience, which may alter the fact that to this end, often empirical models are used in network-based power-system resilience assessment. It is further remarked that the proposed framework can be directly used for modeling a rural distribution system (with multiple radial distribution systems). In this situation, no system redundancy is found and the proposed framework can be separately applied to each independent linear power-distribution subsystem. It is noted that in some wide rural areas with clustered residence units or commercial assets, multiple local substations exist, which allow the adoption of power switches to provide alternative electricity feeding or system redundancy at a possible failure event. In this case, there exists an optimal condition for expressing the resilience at the system level; or more generally, there possibly exists a resilience interval due to the possible combination of binary switches subject to extreme events. This optimization problem is not in the scope of this paper. Nonetheless, the analytical framework presented in this paper provides the basis for computing the resilience of a local linear subsystem as a 'node' in the complex system network with integer variables.

CHAPTER 4. GLOBAL SENSITIVITY ANALYSIS AND DEPENDENCE MODELING USING COPULA

4.1 Introduction

Whilst proposing methodology to quantify the resilience of civil infrastructures, more or less, various uncertainties are included such as uncertainties of hazard loads, material strength, structural capacity, structural capacity degradation over the length of time, scenarios of losses, resources available towards recovery, and response and so on. However, no model/framework to the author's knowledge includes, how resilience is evinced because of these underlying uncertainties. More specifically, the author realizes two paramount gaps first it is not discussed how the variability of the one or more input parameters within the proposed model is affecting the variability of outcome i.e. resilience and if the model is robust such that the decisions based on such model can be taken. And second, the dependence of model outcome i.e. resilience with its direct input or derived input such that effective and efficient decision making can be done to improve resilience.

In this chapter, the author aims to first use the available methodologies to perform Global Sensitivity analysis of TMSR proposed in Chapter 4 with input parameters like aging and three-dimension of resourcefulness and secondly, calculate the dependence of TMSR to input aging and derived input κ_1 and κ_2.

4.2 Global Sensitivity Analysis of the TMSR

Sensitivity analysis determines the robustness of the proposed resilience assessment framework by quantifying the extent to which resilience is affected by the changes in the values of input parameters such as resourcefulness and aging. Essentially, in this study sensitivity analysis addresses the answer to "at what extent the resilience is sensitive to the alteration of

aging and resourcefulness". To that end, the Global Sensitivity Analysis (GSA) that apportion the uncertainty in outputs to the uncertainty in each input factor over the entire range is adopted (Zhou, X. et al. 2008). GSA can be distinguished into two types: the case with independent inputs (i.e. the joint Probability Density Function (PDF) of the inputs variables is expressed as the product of its marginal) and the case with dependent outputs (i.e. the previous does not hold). GSA for the case with independent inputs is appropriate to this study as the input variables aging and resources are assumed to be independent.

For the independent variables, variance-based approach such as Total Sobol Indices proposed by (Sobol′, I. M. 2001) has been widely used because of several desirable properties such as applicable to both linear and nonlinear function, easy to implement and interpret and, can be used for both input ranking. However, these variance-based sensitivity indices implicitly assume that output variance is a sensible measure of the output uncertainty, which is not always the case as will be seen in the resilience distribution in Figures 5.4 and 5.5 (with highly skewed and multi-modal). For such a case, using variance as a proxy of uncertainty may lead to contradictory results (Borgonovo, E. 2007) and should adopt moment–independent approaches which describe the contribution of the input uncertainty on the Cumulative Distribution Function (CDF) of the model output (Liu, Q. and Homma, T. 2010). This study thus adopts the methods proposed by (Pianosi, F. and Wagener, T. 2015) based on CDF to calculate the GSI of aging and resources to resilience.

(Pianosi, F. and Wagener, T. 2015) proposed the PAWN index T_i as the sensitivity index for input variable X_i (i =1, 2,…N) over all possible vlues of x_{ij} (j = 1,2,…J) samples defined as:

$$T_i = \underset{X_i}{\text{stat}}\left[KSM(x_{ij})\right] \tag{4.1}$$

where T_i varies between 0 and 1 such that the lower the value, the less influential the input X_i. statistics (stat) is either maximum or the median over all possible values of x_{ij} and, KSM(x_{ij}) (Kolmogorov Smirnov Metric) is the distance between the empirical unconditional CDF of the output variable Y denoted as $F_Y(y)$ and empirical conditional CDF, $F_{Y|X_i}(y|x_{ij})$ conditional to variable X_i i.e. $KSM = . \ sup_R\left(\left|F_Y(y) - F_{Y|X_i}(y|x_{ij})\right|\right)$. Additional to using KSM statistic as proposed by (Pianosi, F. and Wagener, T. 2015), this study also uses Wasserstein-1/ Earth Mover's Distance (W_1/EMD) statistic quantified as $W_1/EMD = \int_0^1 \left|F_Y{}^{-1}(y) - F_{Y|X_i}{}^{-1}(y|x_{ij})\right| dy$ as later one is proven effective for measuring the resilience variation as will be seen in the resilience aggravation analysis modeling in Chapter 5. Hence, the sensitivity indices for the input variables Aging, and three dimensions of resourcefulness: Social Economic, Organizational Preparedness and Technical dimensions in this study is termed as T_G, T_{R_SE}, T_{R_OP}, T_{R_T} respectively, and is calculated using the following numerical procedure.

First of all J=10000 sets of the sample are generated with Aging (G = uniform random integer (urandi) between 5 and 90) and Latin Hypercube Samples (LHS) with uniform distribution for three dimensions of resourcefulness (R_{SE}, R_{OP}, R_T = *unif* (0.2, 0.98)). Then, using the rural electric distribution setup used in the following section as an example, $R_{sys_j}(A_m | H, G_j, R_{SE_j}, R_{OP_j} R_{T_j})$, $\forall$ (j =1:J) is calculated using Equation 3.15 followed by TMSR using Equation 3.19. It is noted that the Hurricane Category (H) is kept constant to H = III. Hence, with J samples of R_{sys}^t, the unconditional empirical CDF of TMSR denoted as F($TMSR$) is obtained.

Secondly, the Empirical CDF (ECDF) of TMSR conditional to input variables G, R_{SE}, R_{OP}, and R_T denoted as F($TMSR|G_i$) , F($TMSR|R_{SE_i}$), F($TMSR|R_{OP_i}$) and F($TMSR|R_{T_i}$) respectively need to be calculated. Towards obtaining F($T|G_i$), n =100 samples of G = *urandi*

(5, 90) is generated then for each G_i (i = 1,2….n), J sets of LHS for three resourcefulness dimensions with *unif* (0.2, 0.98) is generated. This is followed by calculation of $TMSR|G_i(A_m$ | H, G_i, R_{SE_j}, $R_{OP_j}R_{T_j}$), ∀ (i=1:n and j = 1:J) using Equation 3.15 and consequently (TMSR $|G_i$) using Equation 3.19. Hence the F($TMSR|G_i$) is obtained for all *n* as shown in Figure 4.1.

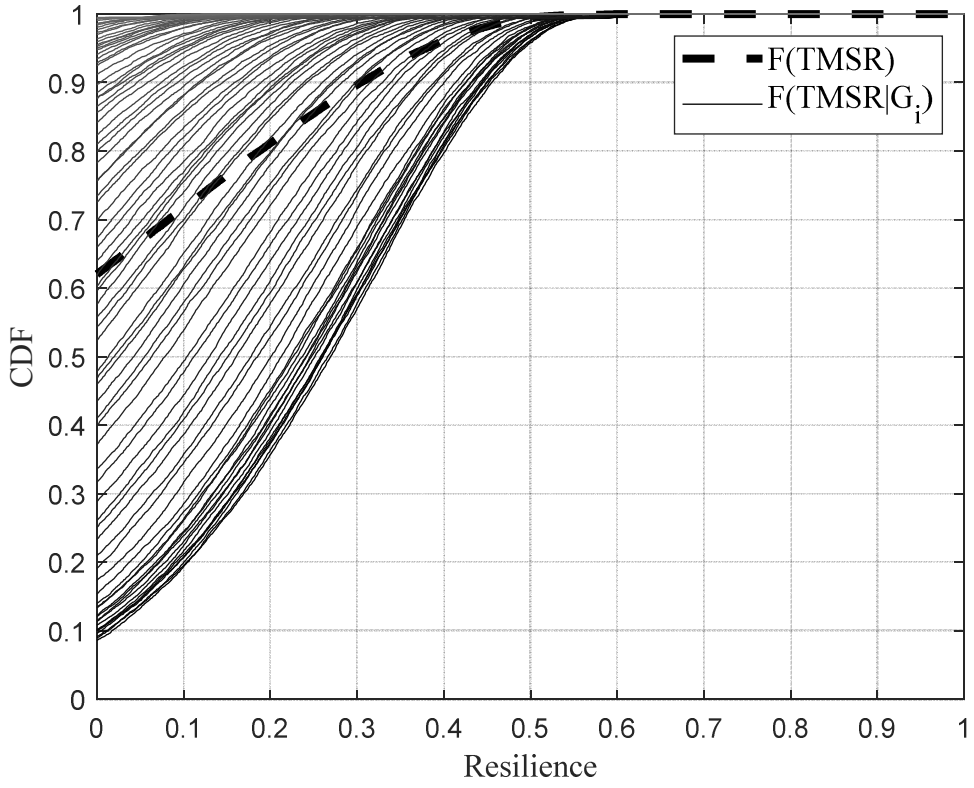

Figure 4.1. ECDF of resilience unconditional to any input variables (dashed line) and ECDF of resilience conditioned to Aging (G_i)

Now, the KSM(G_i) and W_1/EMD(G_i) is approximated respectively between F($TMSR$) and F($TMSR|G_i$) as shown in Figure 4.2 in which it is observed that the EMD statistics varies relatively smoother than the KSM statistics for the unit change of G suggesting W_1/EMD statistics more robust towards sensitivity analysis than KSM statistics for this study.

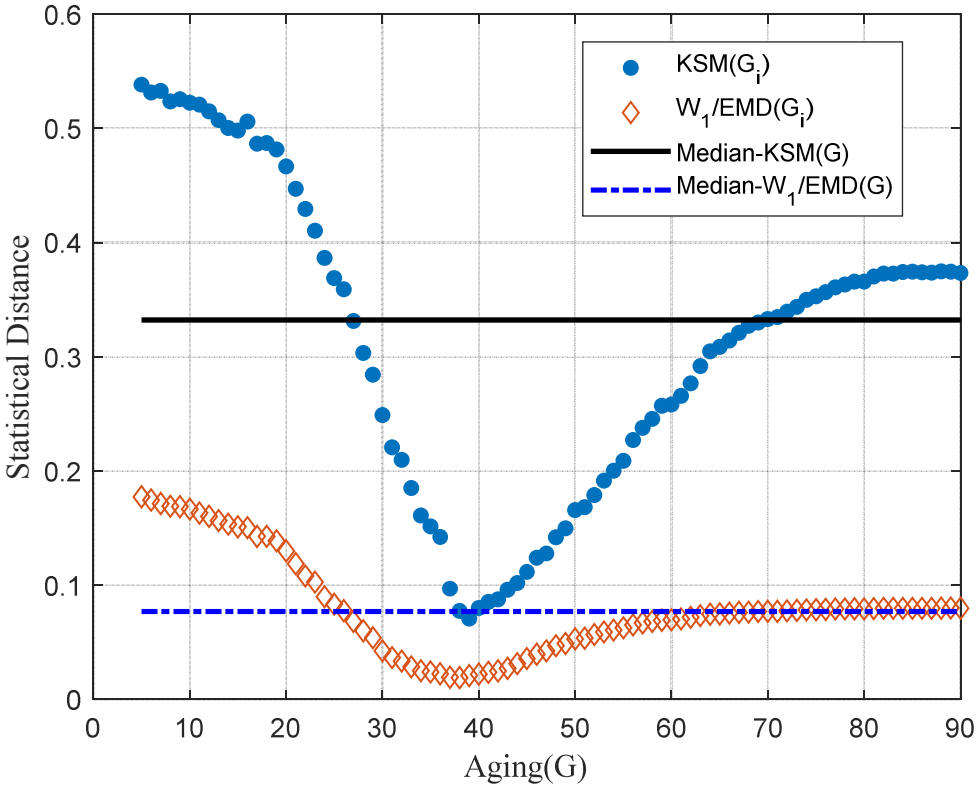

Figure 4.2 Statistical distance between unconditional ECDF of resilience and ECDF of resilience conditional to G using KSM and W_1/EMD statistical distance.

The procedure is repeated to obtain the F ($TMSR|R_{SE_i}$), F($TMSR|R_{OP_i}$) and F($TMSR|R_{T_i}$) and plots are as shown in Figure 4.3 (a-c) respectively.

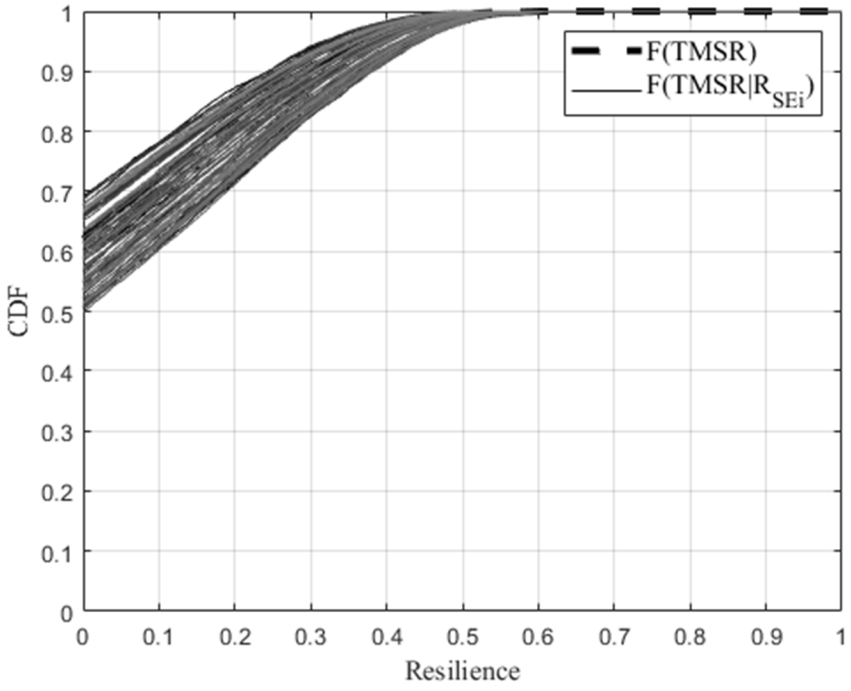
F(TMSR)
F(TMSR|R_SEi)
CDF
Resilience
0
0.1
0.2
0.3
0.4
0.5
0.6
0.7
0.8
0.9
1

(a)

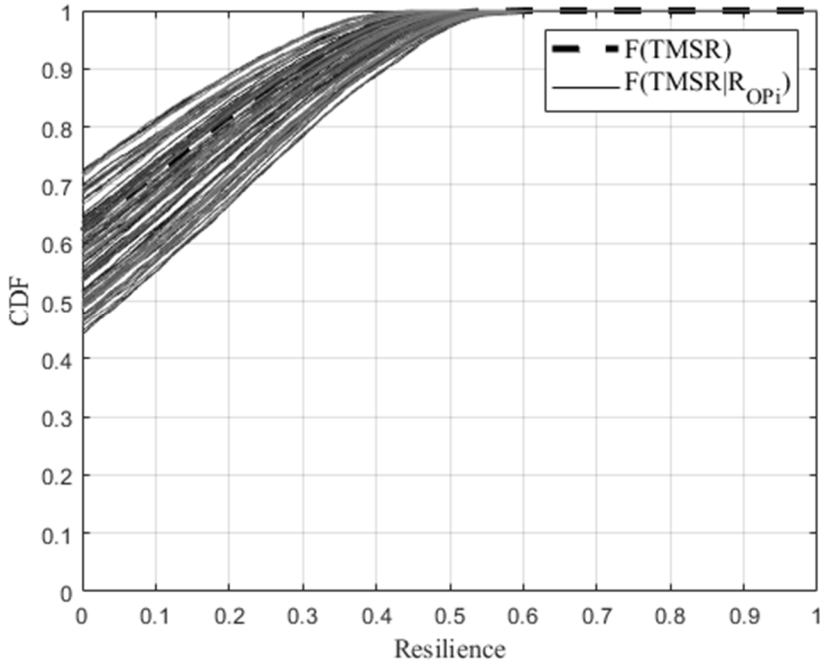
F(TMSR)
F(TMSR|R_OPi)
CDF
Resilience
0
0.1
0.2
0.3
0.4
0.5
0.6
0.7
0.8
0.9
1

(b)

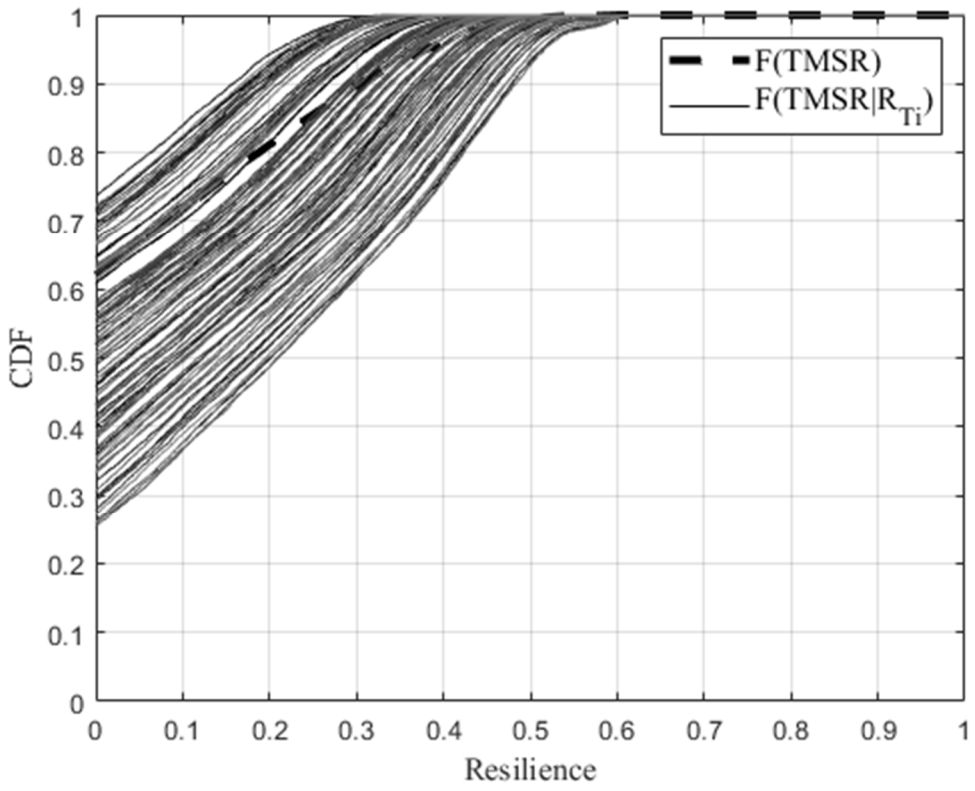

(c)

Figure 4.3. ECDF of resilience unconditional to any input variables (dashed line) and (a). F ($TMSR|R_{SE_i}$), (b) F($TMSR|R_{OP_i}$) and, (c) F ($TMSR$)

Similarly, Figure 4.4(a-c) shows the statistical distance between F($TMSR$) and F ($TMSR|R_{SE_i}$), F($TMSR$ and F($TMSR|R_{OP_i}$) and, F($TMSR$) and F ($TMSR|R_{T_i}$) respectively using KSM and W_1/EMD.

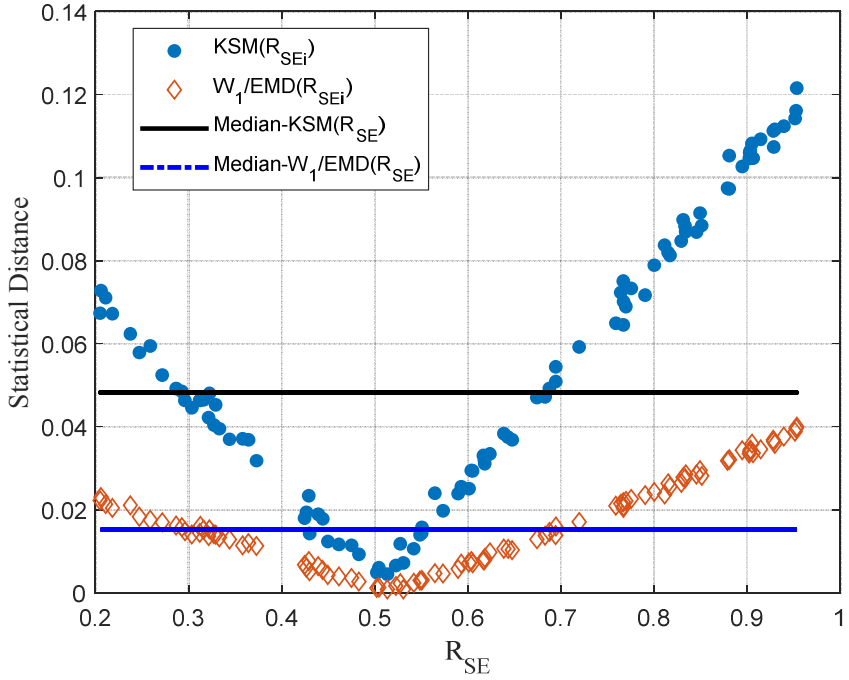
KSM(R_SEi)
W_1/EMD(R_SEi)
Median-KSM(R_SE)
Median-W_1/EMD(R_SE)
Statistical Distance
R_SE
0.14
0.12
0.1
0.08
0.06
0.04
0.02
0
0.2
0.3
0.4
0.5
0.6
0.7
0.8
0.9
1

(a)

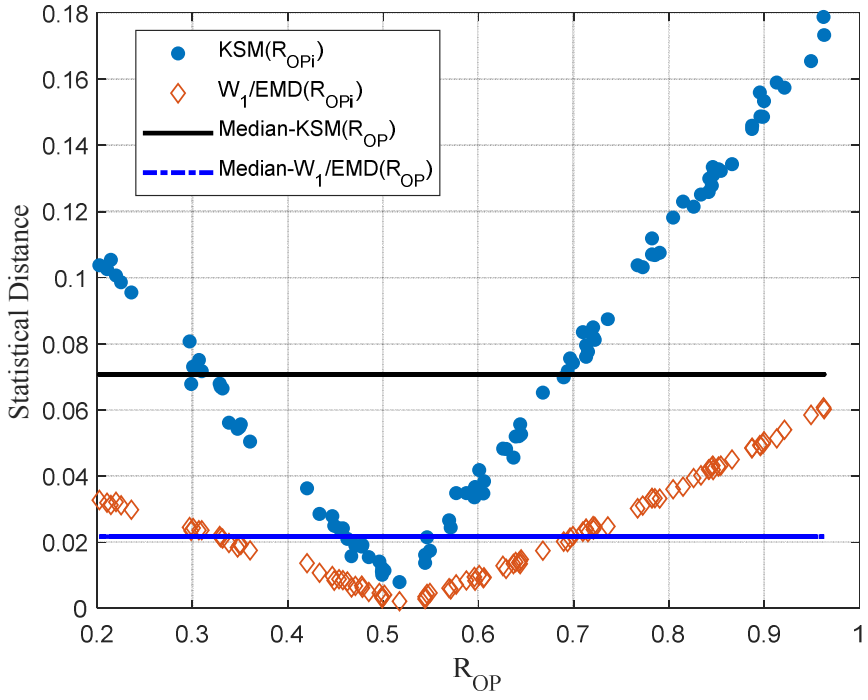
KSM(R_OPi)
W_1/EMD(R_OPi)
Median-KSM(R_OP)
Median-W_1/EMD(R_OP)
Statistical Distance
R_OP
0.18
0.16
0.14
0.12
0.1
0.08
0.06
0.04
0.02
0
0.2
0.3
0.4
0.5
0.6
0.7
0.8
0.9
1

(b)

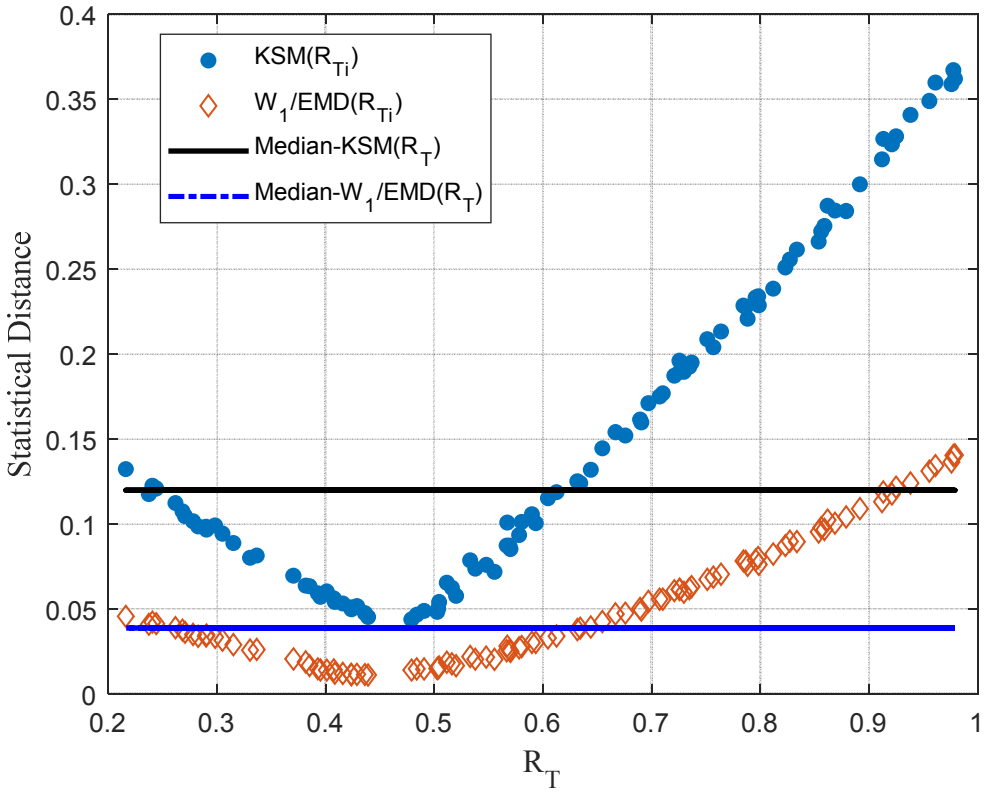

(c)

Figure 4.4. Statistical distance between unconditional ECDF of resilience and (a) F $(TMSR|R_{SE_i})$, (b) F$(TMSR|R_{OP_i})$ and, (c) F $(TMSR|R_{T_i})$ using KSM and W_1/EMD statistical distance

The sensitivity indexes $T_{G,}$ $T_{R\_SE,}$ $T_{R\_OP,}$ T_{R_T} is thus calculated using Equation 4.1 taking median as a stat for KSM as well as W_1/EMD and summarized in Table 4.1.

Table 4.1. $T_{G,}$ $T_{R\_SE,}$ $T_{R\_OP,}$ T_{R_T} using KSM as well as W_1/EMD

	KSM	W_1/EMD
T_G	0.3584	0.0784
T_{R_SE}	0.1110	0.0320
T_{R_OP}	0.1135	0.0332
T_{R_T}	0.1197	0.0387

From Table 4.1, and based on W_1/EMD statistics it can be inferred that although the proposed resilience framework is relatively sensitive to the technical dimension of resourcefulness followed by the Aging, organizational preparedness, and social-economic dimension of the resourcefulness, the framework is indeed robust because not any extreme effect of any input measure is seen.

4.3 Dependence Modeling using Copula

In addition to the moment-independent global sensitivity analysis, this study also explores the dependence measures coming from copula theory to compare the dependence of resilience to aging and resourcefulness. While GSA apportioned the sensitivity of the resilience to the uncertainty of aging or each dimension of resourcefulness over the entire range, copula modeling will allow us to visualize and assess the tail dependency amongst TMSR and aging and, TMSR and derived input parameter (κ_1 and κ_2).

Sklar's Theorem (Sklar, M. 1959), first introduced a copula stating that any multivariate distribution function can be decomposed into the marginal distributions and a copula such that copula captures the dependence between variables. Suppose random vector (X_1, X_2, ……, X_d) $\in \square^d$ with $F_j(x_j) = \mathrm{P}[X_j \leq x_j]$ for $j = 1,\ldots,d$, the continuous CDF of X_j, we can denote another random vector (U_1, U_2, ….U_d) = ($F_1(X_1)$, $F_2(X_2)$,…., $F_d(X_d)$) with uniformly distributed margins. Then the copula, denoted by C is the joint CDF of (U_1, U_2, ….U_d) such as for (u_1, u_2, ….u_d) $\in [0, 1]^d$,

$$C(u_1, u_2, \ldots u_d) = P[U_1 \leq u_1, U_2 \leq u_{2,\ldots,} U_d \leq u_d] \quad (4.2)$$

In other words, copula C is a multivariate joint probability distribution function on the unit square [0, 1] with uniform marginal distributions. This study, however, will explore the bivariate copulas and dependence between resilience and input parameters (aging, three

dimensions of resourcefulness) and derived input (κ_1 and κ_2) individually as resources and aging are independent to each other. As such bivariate copula between variables X and Y with CDF F and G will be denoted as $C(u, v) = P[U \leq u, V \leq v]$. Thus the most familiar measures of dependence such as Pearson's correlation coefficient (r), Spearman's correlation coefficient (ρ), and Kendall's correlation coefficient (τ) can be obtained using copula respectively by

$$r(X,Y) = \frac{1}{D(X)D(Y)} \int_0^1 \int_0^1 [C(u,v) - uv] dF^{-1}(u) dG^{-1}(u) \tag{4.3}$$

$$\rho(X,Y) = 12 \int_0^1 \int_0^1 [C(u,v) - uv] du\, dv \tag{4.4}$$

$$\tau(X,Y) = 4 \int_0^1 \int_0^1 C(u,v) dC(u,v) - 1 \tag{4.5}$$

where F^{-1} and G^{-1} are the usual inverses of F, and G respectively, and D stands for standard deviation. And, ρ and τ are nonparametric dependence measures and distinguished from the measure r in that they are functions of C alone. Additional to ρ and τ study done by (Schweizer, B. and Wolff, E. F. 1981) showed that any suitably normalized measure of distance between the surfaces $C(u,v)$ and uv (e.g. any L_p – distance) should yield a symmetric nonparametric measure of dependence and provided an example with L_1, L_2, and L_∞ respectively as:

$$L_1(X,Y) = 12 \int_0^1 \int_0^1 |C(u,v) - uv| du\, dv \tag{4.6}$$

$$L_2(X,Y) = \left(90 \int_0^1 \int_0^1 [C(u,v) - uv]^2 du\, dv\right)^{\frac{1}{2}} \tag{4.7}$$

$$L_\infty(X,Y) = 4\, sup_{u,v \in [0,1]} |C(u,v) - uv| \tag{4.8}$$

Many parametric copula families with most of them having bi-dimensional dependencies are available (such as Gaussian copulas, t-copulas, Archimedean copulas, extreme-value copulas) and are based on different dependence structures and parameters. However, this study will focus on getting the copula density c and corresponding distribution C between two variables using Kernel Density Estimators (KDE).

While histogram provides the crude estimate of the PDF of a random variable based on a finite data sample, kernel density estimate provides a more effective and smoother PDF for the same data samples. Mathematically, if (x_1, x_2, x_3,…., x_n) are independent and identically distributed (*iid*) samples then PDF f using KDE is

$$f_b(x) = \frac{1}{n}\sum_{i=1}^{n} K_b(x - x_i) \tag{4.9}$$

where K is the suitable nonnegative kernel function (commonly used function are Uniform, Triangle, Biweight, Triweight, Epanechnikov, Gaussian, Cosine, and Quadratic) and $b > 0$ is the smoothing parameter called the bandwidth and, the kernel with subscript b is defined as $K_b(x) = \frac{1}{b}K(\frac{x}{b})$. This KDE can be applied to obtain the corresponding copula density c (u, v) for (U_i, V_i), i=1,…, n as:

$$c(u, v) = \frac{1}{n}\sum_{i=1}^{n} K_b(u - U_i)\, K_b(v - V_i), \qquad (u, v) \in [0, 1]^2 \tag{4.10}$$

Using KDE estimator however has a problem of putting probability mass outside of the unit square for the considerable amount such that the c (u, v) won't integrate to 1 implying it is not a density function on $[0, 1]^2$. Several approaches are proposed to mitigate this problem such as *Mirror-Reflection Technique* by (Gijbels, I. and Mielniczuk, J. 1990), *Beta Kernel Method* and, *Transformation Method* by (Geenens, G. et al. 2017).

In the mirror-reflection method, all the probability mass outside of the unit square is gathered and redistributed back to $[0, 1]^2$ i.e. the original data (U_i, V_i) are augmented by reflecting all original data points with respect to all corners and edges to obtain (U^*_{ik}, V^*_{ik}) as:

$(U^*_{ik}, V^*_{ik})_{k=1,\ldots,9} = \{(U_i, V_i), (-U_i, V_i), (U_i, -V_i), (-U_i, -V_i), (-U_i, 2-V_i), (2-U_i, V_i),$

$(2-U_i, -V_i), (2-U_i, 2-V_i)\}$.

(4.10)

The mirror-reflection estimator is then defined as the usual kernel density estimator on the augmented data as:

$$c^{MR}(u,v) = \frac{1}{n}\sum_{i=1}^{n}\sum_{k=1}^{9} K_b(u - U^*{}_{ik})\, K_b(v - V^*{}_{ik}), \qquad (u,v) \in [0,1]^2 \tag{4.11}$$

The details of a method for automatic bandwidth selection for this estimator can be found on (Nager, T. 2014).

In the beta kernel method, *boundary kernels*, whose support matches the support of the density that we want to estimate, and vary the shape of those kernels depending on the point where density shall be estimated are used. One of the examples of such kernel is Beta(p, q)-distributed random variables as kernels, where the shape parameters vary with each data point. The resulting estimator of the copula density c can thus then be written as follows:

$$c^{\beta}(u,v) = \frac{1}{n}\sum_{i=1}^{n} \beta\left(U_i;\, \frac{u}{b_n} + 1, \frac{1-u}{b_n} + 1\right) \beta\left(V_i;\, \frac{v}{b_n} + 1, \frac{1-v}{b_n} + 1\right), (u,v) \in [0,1]^2 \tag{4.12}$$

where $\beta(\cdot\,; p, q)$ is the density of a Beta(p, q)-distributed random variable and the details of a method for automatic bandwidth selection for this estimator can be found on (Nager, T. 2014).

The idea behind the transformation method is to first transform the initial copula data supported on [0, 1] through the probit function (i.e. quantile function of the standard normal CDF (Φ^{-1})) so that it is supported on the full $\cdot^2$. The density of this transformed data is estimated using KDE and thus an estimate of the initial density on [0, 1] is obtained by back-transformation. Towards TLL2nn, first, define S = $\Phi^{-1}(U)$ and T = $\Phi^{-1}(V)$ transformed variables that follow standard normal distributions and by Sklar's theorem:

$$\mathrm{c}^{T}(u,v) = \frac{f_{ST}\left(\Phi^{-1}(u), \Phi^{-1}(v)\right)}{\phi(\Phi^{-1}(u))\phi(\Phi^{-1}(v))}, \qquad (u,v) \in [0,1]^2 \tag{4.13}$$

where superscript (T) refers to the idea of transformation and f_{ST} is the local likelihood estimator with nearest-neighbor bandwidths.

The option of using any of these techniques and estimating copula density using the copula data (U, V) is provided by an R package "kdecopula" by (Nagler, T. 2018) and is utilized by this study (default method) to get the copula density c (u, v) and dependence measure, $\tau(X, Y)$. The default method within the package is the *Transformation Method* with Local Likelihood (local log-quadratic, p=2) density estimator using nearest-neighbor bandwidth selection procedure (TLL2nn) as devised by (Geenens, G., Charpentier, A. and Paindaveine, D. 2017).

From the defined package, the copula density between resilience and each system parameter can be obtained. And, the exploratory plots for the tail dependencies or multi-modal joint distribution, the surface plot, contour plot, and marginal normal contour plot (i.e. contour plot of the copula density when combined with standard normal margins) of all the copula densities are generated. As such, marginal normal contour plot is the most useful plot to visualize because in the contour plot, contour lines near to the corners become too close to be visually distinguishable thus hiding the tail behavior and marginal normal contour plot overcomes this issue by transforming the margins making the transformed copula density bounded.

If variables are independent, then the marginal normal contour plot of the copula is a perfect concentric circle. With increasing dependencies, the circles will deform. Among important visual signatures, they include that first, if the two variables have tail dependencies, the distorted circle will take the diamond-like shape at the corner of the contours. For example, the contour plot of the t copula as shown in Figure 4.5a shows both the upper and lower tail dependencies and, Gumbel copula and Clayton copula as shown in Figure 4.5b and 4.5c shows

the upper tail and lower tail dependencies respectively. Second, the multiple concentric shapes within the contour plots of the copula density denote a multi-modal joint distribution between two variables.

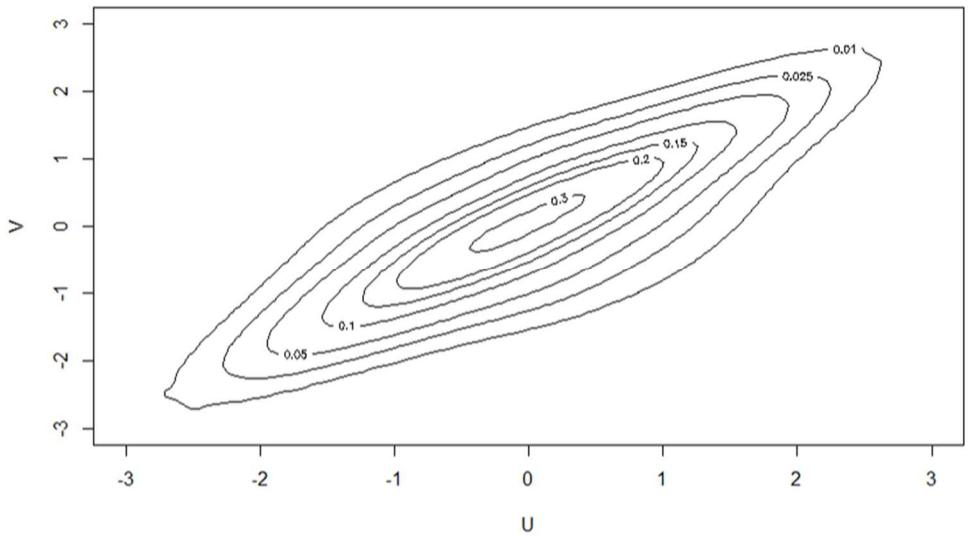

(a)

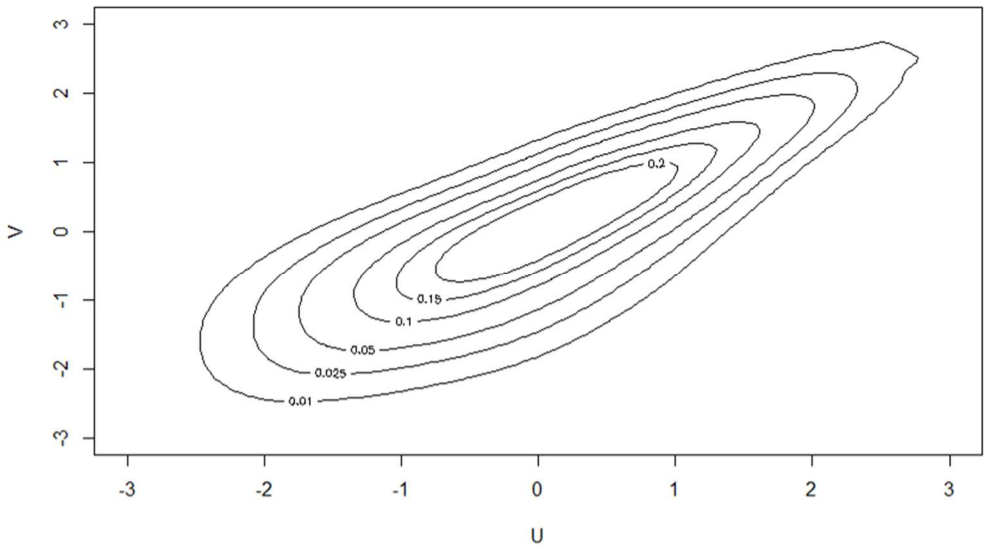

(b)

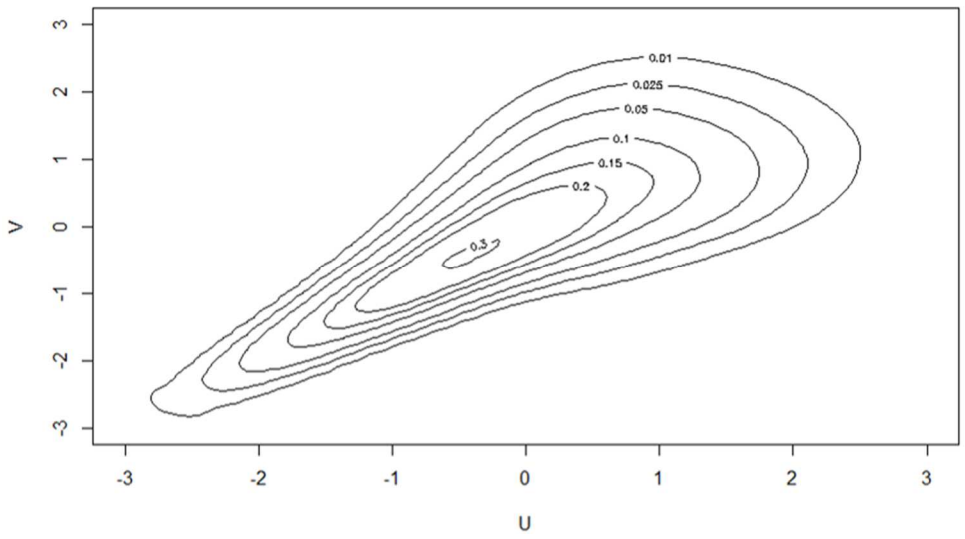

(c)

Figure 4.5 Marginal normal contour plots for a. t copula b. Gumbel copula and c. Clayton Copula

While marginal normal contour plot helps us visualize the dependencies, correlation coefficient quantifies the dependencies, the concept of tail dependence helps to analyze the dependencies between extreme values between variables. As such the upper and lower tail-dependence coefficient termed as λ_U and λ_L respectively for bivariate copula C(U, V) between two random variables X_1 and X_2 defined by (Joe, H. 1997) is given as:

$$\lambda_U \coloneqq \lim_{p \downarrow 0} P\{U > 1 - p | \, V > 1 - p\} = \lim_{p \downarrow 0} \frac{C(1-p,1-p)}{p} \tag{4.14}$$

$$\lambda_L \coloneqq \lim_{p \downarrow 0} P\{U < p | \, V < p\} = \lim_{p \downarrow 0} \frac{C(p,p)}{p} \tag{4.15}$$

Using the above definitions above, various multivariate versions of tail dependence parameters have been introduced and studied in (KLÜPPELBERG, C. et al. 2008; Li, H. 2009; Schmid, F. and Schmidt, R. 2007; Schmid, F. and Schmidt, R. 2007) in which the (Schmid, F. and Schmidt, R. 2007; Schmid, F. and Schmidt, R. 2007) proposed the non-parametric estimation of copula and corresponding tail dependence coefficients. Thus, towards calculating the

coefficients of tail-dependence, the function "fitLambda: Non-Parametric Estimators of the Matrix of Tail Dependence" from the R package "copula" (Marius Hofert, I. k., Martin Maechler, Jun Yan, Johanna G. Neslehova, Rebecca Morger 2020) is used. The function adopts the methodology proposed by (Schmid, F. and Schmidt, R. 2007) for estimating the non-parametric tail dependencies coefficients.

Towards numerical simulations, the J =10000 sets of input sample generated and TMSR calculated towards generating unconditional CDF in sensitivity analysis is utilized. The empirical CDF of TMSR, Aging, κ_1, and κ_2 denoted as U, V_1, V_2, and V_3 respectively is then obtained using the rank transformation method. Now, using the "kdecopula" package in R, the copula density c(u,v_1), c(u, v_2), and c(u,v_3) is obtained and Kendall's correlation coefficient (τ) between TMSR and input parameters are obtained on substituting the value of corresponding c(u,v) on Equation 4.5 and is summarized in Table 4.2. Figure 4.6 (a) is the surface plot of the copula density among TMSR and aging denoted as c(u,v_1), and Figure 4.6 (b) is the contour plot. As seen in Figure 4.6 (b) the density is not reasonably visualized on the whole $[0, 1]^2$ as the densities are exploding at the corners. This thus is hiding the visualization of tail information and is overcome by using the marginal normal contour plot as shown in Figure 4.6(c).

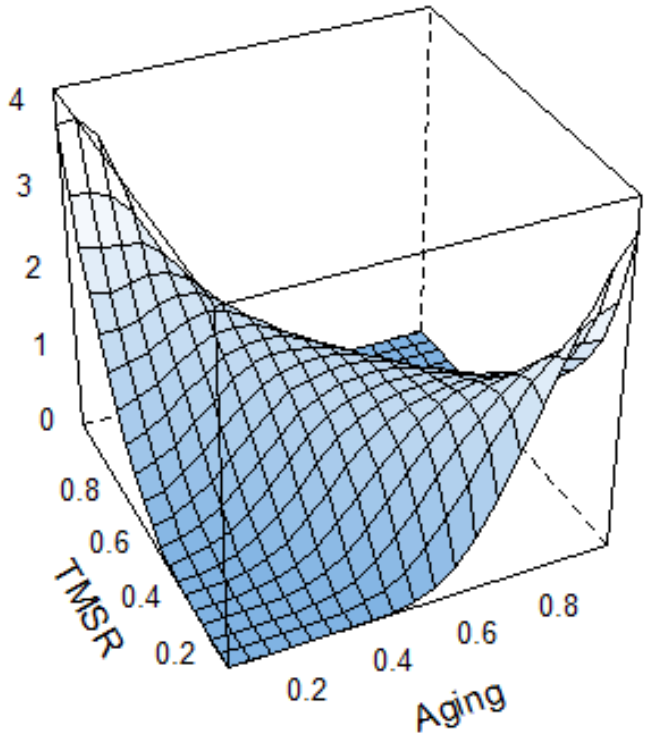
4
3
2
1
0
0.8
0.6
0.4
0.2
TMSR
0.2
0.4
0.6
0.8
Aging

(a)

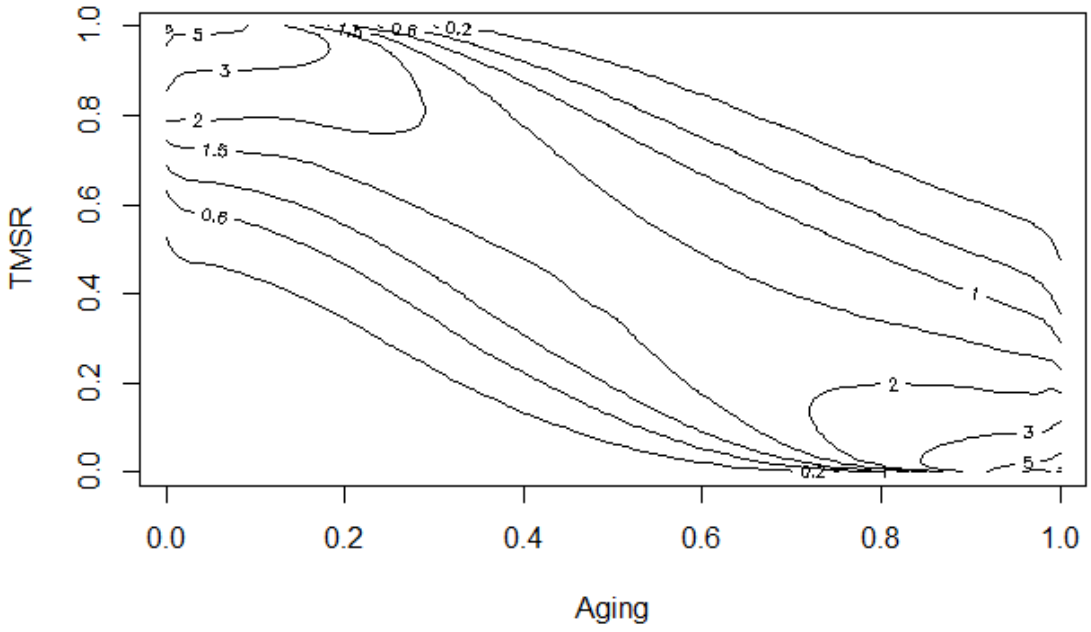
5
3
2
1.5
0.6
0.2
1
2
3
5
TMSR
0.0
0.2
0.4
0.6
0.8
1.0
Aging

(b)

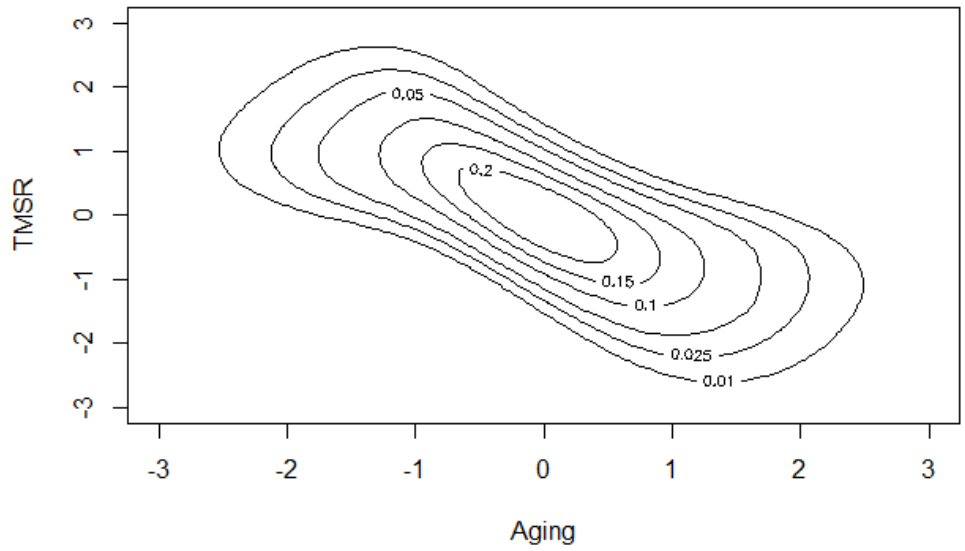

(c)

Figure 4.6 (a) surface plot (b) contour plot and (c) marginal normal contour plot of the copula between aging and TMSR (c(u, v_1)).

Clearly, the contour plot from Figure 4.6 (c) shows the dependencies however not tail dependencies. The upper and lower tail dependencies are found to be null between the TMSR and Aging. The summary of the dependence and tail dependence of TMSR to G, κ_1, and κ_2 are summarized in Table 4.2. Similarly, the copula density plot for TMSR to κ_1 and κ_2 respectively are shown in Figure 4.7 and Figure 4.8.

Table 4.2. Kendall's correlation coefficient (τ) and tail dependencies of TMSR to G, κ_1, and κ_2

	τ	Lower Tail dependence	Upper Tail dependence
Aging (G)	-0.57	0	0
κ_1	0.39	0.425	0.398
κ_2	0.43	0.463	0.429

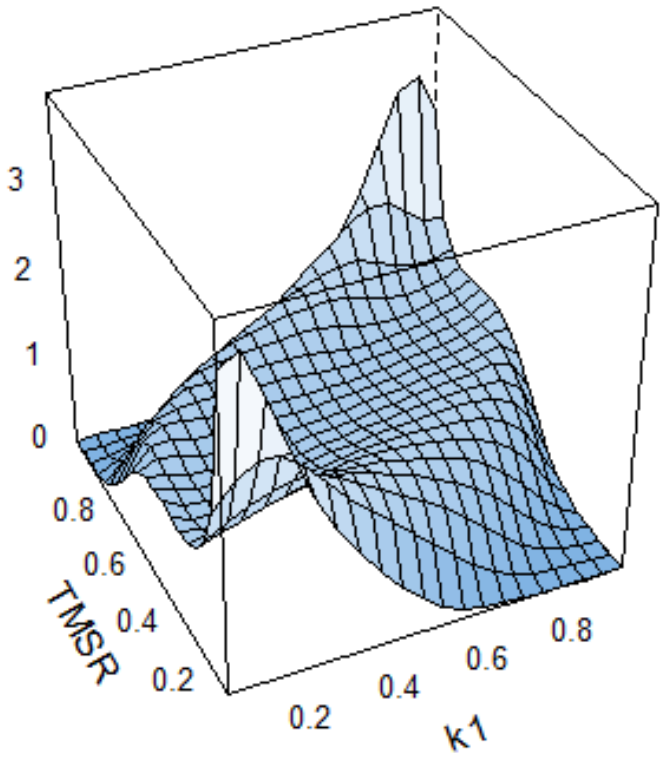
3
2
1
0
0.8
0.6
0.4
0.2
TMSR
0.2
0.4
0.6
0.8
k1

(a)

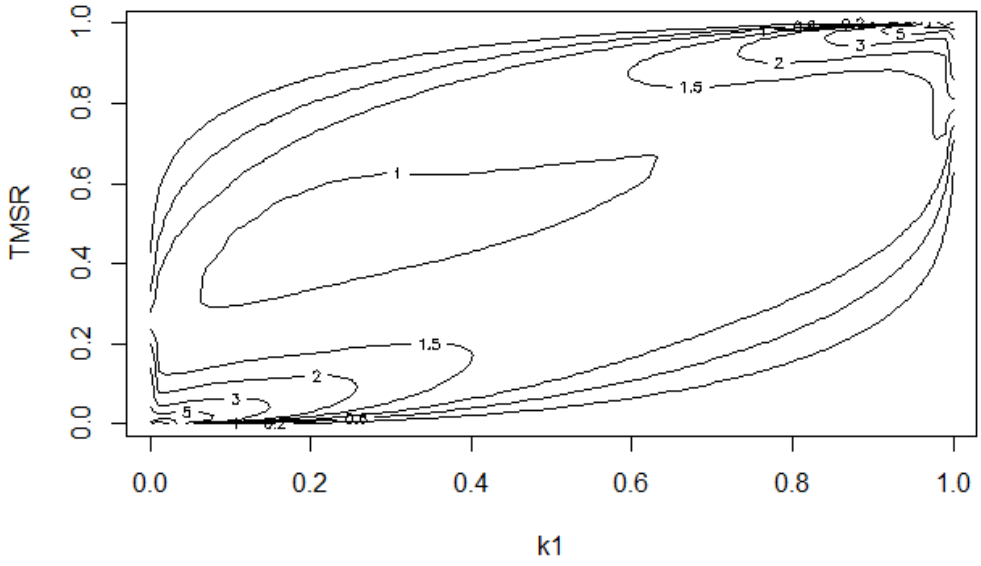
TMSR
0.0
0.2
0.4
0.6
0.8
1.0
k1
1
1.5
2
3
5

(b)

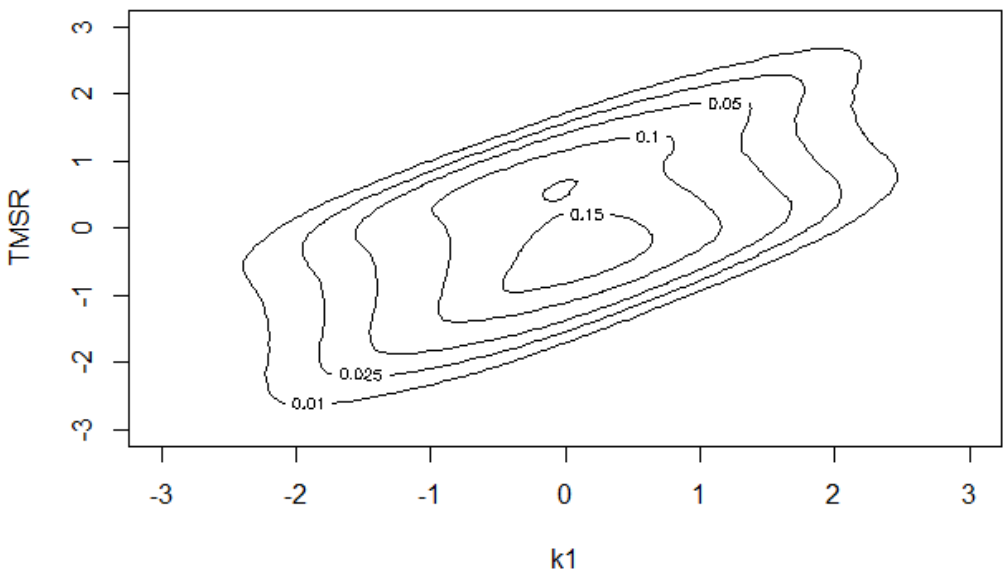

(c)

Figure 4.7 (a) surface plot (b) contour plot and (c) marginal normal contour plot of the copula between κ_1 and TMSR (c(u, v_2)).

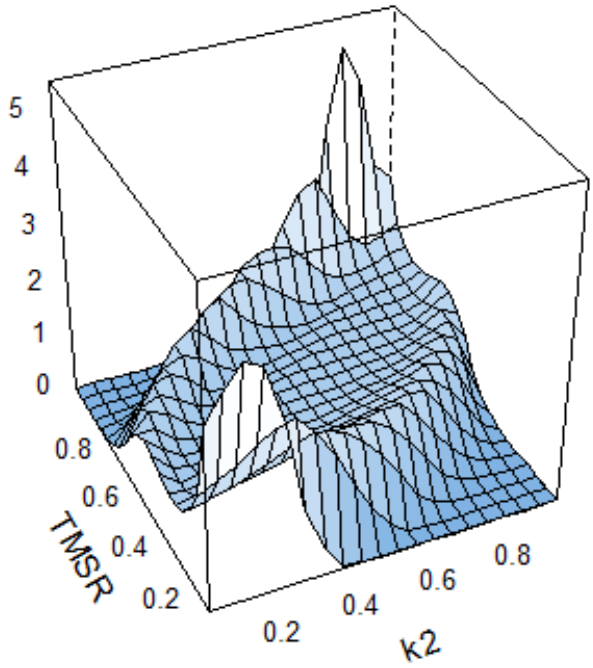

(a)

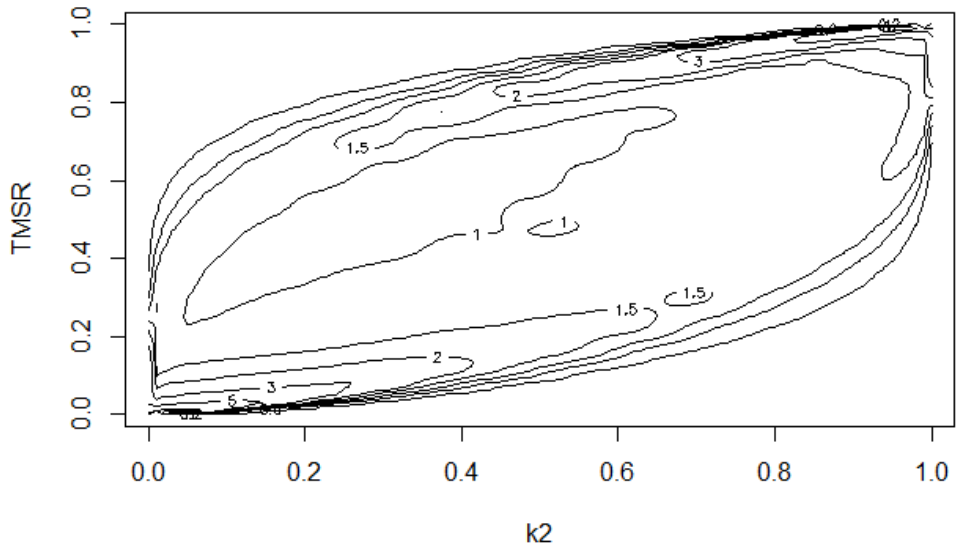

(b)

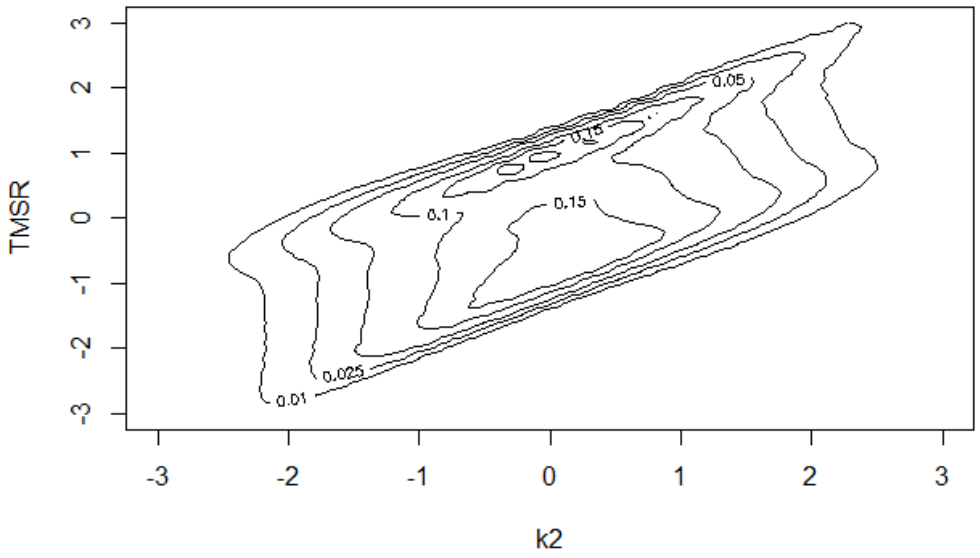

(c)

Figure 4.8 (a) surface plot (b) contour plot and (c) marginal normal contour plot of the copula between κ_2 and TMSR (c(u, v_3)).

The multimodal density function is observed for c(u, v_2) and c(u, v_3). TMSR is more dependent on G κ_2 followed by κ_2 and κ_2. Similarly, TMSR has higher tail dependencies with

κ_2 and zero tail dependencies with aging. It is thus inferred that despite lower age, the system is more prone to less resilience if resources for recovery are low, and even if the system is highly aged the system can achieve high resilience with high resources for recovery.

CHAPTER 5. PROBABILISTIC RESILIENCE DISTANCE MEASURE AND HYPOTHESIS TESTING

5.1 Introduction

After the concept of resilience was first introduced by Holing (Holling, C. S. 1973), researchers in social and engineering sciences have conducted extensive studies for quantifying the social, economic, environmental, technical resilience of infrastructure systems or communities when reacting to manmade or natural disruptions. The abundance of such studies has yielded various definitions of resilience with different statements depending on the systems of concern and the application context (Cimellaro, G. P. 2016). Nonetheless, most definitions converge to describing the notion of resilience as the ability of a physical asset or a community to recover to be fully functional from an extreme event with the loss of part or full functionality (Renschler, C., Frazier, A., Arendt, L., Cimellaro, G., Reinhorn, A. and Bruneau, M. 2010). In the meantime, many quantitative and qualitative approaches exist to date for measuring the resilience of infrastructure and community (with spatial extent from metro areas to country) and, depending on the methodologies, these available assessment approaches can be distinguished into four categories, including Indices, Scorecards, Models and Tools (Cutter, S. L. 2016). Indices [e.g. Community Resilience Index (CRI) (Sherrieb, K. et al. 2010) and, Rural Resilience Index (RRI) (Cox, R. S. and Hamlen, M. 2015)] are the statistical approach in which mostly the quantitative observations or measurements of resilience indicators are aggregated into a single numeric value often by (weighted) average or (weighted) sum. While indices mostly use quantitative data to derive the index value, scorecards [e.g. San Francisco Planning and Urban Research Association (SPUR) (SPUR 2009) and Coastal Resilience Index (CoRI) (Sempier, T. T. et al. 2010) are based on qualitative assessments of resilience indicator

using checklists or questionnaire for which the answers can be dichotomous or multiple choices, statistical values (e.g. counts, percentages, rates, medians), judgments or perceptions. These answers are later assigned with numerical values (1-10) or grades (A-F). Models however use mathematical algorithms and scenario analysis to simplify complex relationships between various dimensions and properties of resilience and, overcome uncertainties and limitations of the nature of the hazard and associated impact. Data obtained from indices and scorecards can be the input to the mathematical algorithms. Lastly, tools are combination of either one or all of above mentioned three categories that provides guidance for assessing resilience with sample procedures and data. The review of these tools/toolkits can be found in (Sharifi, A. 2016).

Resilience-based system quantification model has been witnessed for different categories of infrastructure systems or structures considering different hazards. Cimellaro et al. quantified the seismic resilience of hospital networks using a comprehensive framework that combined economic loss and recovery models (Cimellaro, G. P., Reinhorn, A. M. and Bruneau, M. 2010). One key element of measuring the resilience of a hospital is to define its functional performance as a mathematical function of disruption and recovery. In Cimellaro and Piqué (2016), the waiting time was recognized as the performance parameter against seismic events for medical emergency departments (Cimellaro, G. P. and Piqué, M. 2016). Probabilistic evaluation of the level of damage and the use of a sinusoidal function of time and cost required for rehabilitation were employed to assess the seismic resilience of bridges (Decò, A., Bocchini, P. and Frangopol, D. M. 2013). Sharma et al. used the mathematical approach analogous to probability theory to develop the resilience metrics that quantified the

resilience of engineering systems mainly focusing on the recovery process and was applied to reinforced concrete bridges (Tabandeh, A. and Gardoni, P. 2018).

Despite all these efforts to develop resilience assessment models that can be utilized to majority infrastructure systems, Haimes in (Haimes, Y. Y. 2009) cautioned that given the probabilistic nature of threats and time-variant inherent characteristics of any system, the use of specific numerical descriptor as resilience and comparing it to a different system could be misleading. Only a few studies can be found that quantified resilience comparatively through hypothesizing the standards of the same system resilience. For instance, Chang and Shinozuka in (Chang, S. E. and Shinozuka, M. 2004) predefined the performance standards for robustness and rapidity, then quantify the resilience as the probability of meeting both robustness and rapidity standards for an event. However, the study did not unify the intrinsic dimensions and properties of resilience for comparing the resilience measurements. Hence, the author in this study recognize that critical gaps are the lack of a theoretical basis that can discriminate relatively that how a parametric infrastructure system is more or less resilient when subject to some changed conditions. Therefore, besides measuring the resilience of one system, an objective resilience comparison standard, or more precisely, *a resilience distance measure* between two systems for a given resilience framework is not found in the literature to date.

This chapter thus makes the following contribution to resilience quantification for civil infrastructure systems. First, statistical or information-theoretic resilience-distance (RD) measures, including strictly defined mathematical metrics, are proposed, which answer how a calculated resilience differs when compared to a reference or target system's resilience. Non-parametric two-sample tests are conducted to verify the effectiveness of these measures. More significantly, a resilience aggravation analysis (RAA) model is proposed in this paper for

objectively characterizing how system resilience dynamically varies with critical resilience parameters (such as aging and resourcefulness). Second, using the most suitable resilience distance measures coming from the RAA model, the hypothesis testing is performed to test if the Resilience distribution of the system is similar and acceptable when compared to the targeted resilience distribution of the same system using the non-parametric two-sample test.

The experimental evaluation using the proposed resilience measurement framework in Chapter 3, this section proves the effectiveness of the proposed RD measures, RAA modeling, and hypothesis testing.

5.2 Resilience Measures, Metrics, and Quantification

5.2.1 Resilience Measures and Metrics

In the literature of community or infrastructure system resilience, the terms of *resilience measures or metrics* are commonly used. In many cases, they are interchangeable; sometimes, researchers differentiate them. The authors provide a summary of these usages.

Calling it a *metric* in the literature of system resilience may first arise from the practice of social sciences; on the other hand, the social dimension is indispensable that constructs the space of community resilience. In social sciences, if an objective attribute or a measurable notion can be assigned to an entity, it is then acceptable to call the attribute or notion a *metric.* In this sense, it is closely aligning to a mathematical measure (except the latter needs to satisfy a set of three properties). Typical examples in social studies include literacy rate, poverty rates, average life-expectancy increment, or decrement. *Scorecards,* one of the main categories (among *Indices*, *Scorecards Models*, and, *Tools*) as described above for assessing resilience is a fitting example. In social sciences, a metric can be too treated as a high-level attribute of an entity. A representative explanation can be found in a report by the National Institute of

Standards and Technology (NIST 2016). As such, when NIST proposes to measure community resilience, the following high-level attributes are treated as *metrics*: Recovery Times, Economic Vitality, Social Well-being, Environmental protection towards fewer vulnerabilities and risks, Hybrids (combination of other metrics beyond the four aforementioned attributes), and others given that these metrics can track the situation of the community and help decision-makers understand the implications of the decision at the micro-level.

The confusion further comes from in practice or physical sciences, a metric is treated as a system or standard for measuring something; whereas a measure is a numerical observation. In this context, a metric can be a physical device (e.g., a ruler or a scale for measuring or weighing). Given this practice, a metric can be extended to include a method or process that can be utilized to obtain a measurement. This practice is seen in the literature on community resilience, a recent review that summarizes the major tools, software, models/framework, indices and, scorecards that can be used to *measure* (quantify or assess) community resilience as the resilience metrices (Johansen, C., Horney, J. and Tien, I. 2017). Under this treatment, measures become specific quantities that can be measured by or included in the resilience metric. Notable examples include Community Resilience System (CRS) developed by (CARRI) (CARRI 2011), CRI, CoRI, SPUR, HAZUS-MH, a tool created by FEMA (FEMA 2008) and, Vulnerability-Resilience Indicators Model (Moss, R. et al. 2001).

5.2.2 Mathematical Measures and Metrics

With the proposed notion of resilience distance measures in this paper, considerable confusion may arise. Given the quantitative nature of the resilience quantification efforts, especially for physical assets such as civil structures and infrastructure, one needs to understand the difference between a mathematical measure and a metric.

In mathematical analysis, a *measure* on a set is defined as a non-negative function that assigns a real number to the total set or its subsets. In simple physical instances, it can be the size (e.g. area, length, volume) of the subset. From this point of view, the geometric area- or length-based resilience calculation should be treated as a measure, and a quantity achieved can be termed a resilience measurement. In probability theory, the most essential measure is the *probability measure* on a set (subset) of events, which is more commonly called a *probability distribution*. When one obtains many measurements over a scenario of possible events (disruption and restoration), a resilience distribution as a probability measure can be formed as well.

A probability measure is often considered sufficient in characterizing a variable (denoted by *X*). For example, one can formulate its moments at different orders, including its mean and variance (namely, E[*X*] and Var[*X*]) based on the distribution *P*[*X*]. However, if two random variables, *X1* and *X2,* are concerned and if one attempts to characterize the changes, the answers depend on the disruption types of *X1* and *X2*. If *X1* and *X2* are identically distributed, then one can simply use their first-order moments to characterize the changes, namely to assess if the mean difference, E[*X2*] - E[*X1*], is greater or smaller than zero. However, if such condition is not satisfied or the comparison involves parametrically many other variables, such as in reliability analysis (wherein *X1* and *X2* correspond to engineering demand and capacity), one can evaluate an integral of the joint distribution of *X1* and *X2,* $\iint_{\emptyset(X1,X2)>0} f(X1,X2)\mathrm{d}X1\mathrm{d}X2$, where $\emptyset(X1,X2)$ defines a response surface with $\emptyset(X1,X2) > 0$ defines the subspace of exceedance (where no structural failure occurs), and $f(X1,X2)$ is the joint distribution. In the simplest case, such as both *X1* and *X2* are of Normal distribution, the integration is reduced to a closed-form as a function of the mean difference,

E[*X2*] - E[*X1*]. However, this reliability-like estimation does not apply to resilience quantification, wherein there is no notion of physical exceedance that needs to be concerned, hence no need of defining its joint distribution function $f(X1, X2)$ and their response surface function$\emptyset(X1, X2)$. Instead, given their probability distribution, comparison to quantify the *distance* between the two probability measures: P(*X1*) and P(*X2*), is termed *statistical distance* measure. The authors state that when the sample data of *X1* and *X2* are available, statistical distance measures are much applicable for comparing resilience at different times or under changed parameters to see the efficacy of changes. In certainty domains, such as statistical learning or machine learning, it is often called a dissimilarity measure to emphasize the shape or distribution difference between the two objects; similar terms also include deviance, deviation, discrepancy, discrimination, and divergence.

The notion of metric comes in when the distance measure denoted as $d(X1, X2)$ satisfies a set of four strict properties (i.e., non-negativity ($d(X1, X2) \geq 0$), symmetry ($d(X1, X2) = d(X2, X1)$), the identity of indiscernible ($d(X2, X1) = 0 \leftrightarrow X1 = X2$) , and triangle inequality ($d(X1, X2) \leq d(X1, X3) + d(X3, X2)$)). The simplest or commonly used metric is the Euclidean distance, which can be calculated between a set of two vectors and two probability measures (distribution functions). Many statistical distance measures are not metrics due to lacking one or more of the four properties. The Kullback–Leibler divergence, for example, defined over two distributions, is not a metric as it is not symmetric. To this end, one fundamental difference is that a measure can be assigned to a single entity as a characteristic quantity for the entity or two entities as a distance. However, a metric should be taken as a *distance* between the two entities meeting strictly four metric properties.

In this study, the proposed resilience distance measures are strictly defined based on probability theories and statistics, which include both non-metric (except for the non-symmetric) or metric distances. However, The goal is to quantify or measure the difference of resilience of the same system with different resilience obtained by changing the parameters (such as aging and different dimensions of resourcefulness), for which a system's resilience is a random variable characterized by a probability density distribution (PDF) function. All RD measures are strictly defined between two resilience entities as represented by their PDF functions. To achieve such resilience distribution, a quantification process is indispensable.

5.3. Methods

5.3.1. Resilience Distance Measures

This framework starts with a presumption that probability distributions for the resilience of a constructed system subject to varying parameters exist in terms of continuous or discrete distributions. For the sake of simplicity and a generalization purpose, two notations, $f(x \mid \boldsymbol{p_0})$ and $g(x \mid \boldsymbol{p_1})$, are introduced to denote the resulting distributions; when cumulative distributions are needed, $F(x \mid \boldsymbol{p_0})$ and $G(x \mid \boldsymbol{p_1})$ are defined. To differentiate the underlying system parameters, they are set conditional on the parameter vectors of $\boldsymbol{p_0}$ and $\boldsymbol{p_1}$, respectively. It is noted that when expressing the testing statistics or distance measures as follows, they are treated as continuous functions. When implementing numerically, discrete histograms or empirical cumulative distributions (ECDs) are utilized. This section thus focuses on measuring how similar or far apart the $F(x \mid \boldsymbol{p_0})$ and $G(x \mid \boldsymbol{p_1})$ are using statistical distance measures and termed Resilience Distance measures (RD) herein. From here onwards, $F(x \mid \boldsymbol{p_0})$ is the probability distribution and $f(x \mid \boldsymbol{p_0})$ is the probability density for the resilience measurement of the system marked as the targeted/benchmark system by assigning a desirable high value

for $\boldsymbol{p_0}$. However, these values should be assigned with careful consideration, accounting for the sensitivity of community and system as every service has unique importance within the consumers. And, $G(x \mid \boldsymbol{p_1})$ is a probability distribution and $g(x \mid \boldsymbol{p_1})$ is the probability density measure of the resilience of the system with altered parametric values on $\boldsymbol{p_1}$ and, $x \in \mathbb{R}\,[-\infty, 1]$ is the resilience measure.

Numerous statistical distances and metrics are available in mathematics (Deza, M. M. and Deza, E. 2009) with a plethora of methodologies available to compare two histograms (Sheskin, D. J. 2000). Besides the aforementioned Euclidean distance for distributions, many simple ones exist, including the Bhattacharyya metric and the Mahalanobis metric. Among these measures, many statistical distance measures are not mathematical metrics due to the lack of one or two of the four metric properties. The information-theoretic ones, Kullback–Leibler and Jeffery divergence measures, are not metric as they lack triangle inequality. In this work, the following simple statistical distance measures are considered as candidates for resilience distance measures: Hellinger Metric (HM), Bhattacharya distance (BD), Squared χ^2-distance measure (χ^2D), and Jeffrey divergence (JD) as shown in Equations 5.1-5.4:

$$HM = \left(\frac{1}{2} * \int \left(\sqrt{f(x \mid \boldsymbol{p_0})} - \sqrt{g(x \mid \boldsymbol{p_1})}\right)^2 dx\right)^{\frac{1}{2}} \tag{5.1}$$

$$BD = -\ln\left(\int \sqrt{f(x \mid \boldsymbol{p_0}) * g(x \mid \boldsymbol{p_1})}\, dx\right) \tag{5.2}$$

$$\chi^2 D = \int \frac{\left(f(x \mid \boldsymbol{p_0}) - g(x \mid \boldsymbol{p_1})\right)^2}{f(x \mid \boldsymbol{p_0}) + g(x \mid \boldsymbol{p_1})} dx \tag{5.3}$$

$$JD = \int_0^1 (f(x \mid \boldsymbol{p_0}) - g(x \mid \boldsymbol{p_1})) * ln \frac{f(x \mid \boldsymbol{p_0})}{g(x \mid \boldsymbol{p_1})} dx \tag{5.4}$$

It is noted that HM is always bounded by [0, 1]. The value 0 suggests that two distributions are completely the same. However, value 1 suggests the complete dissimilarity of the distribution. Similarly, the BD, χ^2D measure, and JD are lower bounded by 0 and the value monotonically

increases as the dissimilarity between the probabilities measures increases. JD is the symmetric version of the Kullback-Leibler Distance and behaves like χ^2D measure. Last, for all these chosen measures, only HM measure is strictly defined metrics and the rest are non-metric distances.

For distributions that are complex, or knowledge does not exist about the types of the distributions, a number of cumulative distribution-based distance measures are commonly used in non-parametric sample testing. In this work, the authors select the commonly used Cramer-Von Misses (CVM) and the Kolmogorov-Smirnov (KS) distance measures, both of which are metrics. The analytical expression for the CVMD metric is shown in Equation. 5.5.

$$CVM = \left(\int |F(x \mid \boldsymbol{p_0}) - G(x \mid \boldsymbol{p_1})|^2 \, dx\right)^{\frac{1}{2}} \tag{5.5}$$

The Kolmogorov Smirnov (KS) metric is computed in the form a supremum operation between the cumulative distributions as shown in Equation 5.6.

$$KS = sup_R(|F(x \mid \boldsymbol{p_0}) - \mathrm{G}(x \mid \boldsymbol{p_1})|) \tag{5.6}$$

In recent years, Wasserstein distance has attracted significant attention as a good criterion for discrepancy of two probability measures in fields such as machine learning and genomics (Imaizumi, M. et al. 2019). The reason behind the attraction to various fields is because of two particular characteristics which are incorporation of ground distance on the space and clear physical interpretation as the least amount of work required to transform one probability distribution into another. Mathematically, in general for $p \in [1,\infty)$ the p-Wasserstein distance between two probability measures F, G on $\mathbb{R}$ with finite p-moments is given by:

$$W_p(F,G) = inf_{\pi \in \Gamma(F,G)}\left(\int \|x-y\|^p d\pi(x,y)\right)^{\frac{1}{p}} \tag{5.7}$$

where $\Gamma(F, G)$ is the set of all joint probability Measures on $\mathbb{R} * \mathbb{R}$ whose marginal are *F* and *G*. In the one-dimensional case, however, the *p*-Wasserstein distance is interpreted as the quantile functions F^{-1} and G^{-1} of probability distribution F and G respectively (Ramdas, A. et al. 2017) written as

$$W_p(F, G) = \left(\int_0^1 |F^{-1}(x \mid \boldsymbol{p_0}) - G^{-1}(x \mid \boldsymbol{p_1})|^p dx\right)^{\frac{1}{p}} \tag{5.8}$$

when p = 1, 1- Wasserstein distance (not limited to one dimension) is also called the Earth Mover's Distance (EMD). To understand its physical interpretation more clearly, imagine two piles of earth and the goal is to move one pile of earth to match the second. EMD is the minimum amount of work involved, where "amount of work" is the amount of earth you have to move multiplied by the distance you have to move it. Thus, EMD is a product of changes in location and frequency rather than just changes on one or the other which makes it insensitive to small changes, and therefore the formulation of one-dimensional EMD is utilized in this study. It can be seen from Equations 5.5 and 5.8 that the relationship between the CVMD and EMD is analogous to that of the L1 and L2 norms and thus while EMD is more robust i.e. it is more able to ignore extreme values, CVMD is more stable. Unlike CVMD and EMD, KSM does not include the ground distance but the maximum of the absolute difference between the two empirical CDFs which makes KSM more sensitive to small changes or local deformations. However, KSM is always bounded by [0,1] which makes it easier to interpret the distance but also, on the other hand, its use will be limited to those distributions that are comparatively not far apart.

5.3.2. Resilience Attenuation Analysis Modeling

Resilience attenuation analysis focuses on selecting the RD measures as proposed in section 3.1, that can effectively capture the dissimilarity of resilience with an altered set of

parameters. To proceed, it is assumed that $F(x \mid \boldsymbol{p_0})$ with the variable parameter set $\boldsymbol{p_0} \in \mathcal{R}^n$ is the target resilience distribution of the considered infrastructure system, and the $G(x \mid \boldsymbol{p_1})$ ($\boldsymbol{p_1} \in \mathcal{R}^n$) is the reference system resilience.

The fundamental assumption for performing the RAA is that $F(x \mid \boldsymbol{p_0})$ represents a perfect resilience system. Therefore, it is expected that as system parameters in $\boldsymbol{p_1}$ become more adversarial (such as due to higher-intensity hazard, aging and other hazardous conditions), the resilience will attenuate and the RD measure between $G(x \mid \boldsymbol{p_1})$ and $F(x \mid \boldsymbol{p_0})$ will increase. This notion is analogous to the concept of distance decay, which states that as the distance between two entities or locales increases, their relativity or interactivity decreases. Geometrically, a curve line swooping concavely downward can be used to represent the distance decay as the distance along with the x-axis increases whereas. Mathematically, the distance decay is often expressed as a negative exponential. In this study, a negative exponential expression of $I = e^{-d}$ is adopted as shown in Equation 5.9, where I is a measure of resilience interaction, d is the RD measure, and the x-axis can be one of the causal parameters in $\boldsymbol{p_1}$.

$$I\left(F, G\middle|\boldsymbol{p_{1}}_{i,j}\right) = e^{-d\left(F, G\middle|\boldsymbol{p_{1}}_{i,j}\right)}, \forall\, i = 1,2 \ldots n \text{ paramters in } \boldsymbol{p_1} \text{ and, } j = 1, \ldots N \text{ sample values of parameter } i \tag{5.9}$$

This distance decay curve for through comparing is thus termed as Resilience Attenuation Curve (RAC) and is obtained for all possible n parameters in $\boldsymbol{p_1}$, using all 7 RD measures proposed on section 3.1resulting 7n resilience attenuation curves (RACs). The RD measure for which all n RAC curve swoop concavely downward is thus considered to be the appropriate RD measure as it captured the resilience degradation as the values of any of the system parameters degrades evidently from curve swooping downward.

5.3.3 Nonparametric Two Sample Test

In statistics, a two-sample test is to determine whether the difference between two populations, represented by the corresponding distributions, is statistically significant. As mentioned above, such as two distributions, denoted as $F(x \mid \boldsymbol{p_0})$ and $G(x \mid \boldsymbol{p_1})$, or short as F and G, respectively, it is assumed that F is the target resilience and G is the resilience of concern subject to variable system parameters. Formally, the test is to determine if the difference between the two distributions is statistically significant to reject the null hypothesis H_0: $F = G$ against its alternative H_1: $F \neq G$. Given two resilience distributions F and G, then the rejection of the null hypothesis means that the variable resilience of the system is not acceptable when compared to the targeted resilience. This test then becomes a valuable tool for decision-making that tells if the variable system should be enhanced until the null hypothesis is accepted.

In statistics, given a data sample, parametric methods can be used to fit the data and a distribution type is determined (e.g., to fit a Normal or a Lognormal distribution to the data); hence, parametric tests (e.g., Z test, Student's t-test, and Fisher's F Test). However, in many practical situations, this normality cannot be met. Therefore, non-parametric statistical techniques become necessary, the use of empirical histograms or ECDFs is the simplest approach to understanding the data. As will be confirmed later in this work, resilience distributions in terms of histograms or ECFs demonstrate significant nonparametric characteristics. Therefore, non-parametric two-sample tests are adopted (Sheskin, D. J. 2000). Nonparametric tests are also called distribution-free tests as they do not rely on any underlying mathematical distribution such as assumption of normality or the equal variances and also the test is not to compare the population parameter (such as location, dispersion, shape).

Given two empirical distributions, F and G, the test is performed by calculating two variables: a test statistic and a p-value. The test statistic, often a statistical distance metric, is calculated based on two distributions, measuring the degree of dissimilarity between them. And, based on p-value, the decision is made to support or reject the null hypothesis. The p-value is the probability value that tells how likely the data could have occurred under the null hypothesis. It does so by calculating the likelihood of the test statistic assuming that the null hypothesis is true i.e. the probability of finding the observed, or more extreme, test statistic in the null distribution. And, the null distribution is the probability distribution of the test statistic given the null hypothesis is true. Given the test statistic and p-value, the null hypothesis is rejected if the obtained p-value is lesser than the assigned significance level (a). The significance level is the probability of the study rejecting the null hypothesis given that the null hypothesis is assumed to be true. This significance level is assigned before the testing and is usually 5 %.

The literature on non-parametric two-sample testing is abundant. The Kolmogorov-Smirnov (KS) test has been the standard technique (Lehmann, E. L. 2006). This test is based on the KS statistic, namely, the KS distance defined in Equation 5.6. Because of this supremum function, the KS statistic is sensitive to small deformations; for example if the local deformation is introduced by accumulating the mass around a single point, the KS distance will be highly affected such that the accuracy of KS test is compromised. The Cramer Von Misses (CVM) test is considered a better alternative as the CVM test statistics uses the joint distribution of the samples (Hodges, J. L. 1958). Recently, the Earth Movers Distance (EMD) test or the Wasserstein-distance test gains high popularity, partially due to the wide adoption

of the corresponding distance metric in the literature of machine learning and computer vision where complex and non-parametric distributions are commonly encountered.

In this framework, the authors recommend the use of KS, CVM, and EMD tests to conduct the two-sample tests. The test statistic or equivalently the distance metrics for the three tests are introduced later as the core types of resilience-distance measures. In addition, the *p*-value selection is a critical step. For an approximation of the p-value, the permutation testing method introduced by R.A. Fisher in the 1930s, is applied (Fisher, R. A. 1936). Permutation test also called a randomization test is based on the assumption that under the null hypothesis, data observation from two sets are exchangeable such that new, equally likely data sets can be generated. Thus, the two sets of observed data are shuffled or permuted, and new data sets are generated from the pooled data. The test statistic is then calculated for this resampled data sets. After some sufficient number of permutations and calculating test statistic for each such data sets, null distribution is created. The p-value is thus obtained by observing where our initial test statistic falls within this distribution. It is noted that unlike bootstrapping, permutation resample the data without the replacement.

5.4. Application to Rural Electric Distribution System

5.4.1 Resilience Measures Quantification

The probabilistic resilience measurement framework proposed in Chapter 3 with numerical rural electric distribution system configuration will be utilized in this chapter. However, the addition is the uniform distribution of each resourcefulness dimension such that Equation 3.15 yields the matrix of R_{sys} (κ, A_m). From this resulting matrix, R_{sys} (κ, A_m), the probability density of resilience of the system denoted as $f(R_S)$ will be obtained by

marginalizing the affected customers using the law of total probability and the procedure of which is summarized in the following steps:

1) For each event m, the values of $R_{sys}(\kappa, A_m)$, are sorted within the specified bin-array of resilience measure ($R_s \in \mathbb{R}$ (-∞, 1]) and obtain the frequency counts. The counts are then normalized to get the probability density of resilience conditional to A_m and is denoted as $p(R_s|A_m)$.

2) The probability density of the resilience for a given system denoted as $f(R_s)$ is hence calculated as:

$$f(R_s) = \sum_m p(R_s|A_m) * P_{AC}(A_m) \tag{5.10}$$

From $f(R_s)$, total-mean system-resilience resilience denoted as *Res* can be further calculated as shown in Equation 12:

$$Res = \sum R_s * f(R_s) \tag{5.11}$$

And, if required variance can also be calculated as: $\sum(R_s - Res)^2 * f(R_s)$..

Then, to apply the proposed resilience-distance and nonparametric two sample testing framework, various sample systems are assumed including a benchmark system. The benchmark system (S_B) is newly constructed (e.g., in-service less than five years); in the meantime, very high resourcefulness values are considered. Such a system is taken as a reference system; in practice, any other system should statistically have less resilience. For others systems S_I, S_{II}, and S_{III}, the aging is increased but the value for the resourcefulness dimensions is kept constant when compared to the benchmark system. Similarly, for systems, S_{IV}, and S_V aging is kept constant with decreased resourcefulness dimensions when compared to the benchmark system. However, for the systems S_{VI} and S_{VII} the aging increases and resourcefulness decrease. Table 5.1 summarizes the parameters taken for these systems. For

all these systems, five sectionalizer are assumed to be present at the 42nd, 84th, 127th, 169th pole and, on 211th pole, respectively.

Table 5.1. Parameters considered for Benchmark and other systems

System	Aging	R_{SE}	R_{OP}	R_T
S_B	Not aged (<5 years)	*unif (0.92, 0.98)*	*unif (0.95, 0.98)*	*unif (0.85, 0.98)*
S_I	20 years	*unif (0.92, 0.98*	*unif (0.95, 0.98)*	*unif (0.85, 0.98)*
S_{II}	30 years	*unif (0.92, 0.98)*	*unif (0.95, 0.98)*	*unif (0.85, 0.98)*
S_{III}	60 years	*unif (0.92, 0.98)*	*unif (0.95, 0.98)*	*unif (0.85, 0.98)*
S_{IV}	Not aged	*unif (0.70, 0.88)*	*unif (0.65, 0.85)*	*unif (0.75, 0.83)*
S_V	Not aged	*unif (0.45, 0.79)*	*unif (0.55, 0.79)*	*unif (0.40, 0.79)*
S_{VI}	20 Years	*unif (0.7, 0.88)*	*unif (0.65, 0.85)*	*unif (0.75, 0.83)*
S_{VII}	20 Years	*unif (0.7, 0.88)*	*unif (0.65, 0.85)*	*unif (0.95, 0.98)*
S_{VIII}	25Years	*unif (0.7, 0.98)*	*unif (0.62, 0.98)*	*unif (0.45, 0.98)*

For all these assumed parameters the resilience is calculated using Equation 5.10 and, methodology and the numerical configuration as described in Chapter 3. Table 5.2 below summarizes the total-mean system-resilience calculated using Equation 5.11.

Table 5.2. Total-mean system-resilience of all the systems considered

System	S_B	S_I	S_{II}	S_{III}	S_{IV}	S_V	S_{VI}	S_{VII}	S_{VIII}
Res	0.6102	0.5810	0.5109	0.3025	0.4424	0.3701	0.4431	0.5022	0.3836

The *Res* value of S_I, S_{II}, and S_{III} systems decrease when compared to the B system and each other consecutively as the aging increases with constant κ as summarized in Table 5.2. This decrease is also evident in Figure 5.1(a) (probability density) and 5.1(b) (probability distribution) of resilience measures for the B, S_I, SII, and SIII systems wherein the curve shift consecutively towards the left tail of the B as the aging increases.

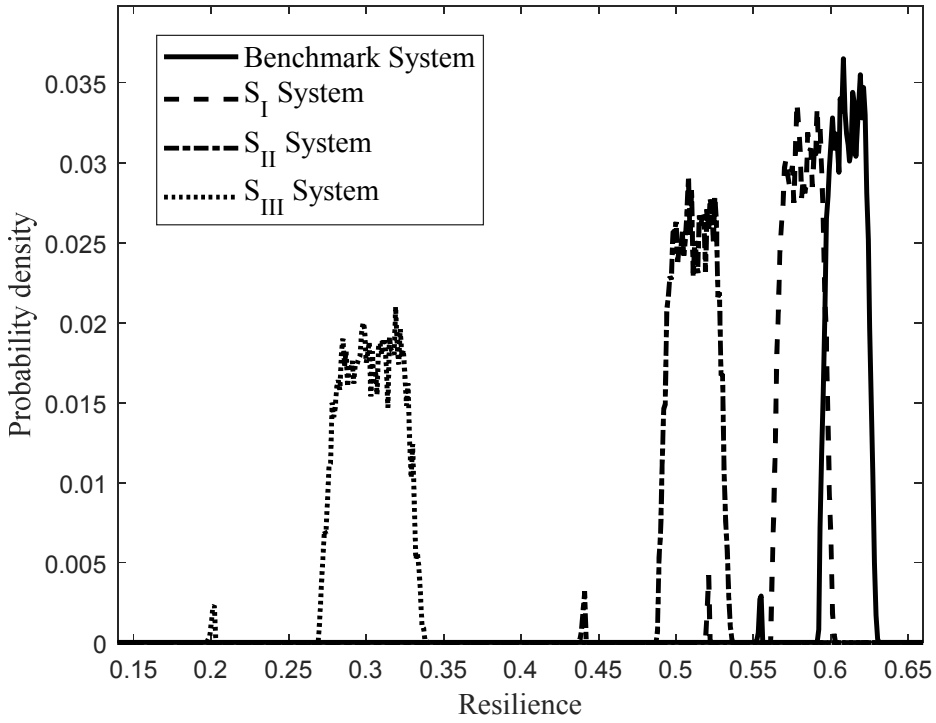
Benchmark System
S_I System
S_II System
S_III System
Probability density
Resilience
0
0.005
0.01
0.015
0.02
0.025
0.03
0.035
0.15
0.2
0.25
0.3
0.35
0.4
0.45
0.5
0.55
0.6
0.65

(a)

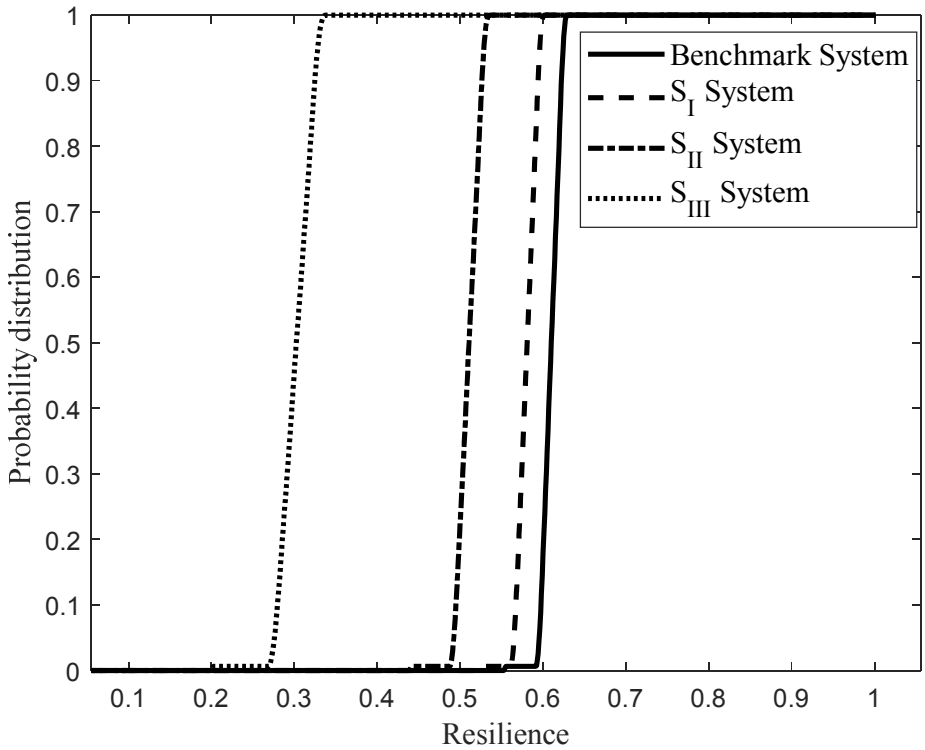
Benchmark System
S_I System
S_II System
S_III System
Probability distribution
Resilience
0
0.1
0.2
0.3
0.4
0.5
0.6
0.7
0.8
0.9
1
0.1
0.2
0.3
0.4
0.5
0.6
0.7
0.8
0.9
1

(b)

Figure 5.1. (a) Probability density and (b) Probability distribution for the resilience measures of S_B, S_I, S_{II}, and S_{III} systems.

Similarly, the *Res* value of S_{IV} and S_V systems decreases when compared to the B system and each other consecutively as each dimension of κ decreases with constant G as summarized in Table 5.2. Probability density and probability distribution for resilience measure of B, S_{IV} and, S_V systems are shown in Figure 5.2 (a) and 5.2(b) respectively and resilience is multimodal for S_V system.

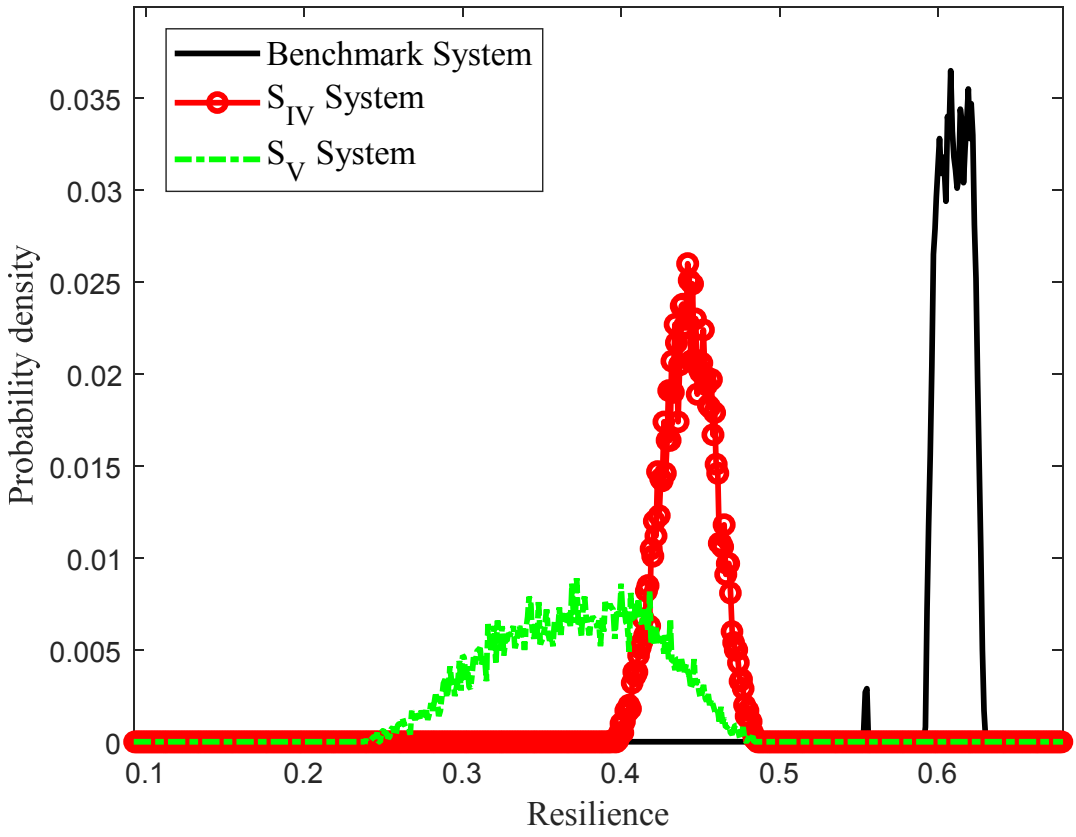

(a)

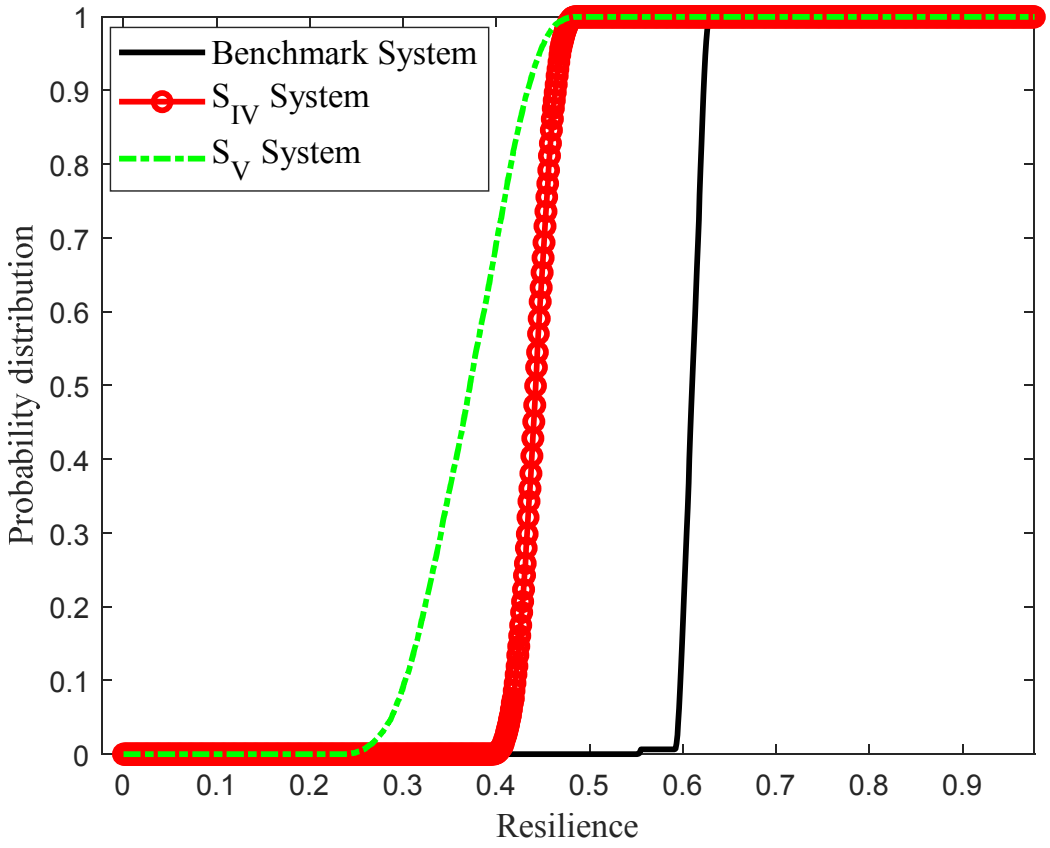

(b)

Figure 5.2. (a) Probability density and (b) Probability distribution for the resilience measures of S_B, S_{IV} and, S_V systems.

For systems S_{VI} and S_{VII} as well in which G is increased and κ decreased when compared to S_B, Res is decreased as summarized in Table 5.2. It is also noted that systems S_{VI} and S_{VII}, when compared to S_I have the same G but decreased κ and Res value is decreased which is evident in Figure 5.3(a) and 5.3(b) where probability density and distribution respectively for resilience measures of S_{VI} and S_{VII} shift to left tail from B and S_I. However, system S_{VII} in which the value of R_T is increased, *Res* is higher when compared to S_{VI} but still lower than S_I since the value of other dimensions of κ is still significantly lower.

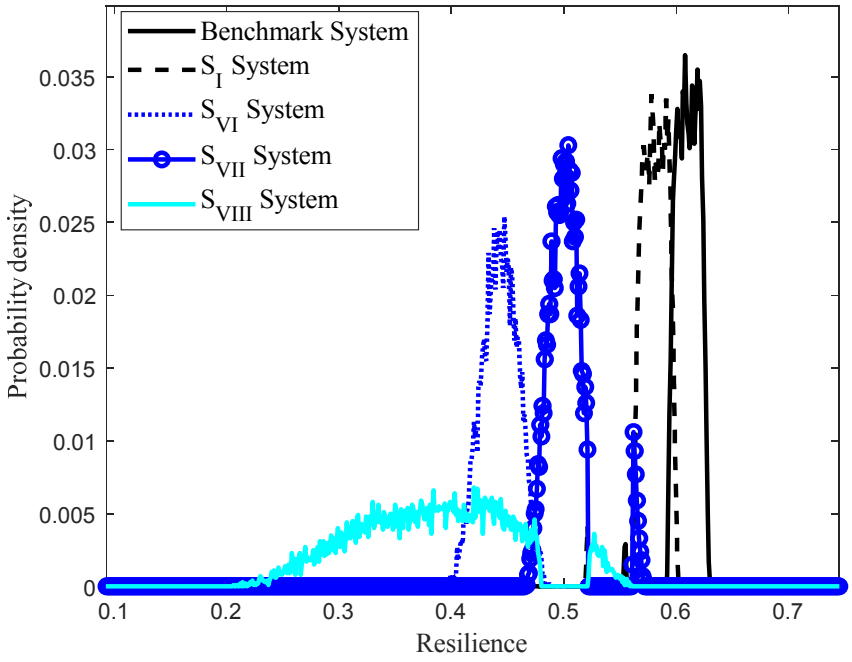
Benchmark System
S_I System
S_VI System
S_VII System
S_VIII System
Probability density
Resilience
0
0.005
0.01
0.015
0.02
0.025
0.03
0.035
0.1
0.2
0.3
0.4
0.5
0.6
0.7

(a)

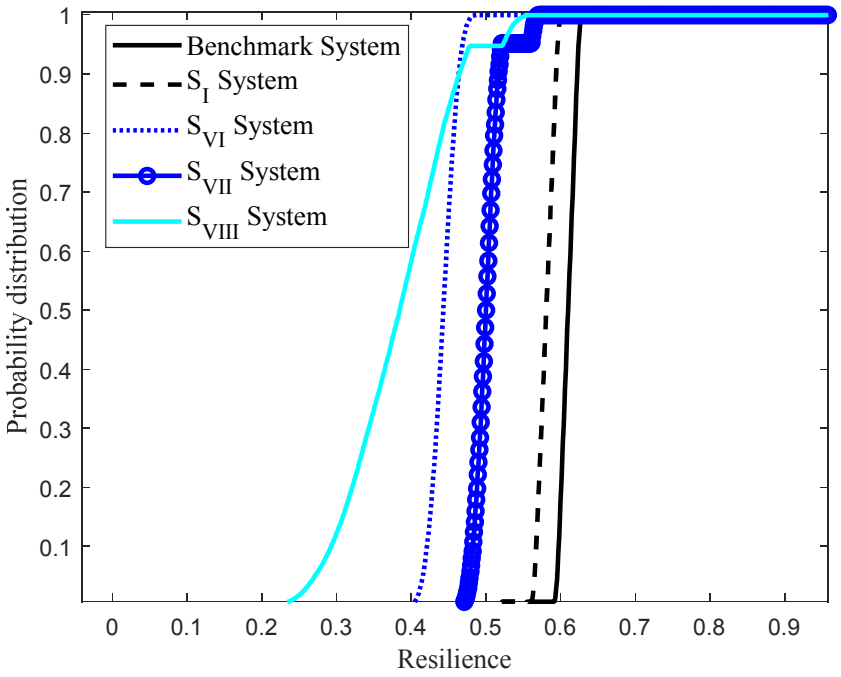
Benchmark System
S_I System
S_VI System
S_VII System
S_VIII System
Probability distribution
Resilience
0.1
0.2
0.3
0.4
0.5
0.6
0.7
0.8
0.9
1
0
0.1
0.2
0.3
0.4
0.5
0.6
0.7
0.8
0.9

(b)

Figure 5.3. (a) Probability density and (b) Probability distribution for the resilience measures of S_B, S_I, S_{VI}, S_{VII} and, S_{VIII} systems.

5.4.2 Resilience Distance

Now, the *RD* (S_B, S_b)) between S_B system and (S_b) system (system with altered parameter) for all {*EMD*/W_1, *CVMD*, *KSM, HM, BD,* χ^2D, *JD*} and *b*= { *I, II, III, IV, V, VI, VII*} are calculated using Equations 5.1-5.7 respectively and values are summarized in Table 5.3. All other resilience distances levels off except for the EMD/W_1 and CVMD and couldn't accurately tell how far the calculated resilience is for every system when compared to benchmark as the resilience aggravates either by increased aging or decreased resources.

Table 5.3. Values of resilience distance measures (*RD*(S_B, S_b)).

	S_I	S_{II}	S_{III}	S_{IV}	S_V	S_{VI}	S_{VII}	S_{VIII}
W_1/EMD	0.0273	0.0927	0.2875	0.1568	0.2233	0.1563	0.1029	0.2122
CVMD	0.1346	0.2946	0.5405	0.3912	0.4543	0.3905	0.3056	0.4269
KSM	0.8871	1	1	1	1	1	0.9952	0.9952
HM	0.0289	0.0316	0.0316	0.0316	0.0316	0.0316	0.0316	0.0316
BD	8.7138	20.3259	47.2335	14.4735	15.0334	15.0945	85.4157	13.167
χ 2D	0.0017	0.0020	0.002	0.002	0.002	0.002	0.002	0.002
JD	0.0516	0.0638	0.0644	0.0471	0.0471	0.0484	0.0646	0.0493

5.4.3 Resilience Attenuation Analysis

Now, towards the RAA, first, RAC as a function of aging is obtained. *RD*(S_B, S_b) is calculated for all possible measures in {*EMD*/W_1, *CVMD*, *KSM, HM, BD,* χ^2*D, JD*} and the parametric systems $S_b \in \{S_{10}, S_{15}, S_{20}, S_{25}, S_{30}, S_{35}, \ldots\ldots, S_{90}\}5$ wherein resourcefulness dimensions are kept constant for S_B and all S_b but the aging is altered. For example, S_{20} is the system 20 years aged whereas S_B is assumed to be not aged (i.e. 5 years). Using, *RD*(S_B, S_b), resilience interaction termed as *I*(S_B, S_b) is thus then calculated and RAC curves for all possible distance measures are hence plotted between *I*(S_B, S_b) vs Aging as shown in Fig. 5.4. It is noted

that the values of $RD(S_B, S_b)$ for BD measure are normalized to 0-1. It is observed in Fig. 5.4 that RAC swoop downward for EMD/W_1 and CVMD complying with the preliminary results of RD measures making them the appropriate RD measures to depict the resilience variations for this work.

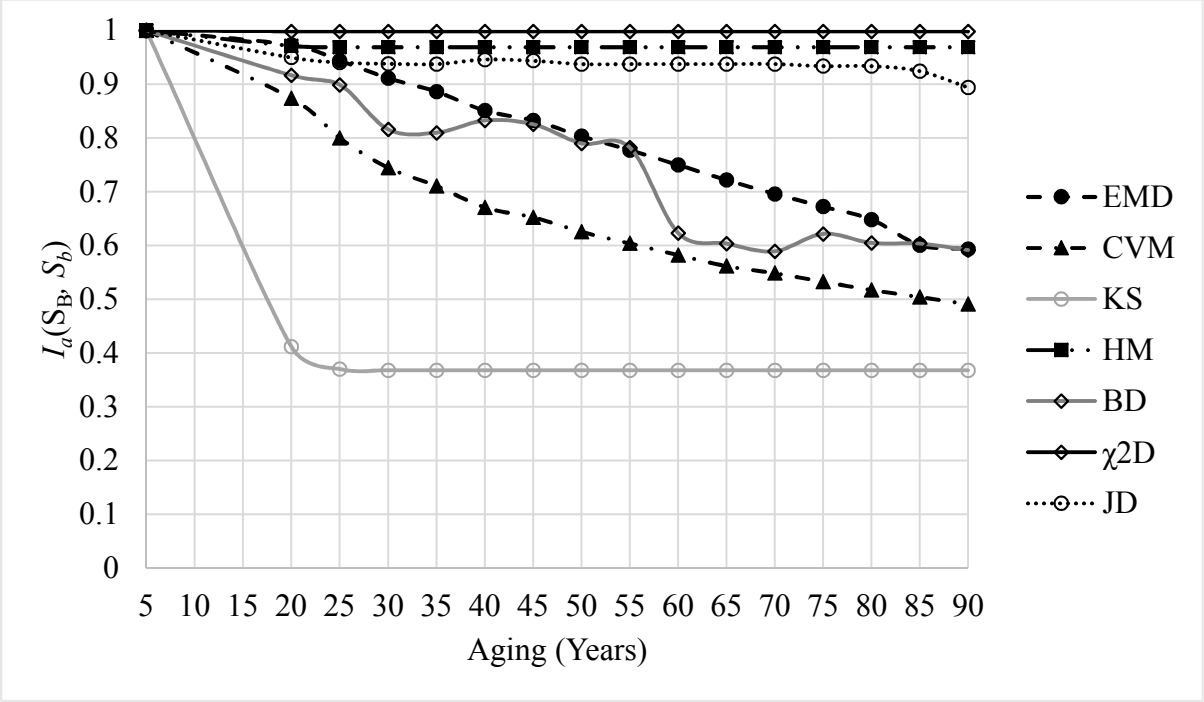

Figure 5.4. RAC as a function of Aging.

Towards the RAC as a function of resourcefulness, aging is kept constant, but resourcefulness dimensions are randomly altered for the parametric systems. 1000 such system having different resourcefulness value such that b = 1:1000 are generated and, for the numerical sampling of the resourcefulness dimensions, the latin hypercube sampling method is adopted with the uniform distribution in the range of (0, 1) to get the upper and lower limit of each dimension. The $RD(S_B, S_b)$) is thus calculated only for EMD/W_1 and CVMD and consecutively $I(S_B, S_b)$ for all these 1000 systems. RAC as a function of resourcefulness is hence the curve drawn by joining the median of each box from the box plot ($I(S_B, S_b)$ vs Mean

Resourcefulness) as shown in Fig. 5.5a for CVMD and Fig. 5.5b for EMD/W_1. Mean Resourcefulness is the mean of κ_1 and κ_2. This Mean Resourcefulness and consecutive $I_a(S_B, S_b)$ are binned to the 5 categories for which the box plot is created. The central mark on each box indicates the median, the bottom and top edges of the box indicate the 25th and 75th percentiles respectively and, the top and bottom mark joined by a dashed line with a box indicates the maximum and minimum value respectively of all $I(S_B, S_b)$.

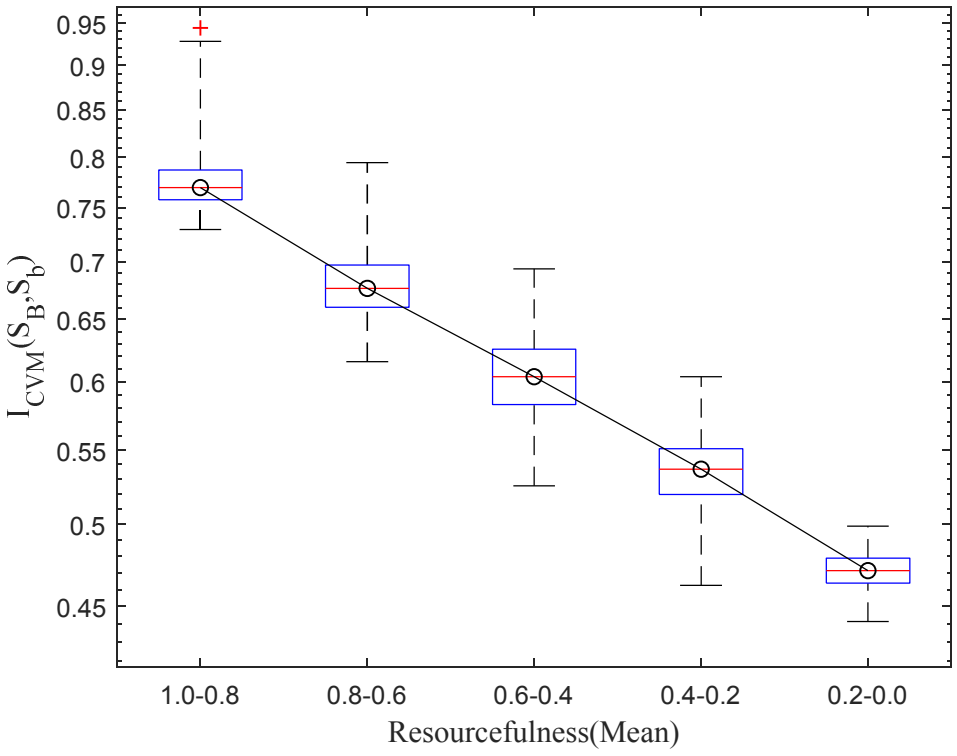

(a)

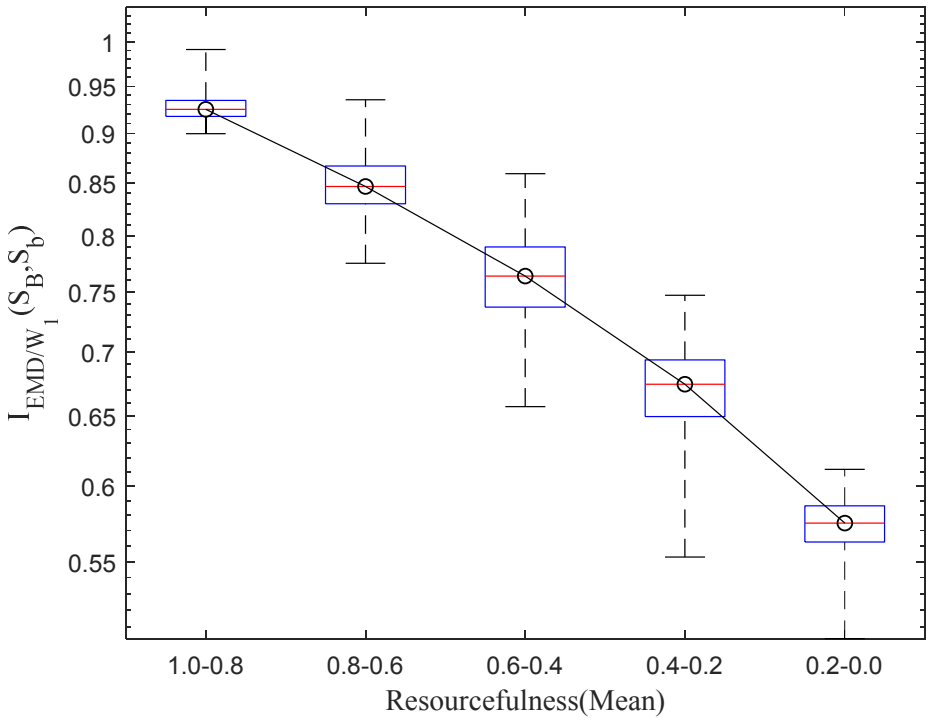

(b)

Figure 5.4. Boxplot and RAC as a function of Resourcefulness using (a) CVM distance and (b) EMD/W_1 Distance

The RAC curve as a function of resourcefulness also swoops downward for the decreased resources confirming the CVMD and EMD/W_1, appropriate RD measures.

Using these two RD measures (CVMD and EMD/W_1), the total system resilience of S_{VI}, S_{VII}, and S_{VIII} now becomes comparable. As seen in Table 5.1, due to the two system parameters of aging and resourcefulness, subjective insight is lost to predict the level of their system resilience. In addition, as illustrated in Fig. 5.2 and Fig.5.3, due to the underlying multi-mode shapes, it confirms too that they are not visually comparable. Nonetheless, by reading the resulting RD measurements in terms of EMD/W1 and CVMD, as shown in Table 5.3, one can reach a conclusion agreed by both EMD/W1and CVMD that their total system resilience levels are ranked as $S_{VII} > S_{VII} > S_{VIII}$. This ranking has vital meaning in practice, as one decides

how to better allocate resources or assess how aging affects the overall resilience of the system when resisting an extreme event.

5.4.4 Nonparametric Two Sample Testing

The null hypothesis (H_0) i.e. $S_B = S_I$ against its alternative (H_1: $S_B \neq S_I$) is set to do the non-parametric hypothesis test. To perform the calculation, 25 resilience samples from B and S_I are obtained from linear interpolation between the probability distribution function plotted in Figure 5.1 as the sample points with corresponding resilience values. Query points are the random values from 0-1. The KS test, EMD/W_1 test and CVM test are thus performed using the "TwoSample" package (Dowd, C. 2018) of R programming Language (Team, R. C. 2020) using these 25 samples for a 1% significance level. For all three tests, the same p-value (0.0025) is obtained which is less than 0.01 (significance value) and hence the test rejects to accept the null hypothesis meaning that the resilience of System S_I is not similar to the acceptable level when compared to the benchmark. The hypothesis test with the same null hypothesis is performed again however in this case S_I is improved by increasing the value of each resourcefulness dimension to *unif (0.94-0.995)*. The notable increase in resilience can be seen in Figure 5.6 where the probability distribution of resilience of improved SI system almost overlaps the probability distribution of the Benchmark system. The resilience measures for this improved SI system are obtained from the interpolation of the probability distribution curve of Figure 5.6 and to perform the hypothesis test. KS, EMD, and CVM all three tests fail to reject the null hypothesis with p-value 0.0458, 0.0566, and 0.082, respectively implying improved S_I system is similar enough to be acceptable when compared to Benchmark. The MATLAB codes to get the probability density i.e. Equation 5.1 and empirical cumulative distribution of

resilience (ECDF), distance calculations i.e. Equations 5.4-5.10 and, codes to get the resilience sample from ECDF are attached as Appendix B.3.

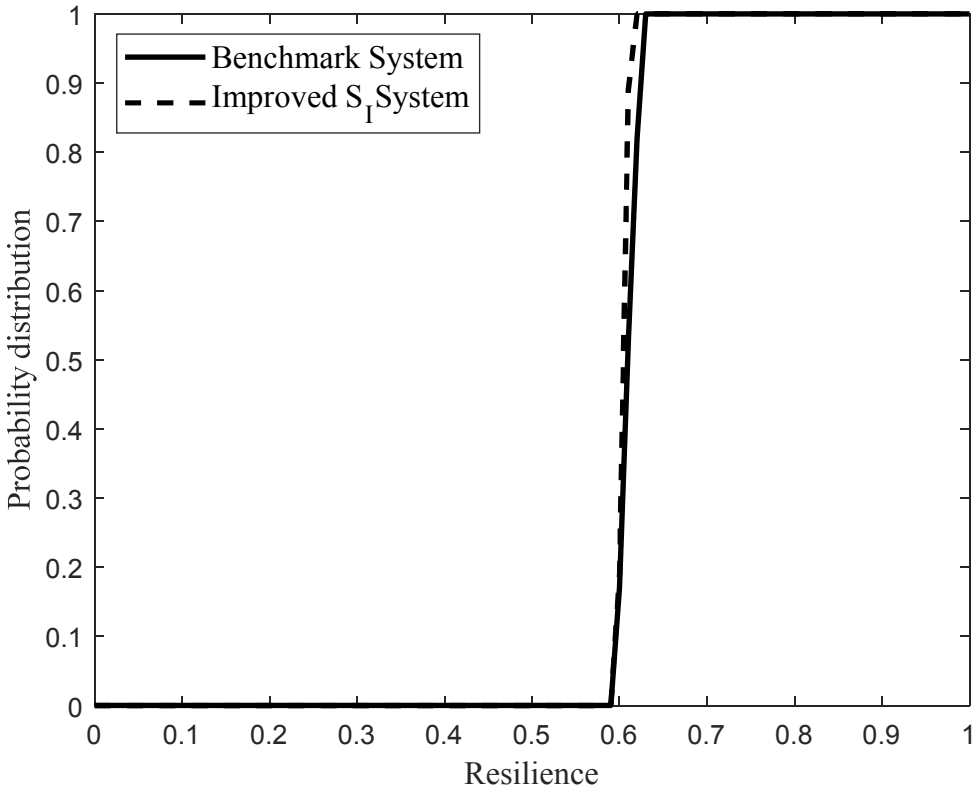

Figure 5.6. The probability distribution function of Benchmark and improved S_I system

5.5 Conclusions

This chapter points out the ambiguity in the use of the term "*resilience metrics*" and suggests the perspective of using the term to identify the approach that compares the resilience measurement and aids in becoming an effective decisive factor. Considering the perspective and complying with the mathematical definition of the metrics this study introduces the use of statistical distance to compare the probabilistic resiliencies of the same system obtained with altered parameters and term it as "*Resilience Distance Measure*". Using several such "*Resilience Distance Measure*", resilience aggravation analysis is numerically performed, and

plot the RAC curve showing W_1/EMD and CVMD perfectly captures the dissimilarities between resilience distributions from targeted resilience. And, also shows numerically that these RD measures can be used as the test statistic to test the hypothesis: "the resilience assessment of the given system is acceptable when compared to target resilience of the same system".

While several pieces of works of literature towards resilience assessment of the infrastructure system or community provides 'a resilience measure' as an entity or the first moment of the parametric data distribution, this study with the numerical evaluation on stochastically modeled rural electric distribution systems proves that the resilience distribution can be multimodal and the decisions based only on the former measure may abridge or exaggerate the situation. Hence, the use of resilience distance measure for the comparison of resiliencies and use of non-parametric hypothesis testing to decide if the resilience is acceptable can be very effective towards decision making.

CHAPTER 6. CONCLUSIONS AND FUTURE WORK

6.1. Conclusions

The key findings of the study are summarized as below:

- The literature synthesis of the most adopted resilience definition and measurement approach towards civil infrastructure and community is provided. The state of art towards assessing the resilience of electrical distribution system against extreme weather events mainly hurricanes is thoroughly studied and summarized. It is realized that the widely accepted framework is yet to be defined. Author found that none of framework fits on the rural electricity distribution system i.e. consideration of geospatial sparseness, and corresponding resourcefulness parameter is not found.
- It is also devised that based on the resilience measurements from several civil infrastructures resilience assessment framework not only limiting to rural electrical distribution system, objective decisions cannot be made. These measurements lack in discriminating relatively that how a parametric infrastructure system is more resilient than a different one or the same one subject to some changed conditions. They lack in answering which input parameter is most influential towards the resilience output and requires more attention and consideration given the resilience need to be strengthened.
- Probabilistic resilience measurement framework for the rural electrical distribution system is developed that includes 1. Mechanics-based fragility modeling against wind speed modeled for different hurricane category for the capacity assessment of power distribution components, which are, coupled wooden pole and conductors. 2. Probabilistic system performance assessed in terms of number of customers without power due to failure of either or both wooden pole and conductor. 3. Analytical

formulation for the recovery of each pole/conductor, mean recovery of system and resilience considering several resourcefulness dimensions towards disaster-response and disaster-recovery and, geospatial sparseness of rural areas.

- Statistical analysis tools for resilience distribution is offered applicable to resilience distribution of any infrastructural system. These tools include 1. Nonparametric methods to assess sensitivity of any input parameters on the proposed framework. 2. Dependence modeling using copula to answer most dependent input parameter to the output resilience and check for the tail dependence. 3. Statistical distance measure termed as resilience distance measure to quantify how far apart or close the calculated resilience measurement of system is when compared to the targeted resilience of same system. 4. Nonparametric two sample test to answer if the calculated resilience is acceptable when compared to targeted resilience.
- Numerical implementation of proposed statistical analysis tools framework to the stochastically modeled linear rural electricity distribution setup shows the nonparametric and multi-mode shapes of resilience at varied input parameters justifying the use of non-parametric approach towards statistical analysis of resilience distribution rather than relying on the first moment of distributions (such as mean or median) and, these statistical tools can be the effective decision making tools following the resilience measurement.

6.2 Potential Future Work

This study although addressed several gaps while assessing the resilience of civil infrastructure and additionally developed framework to quantify resilience of electric

distribution system in the rural setting, there are several arenas for the potential improvements. Immediate and main directions towards future research are as listed below:

- The redundancy to the linear network can be applied by closing the tie switch. The performance assessment of the distribution system can be assessed using the optimization technique including the closure of tie-switch, optimal placement and number of sectionalizer and cost all constrained by the resources available within the rural setup.
- In the fragility modeling of the wooden pole, the level of damage is not considered, rather differentiated as failure and not failed and hence the same recovery period is assigned for all failure poles. In the future, the procedure can be granularized assigning the different limit states and assigning different recovery period based on the damage stage. Additively, the failure of cable because of fallen trees and branches is not included in the fragility modeling which apparently has caused significant cable failure and can be added in the framework.
- The proposed probabilistic resilience measurement framework for rural electrical distribution system is applicable to the single event of hurricane with scenario-based approach to model the hurricane. The framework can be expanded to include the lifecycle resilience assessment including probabilistic based approach and model multiple hazards and their projection within the given lifetime.
- The proposed statistical analysis framework is applied to the stochastically modeled linear distribution system. In the future, the proposed framework can

be applied to the actual rural distribution setup including the actual quantification of each resourcefulness dimension assumed in the framework.

- The statistical analysis tools proposed in the study is very novel and fruition and, applied to the proposed probabilistic resilience measurement framework for rural electrical distribution system only. It can be applied to the probabilistic resilience measurement framework of any other civil infrastructure as the additional case study and improve the tools accordingly.

APPENDIX A. 3.9 AND 3.11 EQUATIONS FORMULATIONS

Considering the power-delivery system in Figure 3.1b that has N poles and N conductors in series, the state of a conductor or a pole is treated binary: s is for a conductor and t for a pole, and $s = 1$ or $t = 1$ denotes failure (0 for success). Then the possible states of a conductor-pole unit form a set of 2-tuple binary state-pairs: {(1, 1), (1, 0), (0, 1), (0, 0)}. To achieve discrete probability density of an event P_{E_i}, i.e. all the customers up to i^{th} pole-conductor from the end unit are affected. it is equivalent to this system state: (1) from the unit N to the unit (i +1), all units need to be in the success state, each leading to a probability measure of (1-Pc) (1-Pw); (2) at the i^{th} unit, the unit is at a state of $\{(s, t) \mid (1-s)(1-t) \neq 1\}$ to create the cascading effect of losing A_m customers, which includes all the unit states but (0, 0) and leads to a probability measure of (Pc + Pw - Pc Pw) from the summation of the probabilities of the three unit states; and (3) from the unit (i -1) to the unit 1 (the end unit), the units can take any of the possible four unit states, which gives a total probability measure (i.e. 1) from the summation of 4^{i-1} different combinations of the unit states. The probability of this system state for ensuring the event A_m gives rise to the mass probability $P_{E_i} = [(1-Pc)^{N-I} (1-Pw)^{N-i}] \times (Pc + Pw - Pc\ Pw) \times 1$. Equation 3.7 further elaborates this expression by defining the special cases at $m = 1$ and $m = N$.

Towards calculating the restoration time-cost for the linear power-delivery system, one needs to separately consider the restoration time of every possible system states. By combination, given an event A_m, it is equivalent to a total number of $3 \times 4^{PS_m - 1}$ system states, each of which corresponds to a different total restoration cost. For each of such system states, the mass probability is a joint function and can be defined as $P(A_m, F_{PS_m})$, where F_{PS_m} is a function of $\mathcal{B} = \{(s_i, t_i) \mid i = PS_m, PS_m - 1, \ldots, 1\}$ that defines one specific scenario of the system

state from the PS_m^{th} to the first conductor-pole unit. This joint probability has the expression of:

$$P[A_m, F_m(\mathcal{B})] = (1-P_c)^{N-PS_m}\,(1-P_w)^{N-PS_m}\;\; {P_c}^{s_{PS_m}}(1-P_c)^{1-s_{PS_m}}\,{P_w}^{t_{PS_m}}(1-P_w)^{1-t_{PS_m}} \quad \ldots \prod_{i=1}^{PS_m-1} {P_c}^{s_i}(1-P_c)^{1-s_i}\,{P_w}^{t_i}(1-P_w)^{1-t_i}$$

where $\{(s_m, t_m) \mid (1\text{-}s_m)(1\text{-}t_m) \neq 1\}$ still holds for the PS_m^{th} unit and (s_i, t_i) takes any of the four binary state-pairs. At this system state, the restoration time for the system is a summation of the individual time cost for each failed pole and conductor. Considering Equation 9 and defining the restoration cost at the i^{th} pole and conductor as $Rw(i)$ and $Rc(i)$, respectively, the total restoration $r[F_{PS_m}(\mathcal{B})]$ has the expression of

$$r[F_{PS_m}(\mathcal{B})] = \sum_{i=1}^{PS_m} Rc(i)\,s_i + Rw(i)\,t_i$$

Given the two expressions above, one can formulate the distribution of the mean restoration time conditional on the event A_m, defined as

$$RC(\kappa_2, A_m) = \mathbf{E}\left[r\left(F_{PS_m}(\mathcal{B})\right) \mid A_m\right] = \frac{\sum_{\mathcal{B}} r\left(F_{PS_m}\right) P(A_m, F_m(\mathcal{B}))}{P(A_m)}$$

$$= P_c\left(\sum_{i=1}^{PS_m-1} Rc(i) + \frac{Rc(PS_m)}{P_c + P_w - P_c P_w}\right) + P_w\left(\sum_{i=1}^{PS_m-1} Rw(i) + \frac{Rw(PS_m)}{P_c + P_w - P_c P_w}\right)$$

It is noted that to achieve the result above (Equation 3.11), a mathematical induction method is recommended for handling the $\mathcal{B}$ set (i.e., by formulating at $PS_m = 1, 2, \ldots PS_m = k$; and then induce at $PS_m = k + 1$). Given $RC(\kappa_2, A_m)$, the total mean restoration time can be further obtained by using the Law of Total Expectation.

APPENDIX B. MAIN MATLAB CODES

B.1 Computation of Failure Probabilities of Wooden Pole and Distribution Lines

```
%This code is the main code with user defined parameters and
call single_span_3d_cable.m function to give failure
probabilities
clear all; clc; close all;
%% units and basic calculation
lbf = 1; ft = 1; kips = lbf * 1000; in = ft / 12; lb=1; sec=1;
%% material property for conductor
E = 17 * 10^6 * lbf / in^2;
alpha = 9.4 * 10^(-6);    % per degree F
d = 0.53 * in;            % diameter, for primary cable
A = pi * d^2 / 4;
EA = E * A;
agecoef = 0.95;
% rated capacity for soft-drawn annealed copper conductor
rC0 =  agecoef*6453*lbf;
% assumed mean and variance of the rated strength
mu_r_co = rC0; va_r_co = (0.1 * rC0)^2;
% parameter a for lognormal distribution of Rated Strength
mu_co= log(mu_r_co^2 / sqrt(va_r_co + mu_r_co^2));
% parameter b for lognormal distribution of Rated Strength
sigma_co= sqrt(log(va_r_co / mu_r_co^2 + 1));
%% initial estimate of geo profile
wb = 0.653 * lbf / ft;          %  bare self-weight
D = 250 * ft;                   % span length
% initial estimate of sag under 20% of rated capacity as
horizontal force
S0_ = wb * D^2 / (8 * (0.2 * rC0));
% initial estimate of conductor cable length
L0_ = D + 8 * S0_^2 / 3 / D;
%% material property for wooden pole
fibre_stress = 8000;          %psi, for southern pine
mu_r_wo = fibre_stress;       % Mean of fiber stress
va_r_wo = (0.15 * fibre_stress)^2;% Variance of fiber Stress
% parameter a for lognormal distribution of fiber stress
mu_wo= log(mu_r_wo^2 / sqrt(va_r_wo + mu_r_wo^2));
% parameter b for lognormal distribution of fiber stress
sigma_wo= sqrt(log(va_r_wo / mu_r_wo^2 + 1));
%% Numerical Simulations
simN=1600;                    % Number of simulations
% create Latin hypercube sample (LHC) for 4 parameters
X = lhsdesign(simN,4);
% Scale factor to create Weibull distribution of wind speed
for different category of hurricane.
```

```
cat1v = 107.196; cat2v = 124.122; cat3v = 145.561; cat4v =
176.027; cat5v = 203.108;
% fixed shape factor value for the Weibull distribution
beta = 2;
%create weibul distribution of velocity for lhc samples
Vw = icdf('wbl',X(:, 1),cat3v,beta);
% create uniform, distribution of theta for lhc samples
directivity=icdf('unif',X(:,2),0,pi);
%create lognormal distribution of rated copper strength
fy_cond = icdf('logn', X(:, 3), mu_co, sigma_co);
%create lognormal distribution of rated wood fibre stress
Fb = icdf('logn', X(:, 4),mu_wo,sigma_wo);
% wood and climate parameter for southern pine and climate
class B
% respectively; decay threshold in inch
kwood = 0.38 ; kclimate = 1.5 ; do=0.2;
% decay rate inch/year
r = 0.0393701*kwood*kclimate;
tlag = 3*r^(-0.4); % year
tdo = tlag+do/r;
c=do/tdo^2;
%Age of the wooden pole
t=[5,20,30,60,90];
for i=1:length(t)
    if t(i) <=tdo
        dt=c*t(i)^2;
    else
        dt = (t(i)-tlag)*r;
    end
     % lbf*ft using Mr= 0.000264* fibre stress* cubic power of
     circumference of pole at ground level
    pole_capacity = 0.000264*Fb*(33-2*pi*dt)^3 ;
    X0 = [0; 0; 0;];      % origin 0
    X1 = [D; 0; 0;];      % origin 1
    % orientation vector of the gravity load
     wa = [0; -1; 0];
     % find out the cable length with zero tension (at slack)
     with fixed support
    K0 = EA / L0_ * 10^4 ; K1 = K0;
     % now  use this to get the slack cable length, which is
     very accurate; no need to find it iteratively
    L0s = L0_ - rC0 * 0.2 / K0;
    K0 = EA / L0s * 1e+6; K1 = K0;  % rigid pin support
     % assume uniform-distributed temperature jump ( -30 to
     100F) -- no much literature
    dT =  rand(simN, 1) * 130 - 30;
    Tmax = zeros(simN, 1); LL = zeros(simN, 1);
```

```
 SAG = zeros(simN, 1);
R1x = zeros (simN, 3); R2x = zeros (simN, 3);
Trx=zeros(simN,3); theta= zeros(simN,1);
 m_pole = zeros(simN,1);
 Wextreme=zeros(simN,1); m_pole2=zeros(simN,1);
 M_pole=zeros(simN,1);
for n=1:simN
    pa1_ = cos(directivity(n));
      pa2_ = sin(directivity(n));
     % orientation vector of the wind load considering
     span 30 degree with horizontal)
    pa_ = [0; 0; 1] + [pa1_; 0; pa2_];
    pa = pa_ / norm(pa_);
      %lbf / ft from N. Impollonia et al.
    p_ = 0.5*0.00237* (Vw(n))^2 * 1.2 * d;
      % the loading vector combining both selfweight and
      wind (note: since I use the slack cable length)
    p = wb * wa+ p_ * pa_;
    P = norm(p); Pa = p/norm(P);
      [R1,R2, Tm,Profile,L, Sag, X0n,X1n,sag_loc] =
      single_span_3d_cable...
    (EA, L0s, P, Pa, dT(n), alpha, K0, K1, X0, X1);
    LL(n) = L;
    SAG(n) = Sag;
    Tmax(n)= norm(Tm);
    R1x(n,:) = R1';
    R2x(n,:) = R2';
    Trx(n,:) = R1'+R2';
    theta(n) = acos(Trx(n,2)/norm(Trx(n,:)));
      m_pole(n) = 3*norm(Trx(n,:)).*sin(theta(n)).*
      23.75*ft;
     % lbf/ft^2 Wextreme= 0.00256*V^2*Kz*Grf*I*Cd from
     pole loading to... calculate moment on pole due to
     wind on face of pole
     Wextreme(n) = 0.00256*(Vw(n))^2*0.876*0.978*1*1;
     % lbf.ft Moment on pole at ground due to wind on the
     face of the pole=
     Wextreme*Hp^2*(Dim_ground+2*Dia_top)/72* OCFw
     m_pole2(n) = Wextreme(n)* 26^2*(10.5+2*9.5)/72*1;
    M_pole(n)= m_pole(n)+m_pole2(n);
end
cable_failure = find((fy_cond-Tmax) <0 );
pole_failure= find(pole_capacity-M_pole<0);
Pc(i) = length(cable_failure)/simN;
Pp(i) = length(pole_failure)/simN;
End
```

```
%% This code is called by Main file. Function name:
single_span_3d_cable.m
function [R1, R2xyz, Tm, Profile, L_, Sag, X0n,X1n,sag_loc] =
single_span_3d_cable...
    (EA, L, P, Pa, dT, alpha, K0, K1, X0, X1)

% EA : E x A sectional stiffness
% L  : Initial length of the cable (single valued)
% P  : Uniformly distributed load (single valued)
% Pa : a 3x1 direction vector for the uniform force P
% dT : temperature jump relative to the ref temperature
(assumed to be 60F)
% alpha: coef of thermal expansion
% K0 and K1: stiffness matrix (3x3 matrix or single valued)
for the supports
% X0 and X1: position coordinates of the supports (3 x 1
vectors)

global chi s pa dt a x0 x1 k0 k1 ; % define normalized
quantities
pa = Pa / norm(Pa);
x0 = X0 / L;
x1 = X1 / L;
chi = P * L / EA;
k0 = K0 / P; k1 = K1 / P;
dt = dT;
a = alpha;
options = optimset('Display','off');   % Option to display
output
s = 1;
r0 = [0.5; -0.5; 0]; % initial reaction force at the start
V0 = [r0; x0; x1]; % x0 is the initial position of the cable
start
[V, fval] = fsolve(@hyperbolic_reaction_with_springs,V0
,options);  % Call solver
r = V(1:3); xi0 = V(4:6); xi1 = V(7:9);
% compute the new catenary parameters
N = 1000; s = linspace(0, 1, N);
xi = hyperbolic_reaction_with_springs(V, s);
L_ = update_cable_length(r, pa, chi) * L;
xm = hyperbolic_reaction_with_springs(V, 1/2);
sag = norm(xm - (x1-x0) / 2);
sag_loc = (xm - (x1 - x0) / 2) * L;
R = r * P * L; R1 = R;
Profile = xi * L;
Sag = sag * L;
X0n = xi0 * L;
```

```
X1n = xi1 * L;
s = linspace(0, 1, 10000);
T = (R * ones(1, 10000)  - P * Pa * s);
Tm = T(:, max(normM(T)) == normM(T));
R2 = T(:, end); % this is the force in the curved s direction.
r2vec = Profile(:,end) - Profile(:, end-1);
cx = r2vec(1)/norm(r2vec); cy = r2vec(2)/norm(r2vec);
cz = r2vec(3)/norm(r2vec);
R2xyz = -norm(R2)* [cx, cy, cz]';

%%%%%%%%%%%%%%%%%%%% catenary solver
%%%%%%%%%%%%%%%%%%%%%%%%%%%%%%%%
function f = hyperbolic_reaction_with_springs(V, s_)
global chi s pa dt a x0 x1 k0 k1;
if nargin == 1

    % define the hyperbolic equation = 0
    r = V(1:3);
    xi0 = V(4:6);
    xi1 = V(7:9);

    f1 = chi * (r * s - pa * s^2 / 2) + ((eye(3) - pa * pa') *
r * ...
        log((norm(r - pa * s) - pa' * (r - pa * s)) / (norm(r)
- pa' * r)) - ...
        pa * (norm(r - pa * s) - norm(r)) + xi0) * (1 + dt *
a) - xi1;

    f2 = r - k0 * (xi0 - x0);
    f3 = (pa - r) - k1 * (xi1 - x1);

    f = [f1; f2; f3];

elseif nargin == 2
    %define the hyperbolic coordinate equation
    iv = ones(1, length(s_));
    r = V(1:3);
    xi0 = V(4:6);
    f  = chi * (r * s_ - pa * s_.^2 / 2) + ((eye(3) - pa *
pa') * r * ...
        log((normM(r * iv - pa * s_) - pa' * (r*iv - pa * s_))
./ (norm(r) - pa' * r)) - ...
        pa * (normM(r * iv - pa * s_) - norm(r)) + xi0 * iv) *
(1 + dt * a);
end
```

```
function n = normM(M)
[i, j] = size(M);
if j == 1
    n = norm(M);
else
    for j = 1:j
        n(j) = norm(M(:, j));
    end
end

function len_ = update_cable_length(r, pa, chi)

r1 = r(1); r2 = r(2); r3 = r(3);
p1 = pa(1); p2 = pa(2); p3 = pa(3);

len_ = chi * (1/2 * (sqrt((p1 - r1)^2 + (p2 - r2)^2 + (p3 -
r3)^2) + ((p1 * r1 + p2 * r2 + p3 * r3) * (-sqrt((p1 - r1)^2 +
(p2 - r2)^2 + (p3 - r3)^2) + ...
    sqrt(r1^2 + r2^2 + r3^2)))/(p1^2 + p2^2 + p3^2) + ((p3^2 *
(r1^2 + r2^2) - 2 * p1 * p3 * r1 * r3 - 2 * p2 * r2 * (p1 * r1
+ p3 * r3) + p2^2 * (r1^2 + r3^2) + p1^2 * (r2^2 + r3^2)) *
...
    (log(p1^2 + p2^2 + p3^2 - p1 * r1 - p2 * r2 + sqrt(p1^2 +
p2^2 + p3^2) * sqrt((p1 - r1)^2 + (p2 - r2)^2 + (p3 - r3)^2) -
p3 * r3) - ...
    log(-p1 * r1 - p2 * r2 - p3 * r3 + sqrt(p1^2 + p2^2 +
p3^2) * sqrt(r1^2 + r2^2 + r3^2))))/(p1^2 + p2^2 +
p3^2)^(3/2))) + 1;
```

B.2 Main Codes for Resilience Quantification

```
clc;
clear all; close all;
%probability of failure of cable conductor conditional to H (I
to V)
Pc = [0.0112, 0.0347, 0.0813, 0.1686, 0.257] ;  %probability
of failure of cable conductor conditional to H (I to V)
Number_of_poles=211; % Number of Poles
Customer_Served=800; % Number of total customer served
Position_of_sectionalizer=[42, 84, 127, 169, 211]; % Position
of the sectionalizer
D = 52800:-250:250;
% constant used to calculate the repair time for pole and
conductor
plambda1 =1.313*10^(-5); clambda1 = 1.06*10^(-5); %
plambda2 = 1.281;         clambda2 = 1.05;
```

```
Tc=30*24;% Control Period
toe=0;
AC = Calculate_Affected_Customer(Number_of_poles,
Customer_Served, Position_of_sectionalizer);
% Probability of failure of wooden pole (G = 5, 20 and 60
Years)(row) and H
% (I to V)(column)
Pp = [0.0517, 0.1074, 0.19, 0.3196, 0.4188; 0.0654, 0.1267,
0.2168, 0.3496, 0.4494; 0.207, 0.3031, 0.431, 0.5414, 0.6342];
RSE=[0.2, 0.65, 0.85 ]; ROP=[0.15,0.55,0.9];
RT = [0.27,0.6,0.97];
kappa1= 0.4*RSE+0.2*ROP+0.4*RT; % Resourcefulness towards
response
kappa2= 0.2*RSE+0.3*ROP+0.5*RT; % Resourcefulness towards
Recovery
RS_min = [2,3,8,16,26]; % Minimum Response time to start
recovery after hurricane
for i = 1: length(kappa2)
     [Rw, Rc] =
     Calculate_Recovery_time_for_each_pole_conductor(D,kappa2(
     i),plambda1,plambda2,clambda1,clambda2);
    for j = 1:size(Pp,1)
      for k = 1:length(Pc)
          [PAc{j,k}, Mean_Ac(j,k),Variance_Ac(j,k)] =
          Probability_of_Affected_Customers(Number_of_poles,Pp
          (j,k),Pc(k),AC,Position_of_sectionalizer);
          [RC{i}{j,k}, Tsys{i}{j,k}, CoVar_Tsys{i}{j,k}]
          =Mean_recovery_time_systems(AC,PAc{j,k},Pp(j,k),Pc(k
          ), Rw, Rc,Position_of_sectionalizer);
        RS = RS_min(k)*exp(1-kappa1(i))
        if kappa2(i)>=0.85

              [Res{i}{j,k},TMSR{i}{j,k},CoVar_TMSR{i}{j,k}] =
              calculate_resilience_exponential_recovery(AC,PA
              c{j,k},RC{i}{j,k}/Ncrews,Tc,toe,RS);
        else
              [Res{i}{j,k},TMSR{i}{j,k},CoVar_TMSR{i}{j,k}] =
              calculate_resilience_trigonometric_recovery(AC,
              PAc{j,k},RC{i}{j,k},Tc,toe,RS);
        end
      end
    end
end
% Plot for probability of affected customers for hurricane
category III
figure
shape = ['d' , 'o', '*'];
```

```
for j=1:size(Pp,1)
    scatter(AC, PAc{j,3},'k',shape(j));
    hold on
end
set(gca,'yscale','log')
xlabel('Affected Customers (A_m)','FontSize', 12,'FontName',
'Times New Roman');
ylabel('Probability of Affected Customers,
P_{AC}(A_m|H,G)','FontSize', 12,'FontName', 'Times New Roman')
legend({'System not aged','System aged 20 years','System aged
60 years'}, 'FontSize',12,'FontName', 'Times New Roman');
hold off
box on; grid on;

% 2. plot for Recovery Time conditional to affected customers
for hurricaen
% categpry III and moderate resourcefulness
figure
plot(AC, RC{2}{1,3},'k-','linewidth', 2); hold on
plot(AC, RC{2}{2,3},'k-.','linewidth', 2);
plot(AC, RC{2}{3,3},'k--','linewidth', 2);
hold off
xlabel('Affected Customers (A_m)','FontSize', 12,'FontName',
'Times New Roman');
ylabel('Mean Recovery Time(RC(k_2,A_m)), Hours','FontSize',
12,'FontName', 'Times New Roman')
legend({'System not aged','System aged 20 years','System aged
60 years'}, 'FontSize',12,'FontName', 'Times New Roman');
box on; grid on;

%3. Plot for Resilience Vs Affected Customers
figure
plot(AC, Res{2}{1,3},'k-','linewidth', 2); hold on
plot(AC, Res{2}{2,3},'k-.','linewidth', 2);
plot(AC, Res{2}{3,3},'k--','linewidth', 2);
hold off
xlabel('Affected Customers (A_m)','FontSize', 12,'FontName',
'Times New Roman');
ylabel('Mean Resilience (R_{sys}(k,A_m))','FontSize',
12,'FontName', 'Times New Roman')
legend({'System not aged','System aged 20 years','System aged
60 years'}, 'FontSize',12,'FontName', 'Times New Roman');
box on; grid on;

function AC = Calculate_Affected_Customer(Number_of_poles,
Customer_Served, Position_of_sectionalizer)
```

```
% creating random number between 3 and 6 such that sum is
equal to Customer_Served
x = randfixedsum(Number_of_poles,1,Customer_Served,3,6);
x1=0;
AC_1= cumsum(round(x));
for i=1:length(Position_of_sectionalizer)

     Affected_Customers(i)=AC_1(Position_of_sectionalizer(i));
end
AC = [x1, Affected_Customers];
end

function [PAC, Mean_AC,Variance_AC ] =
Probability_of_Affected_Customers(Np, Pp,Pc, AC,
Position_of_sectionalizer)
PAc=zeros(Np,1);
f= Pc+Pp-Pc*Pp;
for m = 1: Np+1
    if m==1
     PAc(m) = (1-Pc)^(Np) * (1-Pp)^Np; %length of AC =
     1+Number of poles
    elseif m==Np+1
      PAc(m) = f;
    else
          PAc(m) = power((1-Pc),(Np+1-m)) * power((1-
          Pp),(Np+1-m)) * f;
    end
end
for i = 1:length(AC)
    if i==1
        PAC(i)=PAc(i);
    elseif i==2

          PAC(i)=sum(PAc(i:(Position_of_sectionalizer(i-
          1)+1)));
    else

          PAC(i)=sum(PAc((Position_of_sectionalizer(i-
          2)+1):(Position_of_sectionalizer(i-1)+1)));
    end
end
Mean_AC = sum(AC.*(PAC));
Variance_AC = sum((Mean_AC-AC).^2.*PAC);
end
```

```
function [RCp,RCc] =
Calculate_Recovery_time_for_each_pole_conductor(D,k,plambda1,p
lambda2,clambda1,clambda2)
 RCp = 5.* exp(plambda1.*D).*exp(plambda2*(1-k));
 RCc = 3.* exp(clambda1.*D).*exp(clambda2*(1-k));
end

function [RC, Tsys, CoVar_Tsys] =
Mean_recovery_time_systems(AC,PAC,Pp,Pc, RCc, RCp,p_sec)
f= Pc+Pp-Pc*Pp;
for m = 1:length(AC)
    if m == 1
        RC(m)= 0;
      else
          RC(m)= Pp*(sum (RCp (1: p_sec(m-1)-1))+RCp(p_sec(m-
          1)) / f )+Pc*(sum (RCc (1: p_sec(m-1)-1))+RCc (
          p_sec(m-1)) / f);
    end
end
Tsys=sum(RC.*PAC);
CoVar_Tsys = (sqrt(sum((Tsys-RC).^2.*PAC))/Tsys)*100;
end


function [Res, TMSR, CoVar_TMSR] =
calculate_resilience_exponential_recovery(AC,PAC,Tsys,Tc,toe,R
S)
Q100=AC(end);
Res =zeros(length(AC):1); % Resilience of system conditional
to event
for m = 1:length(AC)
    Qr = Q100-AC(m);
    gamma =(AC(m))/(exp(1)-1);
     fun_e = @(t)(gamma.*exp((t-RS)./Tsys(m)))+Qr-gamma;
    q_e = integral(fun_e,RS,(Tsys(m)+RS));
     Res(m) = ((RS*Qr)+q_e+((Tc-Tsys(m)-
     RS).*Q100))./(Tc.*Q100);
end
Res(1) = 1;
TMSR = sum(Res.*PAC);
CoVar_TMSR=abs(sqrt(sum((TMSR-Res).^2.*PAC))/TMSR)*100;
end


function [Res, TMSR, CoVar_TMSR] =
calculate_resilience_trigonometric_recovery(AC,PAC,RC,Tc,toe,R
S)
```

```
Q100=AC(end);
for m = 1:length(AC)
    Qr = Q100-AC(m);
     fun_t = @(t)(AC(m).*(1-cos((pi.*(t-RS))./(2*RC(m))))+Qr;
    q_l = integral(fun_t,RS,(RC(m)+RS));
     Res(m) = ((RS*Qr)+q_l+((Tc-RC(m)-RS).*Q100))./(Tc.*Q100);
end
Res(1) = 1;
TMSR = sum(Res.*PAC);
CoVar_TMSR= abs((sqrt(sum((TMSR-Res).^2.*PAC))/TMSR)*100);
end
```

B.3 Codes to get the probability density, ecdf, resilience

distance and, resilience samples.

```
%%This function calculates the probability density and
empirical cumulative distribution of resilience
%inputs are: bins= bin_edges to categorize the resilience
%               PAC = Probability of affected customers
%                Rsys = Calculated resilience matrix
          conditional kappa (row) to affected
          customers(column)
function [P_res,P_res_ cum]= get_probability_density(R_sys,
bins,PAC)
P_res=zeros(1,length(bins)-1);
for m=1: size(R_sys,2)

h(:,m)=histcounts(Rsys(:,m),bins,'Normalization','probability'
);
end
for i=1:length(bins)-1
    for j = 1: length(PAC)
        P_res(i) = h(i,j).*PAC(j)+P_res(i);
    end
end
P_res = [0,P_res];
P_res_cum=cumsum(P_res);
end

%% Calculate resilience distance
% % Kolmogorov-Smirnov metric (KS)
KSM = max(abs(P_res_cum_B-P_res_cum_SI));
CVMD = sqrt(trapz(bins, (P_res_cum_B-P_res_cum_SI).^2));
HM = (1/2*trapz(bins, (sqrt(P_res_B)-sqrt(P_res_SI)).^2))^0.5;
BD = -log(trapz(bins, sqrt(P_res_B.*P_res_SI)));
```

```
X^2D = trapz(bins, ((P_res_B-
P_res_SI).^2)./(P_res_SI+P_res_B));
JD = trapz(bins, ((P_res_B-
P_res_SI).*log(P_res_B./P_res_SI)));
EMD = wass_test(P_res_cum_B, P_res_cum_SI, 1000,1000, bins);

function wass_distance= wass_test(Fn, Gm, n,m, bins)
% This function calculates the Wasserstein-1 distance
% Fn is the empirical distribution of the first samples
% Gm is the empirical distribution of the second sample
% n= length(sample_1); m=length(sample_2);
t = 0:0.1:1; %samples to interpolate on
[x1, index] = unique(Fn);
 y1= bins(index);
InvFn= interp1(x1,y1,t,'next');
[x2, index] = unique(Gm);
 y2= edges(index);
InvGm= interp1(x2,y2,t,'next');
wass_distance = trapz(t, (abs(InvFn-InvGm)));
end

function Samples = Create_Res_Samples(Prob_dist,N,edges)
%%this function creates the resilience sample based on the
%probability distribution of resilience desired
% Number of samples required
% Bin edges
rand_Vals = rand(N,1);
[x, index] = unique(Prob_dist);
index(1)=index(2)-1;
index(length(index)) = 101;
Samples = interp1(x,edges(index),rand_Vals);
end
```

REFERENCES

(ANSI) American National Standards Institute 05.1 2017. "Wood poles: Specifications and dimensions." American Wood Protection Association (AWPA), AL, USA.

Altman, J., O.N. Ukhvatkina, A.M. Omelko, M. Macek, T. Plener, V. Pejcha, T. Cerny, P. Petrik, M. Srutek, J.-S. Song, A.A. Zhmerenetsky, A.S. Vozmishcheva, P.V. Krestov, T.Y. Petrenko, K. Treydte, and J. Dolezal 2018. "Poleward migration of the destructive effects of tropical cyclones during the 20th century." *Proceedings of the National Academy of Sciences.* 115 (45), 11543. https://doi.org/10.1073/pnas.1808979115

Anghel, M., K.A. Werley, and A.E. Motter 2007. "Stochastic model for power grid dynamics." *Proc., 2007 40th Annual Hawaii International Conference on System Sciences (HICSS'07)*, IEEE, 113-113. https://doi.org/10.1109/HICSS.2007.500

Archer, C.L., and M.Z. Jacobson 2003. "Spatial and temporal distributions of u.S. Winds and wind power at 80 m derived from measurements." *Journal of Geophysical Research: Atmospheres.* 108 (D9). https://doi.org/10.1029/2002JD002076

Bazargani, N.T., and S.M.T. Bathaee "A novel approach for probabilistic hurricane resiliency assessment of an active distribution system using point estimate method." *Proc., 2018 19th IEEE Mediterranean Electrotechnical Conference (MELECON)*, 275-280. https://doi.org/10.1109/MELCON.2018.8379107

Bhat, R., Y.M. Darestani, A. Shafieezadeh, A.P. Meliopoulos, and R. DesRoches "Resilience assessment of distribution systems considering the effect of hurricanes." *Proc., 2018 IEEE/PES Transmission and Distribution Conference and Exposition (T&D)*, 1-5. https://doi.org/10.1109/TDC.2018.8440320

Bhatia, K.T., G.A. Vecchi, T.R. Knutson, H. Murakami, J. Kossin, K.W. Dixon, and C.E. Whitlock 2019. "Recent increases in tropical cyclone intensification rates." *Nature Communications.* 10 (1), 635. https://doi.org/10.1038/s41467-019-08471-z

Bier, V.M., E.R. Gratz, N.J. Haphuriwat, W. Magua, and K.R. Wierzbicki 2007. "Methodology for identifying near-optimal interdiction strategies for a power transmission system." *Reliability Engineering & System Safety.* 92 (9), 1155-1161. https://doi.org/10.1016/j.ress.2006.08.007

Bilal, A., M. 2015. "Practical resilience metrics for planning, design, and decision making." *ASCE-ASME Journal of Risk and Uncertainty in Engineering Systems, Part A: Civil Engineering.* 1 (3), 04015008. https://doi.org/10.1061/AJRUA6.0000826

Bilal, A.M., and K.-L. Lai 1990. "Structural reliability assessment using latin hypercube sampling." *Proc., 5th International Conferene on Structural Safety and Reliability 1989 (ICOSSAR'89)*, ASCE, New York, NY, 1177-1184.

Borgonovo, E. 2007. "A new uncertainty importance measure." *Reliability Engineering & System Safety.* 92 (6), 771-784. https://doi.org/10.1016/j.ress.2006.04.015

Brennan, M.A., and C.G. Flint 2007. "Uncovering the hidden dimensions of rural disaster mitigation: Capacity building through community emergency response teams." *Southern Rural Sociology.* 22 (22), 1-5.

Britt, E. 2017. "Hurricanes harvey and irma: Electric industry impacts, restoration, and cost recovery." *Infrastructre.* 57 (1), 6. http://www.dwmrlaw.com/wp-content/uploads/2018/04/ABA_INFRA57-1.pdf

Brown, R.E., and H.L. Willis 2006. "The economics of aging infrastructure." *IEEE Power and Energy Magazine.* 4 (3), 36-43. https://doi.org/10.1109/MPAE.2006.1632452

Bruneau, M., S.E. Chang, R.T. Eguchi, G.C. Lee, T.D. O'Rourke, A.M. Reinhorn, M. Shinozuka, K. Tierney, W.A. Wallace, and D.v. Winterfeldt 2003. "A framework to quantitatively assess and enhance the seismic resilience of communities." *Earthquake Spectra.* 19 (4), 733-752. https://doi.org/10.1193/1.1623497

Bruneau, M., and A. Reinhorn 2007. "Exploring the concept of seismic resilience for acute care facilities." *Earthquake Spectra.* 23 (1), 41-62. https://doi.org/10.1193/1.2431396

Bruneau, M., and A.M. Reinhorn 2019. "Structural engineering dilemmas, resilient epcot, and other perspectives on the road to engineering resilience." *ASCE-ASME Journal of Risk and Uncertainty in Engineering Systems, Part A: Civil Engineering.* 5 (3), 02519001. https://doi.org/10.1061/AJRUA6.0001011

Burbank, K., T. Davison, S. Saifee, G. WHite, C. Beck, and D. Quan 2005. "An estimate of lost earnings due to electric supply disruption; *the case of florida's 2004 hurricane season*." FEMA, Orlando.

Carlos Agustín, E.-S. 2013. "Estimation of extreme wind speeds by using mixed distributions." *Ingeniería, Investigación y Tecnología.* 14 (2), 153-162. https://doi.org/10.1016/S1405-7743(13)72233-9

CARRI 2011. "Community resilience system initiative (crsi) steering committee final report — a roadmap to increased community resilience." Community and Regional Resilience Institute Washington DC., 156. https://s31207.pcdn.co/wp-content/uploads/2019/08/CRSI-Final-Report.pdf

2020. "Power off: Extreme weather and power outages." Climate Central.

Chang, S.E., and M. Shinozuka 2004. "Measuring improvements in the disaster resilience of communities." *Earthquake Spectra.* 20 (3), 739-755. https://doi.org/10.1193/1.1775796

Chen, C., J. Wang, F. Qiu, and D. Zhao 2016. "Resilient distribution system by microgrids formation after natural disasters." *IEEE Transactions on Smart Grid.* 7 (2), 958-966. https://doi.org/10.1109/TSG.2015.2429653

Chi, Y., Y. Xu, C. Hu, and S. Feng "A state-of-the-art literature survey of power distribution system resilience assessment." *Proc., 2018 IEEE Power & Energy Society General Meeting (PESGM)*, 1-5. https://doi.org/10.1109/PESGM.2018.8586495

Choi, J.-W., Y. Cha, H.-D. Kim, and S.-D. Kang 2016. "Latitudinal change of tropical cyclone maximum intensity in the western north pacific." *Advances in Meteorology.* 2016, 8. https://doi.org/10.1155/2016/5829162

Choi, W., C.-H. Ho, J. Kim, and J.C.L. Chan 2019. "Near-future tropical cyclone predictions in the western north pacific: Fewer tropical storms but more typhoons." *Climate Dynamics.* 53 (3), 1341-1356. https://doi.org/10.1007/s00382-019-04647-x

Cimellaro, G.P. 2016. *Urban resilience for emergency response and recovery: Fundamentals concepts and applications*, Springer, Switzerland.

Cimellaro, G.P., and M. Piqué 2016. "Resilience of a hospital emergency department under seismic event." *Advances in Structural Engineering.* 19 (5), 825-836. https://doi.org/10.1177/1369433216630441

Cimellaro, G.P., A.M. Reinhorn, and M. Bruneau 2010. "Framework for analytical quantification of disaster resilience." *Engineering Structures.* 32 (11), 3639-3649. https://doi.org/10.1016/j.engstruct.2010.08.008

Cimellaro, G.P., A.M. Reinhorn, and M. Bruneau 2010. "Seismic resilience of a hospital system." *Structure and Infrastructure Engineering.* 6 (1-2), 127-144. https://doi.org/10.1080/15732470802663847

Colbert, A.J., B.J. Soden, G.A. Vecchi, and B.P. Kirtman 2013. "The impact of anthropogenic climate change on north atlantic tropical cyclone tracks." *Journal of Climate.* 26 (12), 4088-4095. https://doi.org/10.1175/jcli-d-12-00342.1

Cox, R.S., and M. Hamlen 2015. "Community disaster resilience and the rural resilience index." *American Behavioral Scientist.* 59 (2), 220-237. https://doi.org/10.1177/0002764214550297

Cutter, S.L. 2016. "The landscape of disaster resilience indicators in the USA." *Natural Hazards.* 80 (2), 741-758. https://doi.org/10.1007/s11069-015-1993-2

Cutter, S.L., L. Barnes, M. Berry, C. Burton, E. Evans, E. Tate, and J. Webb 2008. "A place-based model for understanding community resilience to natural disasters." *Global Environmental Change.* 18 (4), 598-606. https://doi.org/10.1016/j.gloenvcha.2008.07.013

Dagher, H.J. 2006. *Reliability-based design of utility pole structures*, ASCE, SEI, Reston,Virginia.

Danica Coto 2018, July 16. "Lights slowly come on for puerto ricans in rural areas." <https://www.csmonitor.com/USA/2018/0716/Lights-slowly-come-on-for-Puerto-Ricans-in-rural-areas>. (https://www.csmonitor.com/USA/2018/0716/Lights-slowly-come-on-for-Puerto-Ricans-in-rural-areas).

Darestani, Y.M., and A. Shafieezadeh "A framework for hurricane resilience assessment of power distribution systems." *Proc., 13th International Conference on Applications of Statistics and Probability in Civil Engineering, ICASP13*.

Davidson, R., A., H. Liu, I. Sarpong, K., P. Sparks, and D. Rosowsky, V. 2003. "Electric power distribution system performance in carolina hurricanes." *Natural Hazards Review.* 4 (1), 36-45. 10.1061/(ASCE)1527-6988(2003)4:1(36)

Decò, A., P. Bocchini, and D.M. Frangopol 2013. "A probabilistic approach for the prediction of seismic resilience of bridges." *Earthquake Engineering & Structural Dynamics.* 42 (10), 1469-1487. https://doi.org/10.1002/eqe.2282

Deza, M.M., and E. Deza 2009. *Encyclopedia of distances*, Springer Berlin Heidelberg.

DHS 2011. "Presidential policy directive / ppd-8: National preparedness." <https://www.dhs.gov/xlibrary/assets/presidential-policy-directive-8-national-preparedness.pdf>. (https://www.dhs.gov/xlibrary/assets/presidential-policy-directive-8-national-preparedness.pdf).

Dowd, C. 2018. Twosamples: Fast permutation based two sample testsR package Version 1.0.0.

Dueñas-Osorio, L., J.I. Craig, B.J. Goodno, and A. Bostrom 2007. "Interdependent response of networked systems." *Journal of Infrastructure Systems.* 13 (3), 185-194. https://doi.org/10.1061/(ASCE)1076-0342(2007)13:3(185)

Edwards, P., and R. B. Hurst 2001. "Level-crossing statistics of the horizontal wind speed in the planetary surface boundary layer." *Chaos (Woodbury, N.Y.).* 11, 611-618. https://doi.org/10.1063/1.1379310

Espinoza, S., M. Panteli, P. Mancarella, and H. Rudnick 2016. "Multi-phase assessment and adaptation of power systems resilience to natural hazards." *Electric Power Systems Research.* 136, 352-361. https://doi.org/10.1016/j.epsr.2016.03.019

FEMA 2008. "Hazus-mh: Preparedness and response planning." Federal Emergency Management Agency, Washington DC.

Fisher, R.A. 1936. "The design of experiments." *Nature.* 137 (3459), 252-254. https://doi.org/10.1038/137252a0

Gao, H., Y. Chen, Y. Xu, and C. Liu 2016. "Resilience-oriented critical load restoration using microgrids in distribution systems." *IEEE Transactions on Smart Grid.* 7 (6), 2837-2848. https://doi.org/10.1109/TSG.2016.2550625

Gascó-Hernandez, M., M. Zheleva, P. Bogdanov, and J.R. Gil-Garcia 2019. "Towards a socio-technical framework for bridging the digital divide in rural emergency preparedness and response: Integrating user adoption, heterogeneous wide-area networks, and advanced data science." *Proc., 20th Annual International Conference on Digital Government Research, Mohamed bin Rashid School of Govrnment.*, ACM, NY, USA, 362-369. https://doi.org/10.1145/3325112.3325217

Gasser, P., P. Lustenberger, M. Cinelli, W. Kim, M. Spada, P. Burgherr, S. Hirschberg, B. Stojadinovic, and T.Y. Sun 2019. "A review on resilience assessment of energy systems." *Sustainable and Resilient Infrastructure.* https://doi.org/10.1080/23789689.2019.1610600, 1-27. https://doi.org/10.1080/23789689.2019.1610600

Gautam, P., P. Piya, and R. Karki 2021. "Resilience assessment of distribution systems integrated with distributed energy resources." *IEEE Transactions on Sustainable Energy.* 12 (1), 338-348. https://doi.org/10.1109/TSTE.2020.2994174

Geenens, G., A. Charpentier, and D. Paindaveine 2017. "Probit transformation for nonparametric kernel estimation of the copula density." *Bernoulli.* 23 (3), 1848-1873. https://doi.org/10.3150/15-BEJ798

Gijbels, I., and J. Mielniczuk 1990. "Estimating the density of a copula function." *Communications in Statistics - Theory and Methods.* 19 (2), 445-464. https://doi.org/10.1080/03610929008830212

Guikema, S., D., and J. Goffelt, P. 2008. "A flexible count data regression model for risk analysis." *Risk Analysis.* 28 (1), 213-223. https://doi.org/10.1111/j.1539-6924.2008.01014.x

Haimes, Y.Y. 2009. "On the definition of resilience in systems." *Risk Analysis.* 29 (4), 498-501. https://doi.org/10.1111/j.1539-6924.2009.01216.x

Hashimoto, T., J.R. Stedinger, and D.P. Loucks 1982. "Reliability, resiliency, and vulnerability criteria for water resource system performance evaluation." *Water Resources Research.* 18 (1), 14-20. https://doi.org/10.1029/WR018i001p00014

He, H., J. Yang, D. Gong, R. Mao, Y. Wang, and M. Gao 2015. "Decadal changes in tropical cyclone activity over the western north pacific in the late 1990s." *Climate Dynamics.* 45 (11), 3317-3329. https://doi.org/10.1007/s00382-015-2541-1

Henry, D., and J. Emmanuel Ramirez-Marquez 2012. "Generic metrics and quantitative approaches for system resilience as a function of time." *Reliability Engineering & System Safety.* 99, 114-122. https://doi.org/10.1016/j.ress.2011.09.002

Hodges, J.L. 1958. "The significance probability of the smirnov two-sample test." *Ark. Mat.* 3 (5), 469-486. https://doi.org/10.1007/BF02589501

Holland, G., and C.L. Bruyère 2014. "Recent intense hurricane response to global climate change." *Climate Dynamics.* 42 (3), 617-627. https://doi.org/10.1007/s00382-013-1713-0

Holling, C.S. 1973. "Resilience and stability of ecological systems." *Annual Review of Ecology and Systematics.* 4 (1), 1-23. https://doi.org/10.1146/annurev.es.04.110173.000245
IEEE 2012. "Ieee guide for electric power distribution reliability indices." *IEEE Std 1366-2012 (Revision of IEEE Std 1366-2003).* https://doi.org/10.1109/IEEESTD.2012.6209381, 1-43. https://doi.org/10.1109/IEEESTD.2012.6209381
2019. "Hypothesis test and confidence analysis with wasserstein distance with general dimension." arXiv:1910.07773.
Impollonia, N., G. Ricciardi, and F. Saitta 2011. "Statics of elastic cables under 3d point forces." *International Journal of Solids and Structures.* 48 (9), 1268-1276. https://doi.org/10.1016/j.ijsolstr.2011.01.007
Joe, H. 1997. *Multivariate models and multivariate dependence concepts*, Chapman and Hall/CRC.
Johansen, C., J. Horney, and I. Tien 2017. "Metrics for evaluating and improving community resilience." *Journal of Infrastructure Systems.* 23 (2), 04016032. https://doi.org/doi:10.1061/(ASCE)IS.1943-555X.0000329
Kapucu, N., C.V. Hawkins, and F.I. Rivera 2013. "Disaster preparedness and resilience for rural communities." *Risk, Hazards & Crisis in Public Policy.* 4 (4), 215-233. https://doi.org/10.1002/rhc3.12043
Kenward, A., and U. Raja 2014. "Blackout: Extreme weather, climate change and power outages." *Climate Central.* 23.
Klotzbach, P.J. 2006. "Trends in global tropical cyclone activity over the past twenty years (1986–2005)." *Geophysical Research Letters.* 33 (10). https://doi.org/10.1029/2006gl025881
KLÜPPELBERG, C., G. KUHN, and L. PENG 2008. "Semi-parametric models for the multivariate tail dependence function – the asymptotically dependent case." *Scandinavian Journal of Statistics.* 35 (4), 701-718. https://doi.org/10.1111/j.1467-9469.2008.00602.x
Knutson, T., S.J. Camargo, J.C.L. Chan, K. Emanuel, C.-H. Ho, J. Kossin, M. Mohapatra, M. Satoh, M. Sugi, K. Walsh, and L. Wu 2019. "Tropical cyclones and climate change assessment: Part i: Detection and attribution." *Bulletin of the American Meteorological Society.* 100 (10), 1987-2007. https://doi.org/10.1175/bams-d-18-0189.1
Knutson, T.R., J.J. Sirutis, G.A. Vecchi, S. Garner, M. Zhao, H.-S. Kim, M. Bender, R.E. Tuleya, I.M. Held, and G. Villarini 2013. "Dynamical downscaling projections of twenty-first-century atlantic hurricane activity: Cmip3 and cmip5 model-based scenarios." *Journal of Climate.* 26 (17), 6591-6617. https://doi.org/10.1175/jcli-d-12-00539.1
Kossin, J. 2018. "Comment on “spatial and temporal trends in the location of the lifetime maximum intensity of tropical cyclones” by tennille and ellis." *Atmosphere.* 9 (7), 241. https://doi.org/10.3390/atmos9070241
Kossin, J.P., K.A. Emanuel, and S.J. Camargo 2016. "Past and projected changes in western north pacific tropical cyclone exposure." *Journal of Climate.* 29 (16), 5725-5739. https://doi.org/10.1175/jcli-d-16-0076.1
Kossin, J.P., K.A. Emanuel, and G.A. Vecchi 2014. "The poleward migration of the location of tropical cyclone maximum intensity." *Nature.* 509 (7500), 349-352. https://doi.org/10.1038/nature13278

Kossin, J.P., T.L. Olander, and K.R. Knapp 2013. "Trend analysis with a new global record of tropical cyclone intensity." *Journal of Climate.* 26 (24), 9960-9976. https://doi.org/10.1175/jcli-d-13-00262.1

Kwasinski, A. 2016. "Quantitative model and metrics of electrical grids' resilience evaluated at a power distribution level." *Energies.* 9 (2), 93. https://doi.org/10.3390/en9020093

Lehmann, E.L. 2006. *Nonparametrics: Statistical methods based on ranks*, Springer-Verlag, New York.

Li, H. 2009. "Orthant tail dependence of multivariate extreme value distributions." *Journal of Multivariate Analysis.* 100 (1), 243-256. https://doi.org/10.1016/j.jmva.2008.04.007

Li, J., X. Ma, C. Liu, and K.P. Schneider 2014. "Distribution system restoration with microgrids using spanning tree search." *IEEE Transactions on Power Systems.* 29 (6), 3021-3029. https://doi.org/10.1109/TPWRS.2014.2312424

Liang, A., L. Oey, S. Huang, and S. Chou 2017. "Long-term trends of typhoon-induced rainfall over taiwan: In situ evidence of poleward shift of typhoons in western north pacific in recent decades." *Journal of Geophysical Research: Atmospheres.* 122 (5), 2750-2765. https://doi.org/10.1002/2017jd026446

Liu, H., R. Davidson, A., D. Rosowsky, V., and J. Stedinger, R. 2005. "Negative binomial regression of electric power outages in hurricanes." *Journal of Infrastructure Systems.* 11 (4), 258-267. 10.1061/(ASCE)1076-0342(2005)11:4(258)

Liu, Q., and T. Homma 2010. "A new importance measure for sensitivity analysis." *Journal of Nuclear Science and Technology.* 47 (1), 53-61. https://doi.org/10.1080/18811248.2010.9711927

Mahzarnia, M., M. Parsa Moghaddam, P. Siano, and M.-R. Haghifam 2020. "A comprehensive assessment of power system resilience to a hurricane using a two-stage analytical approach incorporating risk-based index." *Sustainable Energy Technologies and Assessments.* 42, 100831. https://doi.org/10.1016/j.seta.2020.100831

Marius Hofert, I.k., Martin Maechler, Jun Yan, Johanna G. Neslehova, Rebecca Morger. 2020. Multivariate dependence with copulas version 1.0-1CRAN.

Mei, W., and S.-P. Xie 2016. "Intensification of landfalling typhoons over the northwest pacific since the late 1970s." *Nature Geoscience.* 9 (10), 753-757. https://doi.org/10.1038/ngeo2792

Mensah, A.F., and L. Dueñas-Osorio 2016. "Efficient resilience assessment framework for electric power systems affected by hurricane events." *Journal of Structural Engineering.* 142 (8), C4015013. https://doi.org/10.1061/(ASCE)ST.1943-541X.0001423

Miles, S.B., and S.E. Chang 2006. "Modeling community recovery from earthquakes." *Earthquake Spectra.* 22 (2), 439-458. https://doi.org/10.1193/1.2192847

Mileti, D. 1999. *Disasters by design: A reassessment of natural hazards in the united states*, The National Academies Press, Washington, DC.

Mohammadi Darestani, Y., and A. Shafieezadeh 2019. "Multi-dimensional wind fragility functions for wood utility poles." *Engineering Structures.* 183, 937-948. https://doi.org/10.1016/j.engstruct.2019.01.048

Moon, I.-J., S.-H. Kim, P. Klotzbach, and J.C.L. Chan 2015. "Roles of interbasin frequency changes in the poleward shifts of the maximum intensity location of tropical cyclones." *Environmental Research Letters.* 10 (10), 104004. https://doi.org/10.1088/1748-9326/10/10/104004

Morrell, J.J. 2012. "Wood pole maintenance manual: 2012 edition, research contribution 51." Oregon State University. Forest Research Laboratory, Corrvallis.
Moss, R., A. Brenkert, and E. Malone 2001. "Vulnerability to climate change: A quantitative approach." U.S. Dept. of Energy, Oak Ridge, TN.
Mukherjee, S., R. Nateghi, and M. Hastak 2018. "A multi-hazard approach to assess severe weather-induced major power outage risks in the u.S." *Reliability Engineering & System Safety.* 175, 283-305. https://doi.org/10.1016/j.ress.2018.03.015
Nager, T. 2014. "Kernel methods for vine copula estimation." Master's, Technische Universität München.
Nagler, T. 2018. "Kdecopula: An r package for the kernel estimation of bivariate copula densities." *Journal of Statistical Software.* 84 (7). 10.18637/jss.v084.i07
Nateghi, R. 2018. "Multi-dimensional infrastructure resilience modeling: An application to hurricane-prone electric power distribution systems." *IEEE Access.* 6, 13478-13489. https://doi.org/10.1109/ACCESS.2018.2792680
NIST 2016. "Community resilience planning guide for building and infrastructure systems-volume ii." 258. http://dx.doi.org/10.6028/NIST.SP.1190v2
Oey, L.-Y., and S. Chou 2016. "Evidence of rising and poleward shift of storm surge in western north pacific in recent decades." *Journal of Geophysical Research: Oceans.* 121 (7), 5181-5192. https://doi.org/10.1002/2016jc011777
Onyewuchi, U.P., A. Shafieezadeh, M.M. Begovic, and R. DesRoches 2015. "A probabilistic framework for prioritizing wood pole inspections given pole geospatial data." *IEEE Transactions on Smart Grid.* 6 (2), 973-979. https://doi.org/10.1109/TSG.2015.2391183
Ouyang, M., and L. Dueñas-Osorio 2014. "Multi-dimensional hurricane resilience assessment of electric power systems." *Structural Safety.* 48, 15-24. https://doi.org/10.1016/j.strusafe.2014.01.001
Ouyang, M., L. Dueñas-Osorio, and X. Min 2012. "A three-stage resilience analysis framework for urban infrastructure systems." *Structural Safety.* 36-37, 23-31. https://doi.org/10.1016/j.strusafe.2011.12.004
ATC & SEI Conference on Advances in Hurricane Engineering 2012 2013. "Failure risk of 230 kv electricity transmission lines in south carolina under hurricane wind hazards." ASCE, Miami, Florida, USA.
Panteli, M., and P. Mancarella 2017. "Modeling and evaluating the resilience of critical electrical power infrastructure to extreme weather events." *IEEE Systems Journal.* 11 (3), 1733-1742. https://doi.org/10.1109/JSYST.2015.2389272
Panteli, M., C. Pickering, S. Wilkinson, R. Dawson, and P. Mancarella 2017. "Power system resilience to extreme weather: Fragility modeling, probabilistic impact assessment, and adaptation measures." *IEEE Transactions on Power Systems.* 32 (5), 3747-3757. https://doi.org/10.1109/TPWRS.2016.2641463
Park, D.-S.R., C.-H. Ho, and J.-H. Kim 2014. "Growing threat of intense cyclones to east asia over the period 1977-2010." *Environmental Research Letters.* 9 (1). https://doi.org/10.1088/1748-9326/9/1/014008
Park, D.-S.R., C.-H. Ho, J.-H. Kim, and H.-S. Kim 2013. "Spatially inhomogeneous trends of tropical cyclone intensity over the western north pacific for 1977–2010." *Journal of Climate.* 26 (14), 5088-5101. https://doi.org/10.1175/jcli-d-12-00386.1

AGU Fall Meeting Abstracts 2015. "Does weakening vertical ocean mixing contribute to the poleward shift of tropical cyclone maximum intensity?".

Pianosi, F., and T. Wagener 2015. "A simple and efficient method for global sensitivity analysis based on cumulative distribution functions." *Environmental Modelling & Software.* 67, 1-11. https://doi.org/10.1016/j.envsoft.2015.01.004

Poudel, S., A. Dubey, and A. Bose 2020. "Risk-based probabilistic quantification of power distribution system operational resilience." *IEEE Systems Journal.* 14, 3506-3517.

Preston, B.L., S.N. Backhaus, M. Ewers, J.A. Phillips, C.A. Silva Monroy, A.G. Tarditi, J.P. Looney, and T.J. King, Jr. 2016. "Resilience of the u.S. Electricity system: A multi-hazard perspective."
https://www.hsdl.org/?view&did=818859

Ramdas, A., N.G. Trillos, and M. Cuturi 2017. "On wasserstein two-sample testing and related families of nonparametric tests." *Entropy.* 19 (2), 47. https://doi.org/10.3390/e19020047

Reed, D.A., K.C. Kapur, and R.D. Christie 2009. "Methodology for assessing the resilience of networked infrastructure." *IEEE Systems Journal.* 3 (2), 174-180. https://doi.org/10.1109/JSYST.2009.2017396

Renschler, C., A. Frazier, L. Arendt, G. Cimellaro, A. Reinhorn, and M. Bruneau 2010. "Framework for defining and measuring resilience at the community scale: The peoples resilience framework." https://www.hsdl.org/?view&did=790013

Sakai, T., M. Nakajima, K. Tokaji, and N. Hasegawa 1997. "Statistical distribution patterns in mechanical and fatigue properties of metallic materials." *Materials Science Research International,* . 3, 63-74.

Schmid, F., and R. Schmidt 2007. "Multivariate conditional versions of spearman's rho and related measures of tail dependence." *Journal of Multivariate Analysis.* 98 (6), 1123-1140. https://doi.org/10.1016/j.jmva.2006.05.005

Schmid, F., and R. Schmidt 2007. "Nonparametric inference on multivariate versions of blomqvist's beta and related measures of tail dependence." *Metrika.* 66 (3), 323-354. https://doi.org/10.1007/s00184-006-0114-3

Schweizer, B., and E.F. Wolff 1981. "On nonparametric measures of dependence for random variables." *The Annals of Statistics.* 9 (4), 879-885. http://www.jstor.org/stable/2240856

2010. "Coastal community resilience index: A community self-assessment." MASGP-08-014, Mississippi-Alabama, Sea Grant Consortium.

Sharifi, A. 2016. "A critical review of selected tools for assessing community resilience." *Ecological Indicators.* 69, 629-647. https://doi.org/10.1016/j.ecolind.2016.05.023

Sherrieb, K., F.H. Norris, and S. Galea 2010. "Measuring capacities for community resilience." *Social Indicators Research.* 99 (2), 227-247. https://doi.org/10.1007/s11205-010-9576-9

Sheskin, D.J. 2000. *Handbook of parametric and nonparametric statistical procedures, 2nd ed*, Chapman & Hall/CRC, Boca Raton, FL.

Sklar, M. 1959. "Fonctions de repartition a n dimensions et leurs marges." *Inst. Statist. Univ. Paris.* 8, 229-231.

Sobol′, I.M. 2001. "Global sensitivity indices for nonlinear mathematical models and their monte carlo estimates." *Mathematics and Computers in Simulation.* 55 (1), 271-280. https://doi.org/10.1016/S0378-4754(00)00270-6

Song, J., and P.J. Klotzbach 2018. "What has controlled the poleward migration of annual averaged location of tropical cyclone lifetime maximum intensity over the western north pacific since 1961?" *Geophysical Research Letters.* 45 (2), 1148-1156. https://doi.org/10.1002/2017gl076883

2013. "Bare copper wire and cable." Southwire Company, Georgia, USA.

2009. "Defining resilience: What san francisco needs from its seismic mitigation policies."

Studholme, J., and S. Gulev 2018. "Concurrent changes to hadley circulation and the meridional distribution of tropical cyclones." *Journal of Climate.* 31 (11), 4367-4389. https://doi.org/10.1175/jcli-d-17-0852.1

Sun, S., Q. Lyu, G. Li, Y. Lin, Z. Bie, and W. Wen "Resilience modeling and assessment for power distribution systems under typhoon disasters." *Proc., 2019 IEEE Sustainable Power and Energy Conference (iSPEC)*, 2413-2418. https://doi.org/10.1109/iSPEC48194.2019.8975030

Tabandeh, A., and P. Gardoni 2018. "Resilience analysis: A mathematical formulation to model resilience of engineering systems au - sharma, neetesh." *Sustainable and Resilient Infrastructure.* 3 (2), 49-67. https://doi.org/10.1080/23789689.2017.1345257

Team, R.C. 2020. R: A language and environment for statistical computing. R foundation for Statistical Computing, Vienne, Austria.

Technology, Q. 2008. "Undergrounding assessment phase 3 report: Ex ante cost and benefit modeling ", Quanta Technology, 97. https://woodpoles.org/portals/2/documents/UndergroundingAssessment_P3.pdf

Technology, Q. 2009. "Cost-benefit analysis of the deployment of utility infrastructure upgrades and storm hardening programs." Quanta Technology, 108. http://www.puc.texas.gov/industry/electric/reports/infra/utlity_infrastructure_upgrades_rpt.pdf

Tennille, S.A., and K.N. Ellis 2017. "Spatial and temporal trends in the location of the lifetime maximum intensity of tropical cyclones." *Atmosphere.* 8 (10), 198. https://doi.org/10.3390/atmos8100198

Torrent, R.J. 1978. "The log-normal distribution" a better fitness for the results of mechanical testing of materials " *Materials and structures*, Kluwer Academic Publishers, 235–245.

Vivekanandan, N. 2012. "Comparison of estimators of extreme value distributions for wind data analysis." *Bonfring International Journal of Data Mining.* 2, 16-20. https://doi.org/10.9756/BIJDM.1503

Vugrin, E.D., A.R. Castillo, and C.A. Silva-Monroy 2017. "Resilience metrics for the electric power system: A performance-based approach, sand2017-1493." Sandia National Laboratories, CA, United States. https://www.osti.gov/servlets/purl/1367499

Wang, C.-h., R.H. Leicester, and M. Nguyen 2008. "Probabilistic procedure for design of untreated timber poles in-ground under attack of decay fungi." *Reliability Engineering & System Safety.* 93 (3), 476-481. https://doi.org/10.1016/j.ress.2006.12.007

Wang, R., and L. Wu 2019. "Influence of track changes on the poleward shift of lmi location of western north pacific tropical cyclones." *Journal of Climate.* 32 (23), 8437-8445. https://doi.org/10.1175/jcli-d-18-0855.1

Warwick, M., and M. Hoffman 2016. "Electricity distribution system baseline report for doe quadrennial energy review, pnnl-25187." Pacific Northwest National Laboratory, Richland, Washington.

Webster, P.J., G.J. Holland, J.A. Curry, and H.-R. Chang 2005. "Changes in tropical cyclone number, duration, and intensity in a warming environment." *Science.* 309 (5742), 1844-1846. https://doi.org/10.1126/science.1116448

Yao, Y., T. Edmunds, D. Papageorgiou, and R. Alvarez 2007. "Trilevel optimization in power network defense." *IEEE Transactions on Systems, Man, and Cybernetics, Part C (Applications and Reviews).* 37 (4), 712-718. https://doi.org/10.1109/TSMCC.2007.897487

Yuan, H., W. Zhang, J. Zhu, and A.C. Bagtzoglou 2018. "Resilience assessment of overhead power distribution systems under strong winds for hardening prioritization." *ASCE-ASME Journal of Risk and Uncertainty in Engineering Systems, Part A: Civil Engineering.* 4 (4), 04018037. https://doi.org/doi:10.1061/AJRUA6.0000988

Zhan, R., and Y. Wang 2017. "Weak tropical cyclones dominate the poleward migration of the annual mean location of lifetime maximum intensity of northwest pacific tropical cyclones since 1980." *Journal of Climate.* 30 (17), 6873-6882. https://doi.org/10.1175/jcli-d-17-0019.1

Zhang, C., and Y. Wang 2017. "Projected future changes of tropical cyclone activity over the western north and south pacific in a 20-km-mesh regional climate model." *Journal of Climate.* 30 (15), 5923-5941. 10.1175/jcli-d-16-0597.1

Zhou, H., J.a. Wang, J. Wan, and H. Jia 2010. "Resilience to natural hazards: A geographic perspective." *Natural Hazards.* 53 (1), 21-41. https://doi.org/10.1007/s11069-009-9407-y

Zhou, X., H. Lin, and H. Lin 2008. "Global sensitivity analysis." *Encyclopedia of gis*, S. Shekhar, and H. Xiong, eds., Springer US, Boston, MA, 408-409.

Zhu, D., D. Cheng, R.P. Broadwater, and C. Scirbona 2007. "Storm modeling for prediction of power distribution system outages." *Electric Power Systems Research.* 77 (8), 973-979. https://doi.org/10.1016/j.epsr.2006.08.020

Zona, A., O. Kammouh, and G.P. Cimellaro 2020. "Quantification of resourcefulness for community resilience framework." *International Journal of Disaster Risk Reduction.* 46. https://doi.org/10.1016/j.ijdrr.2020.101509

VITA

Prativa Sharma was born in 1992 in Kathmandu, Nepal. She completed her high school study at Kathmandu Model Higher Secondary School, Kathmandu, Nepal, in 2010, and her Bachelor's degree from Himalaya College of Engineering, Tribhuvan University, Nepal, in 2014. After graduating, she worked for two years as a civil engineer at Development Support Consult Pvt Ltd, Nepal.

In January 2017, Ms. Prativa joined the University of Missouri Kansas City (UMKC) under the supervision of Professor ZhiQiang Chen to obtain an interdisciplinary Ph.D. degree with civil engineering as the coordinating discipline and geosciences as the co-discipline. She received her Master of Science in civil engineering degree in May 2019. During her stay at UMKC, she worked as a graduate research assistant, teaching assistant and also did a 2021 summer internship as a research assistant in the Oak Ridge National Laboratory.

Ms. Prativa Sharma has authored one paper in a peer-reviewed journal and has authored and co-authored four conference papers, has presented on three conference talks and two university symposium posters.